
International Panel Report


International Collaborative
Project to Evaluate Fire Models
for Nuclear Power Plant
Applications

International Panel Report on
Benchmark Exercise # 2 - Pool
Fires in Large Halls

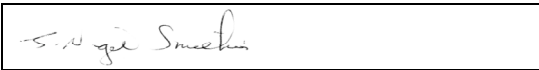
BRE client report number
212214

May 2004

Prepared by ¹

Signature	
Name	Stewart Miles
Position	Senior Consultant, BRE Fire Division

Approved on behalf of BRE ²

Signature	
Name	Nigel Smithies
Position	Director, BRE Fire Division
Date	May 2004

BRE
Bucknalls Lane
Garston
Watford
WD25 9XX

Tel : +44 1923 664000
Fax : +44 1923 664010

Email : enquiries@bre.co.uk
Website : www.bre.co.uk

¹ The overall document has been compiled by the S Miles of the Building research establishment (BRE), UK. The appendices have been written by the individual authors.

² BRE approval is for the main body of the report, and does not extend to the appendices.

International Panel Report

Benchmark Exercise # 2 - Pool Fires in Large Halls

CONTENTS

FORWARD	4
ABSTRACT	5
ACRONYMS	6
EXECUTIVE SUMMARY	7
INTRODUCTION	11
DEFINITION OF BENCHMARK EXERCISE # 2	13
<i>Part I – Large Hall Tests</i>	13
<i>Part II – Extended NPP Scenarios</i>	21
RESULTS OF ANALYSES	27
<i>Part I – Large Hall Tests</i>	27
<i>Part II – Extended NPP Scenarios</i>	35
GENERAL CONCLUSIONS AND RECOMMENDATIONS	51
REVIEW OF HEAT RELEASE RATE AND COMBUSTION TERMS	53
REFERENCES	55
ACKNOWLEDGEMENTS	57
FIGURES	58
<i>Appendix A - K. McGrattan (NIST): Benchmark Exercise #2 - Fire in a large hall - NIST Fire Dynamics Simulator</i>	
<i>Appendix B - D. Roubineau (IRSN): Benchmark Exercise 2 - Study of the consequences of a fire in a turbine hall</i>	
<i>Appendix C - W. Klein-Heßling (GRS): Technical Note TN-KLH 1/2003 - Fire Benchmark #2 - COCOSYS Results</i>	
<i>Appendix D - L. Gay and B Gautier (EDF): MAGIC Calculation for Benchmark #2 - Fire in a large hall</i>	
<i>Appendix E - M. Heitsch (GRS): Benchmark Exercise #2 Simulations with CFX</i>	
<i>Appendix F - M. Dey (USNRC): Analysis of Pool Fires in Large Multi-Level Halls with the CFAST and FDS Fire Codes</i>	
<i>Appendix G – D. Joyeux and O. Lecoq-Jammes (CTICM): Simulations with MAGIC (V 3.4.8)</i>	

Appendix H - S. Miles (BRE): Benchmark Exercise #2 Simulations with JASMINE and CFAST

Appendix I - J. Will (HHP Braunschweig): Benchmark Exercise #2 - Fire in a Large Hall - Results of Kobra-3D Calculations

FORWARD

The objective of the International Collaborative Project to Evaluate Fire Models for Nuclear Power Plant Applications is to share the knowledge and resources of various organisations to evaluate and improve the state of the art of fire models for use in nuclear power plant fire safety and fire hazard analysis. The project is divided into two phases. The purpose of the first phase is to evaluate the capabilities of current fire models for fire safety analysis in nuclear power plants. The second phase will extend the validation database of those models, and implement beneficial improvements to the models that are identified in the first phase.

A series of benchmark exercises are being conducted as part of the first phase of the collaborative project. An international collaborative project has been set up to share knowledge and resources from various organisations and to evaluate and improve the state of fire modelling for nuclear power plant fire safety. As part of this project, participants are undertaking a series of benchmark exercises. Predictions from a range of numerical fire models are being analysed by comparing the results from different models, and also against experimental measurements where available. Benchmark exercise # 1, comprising a set of fire scenarios inside a switchgear room, has been completed and reported.

This panel report covers the work of Benchmark exercise # 2, which was designed to challenge fire models in respect to their application to large enclosures, and to address complexities introduced by features such as horizontal (hatch) flows between compartments. The exercise was divided into two parts. For *Part I* experimental measurements of gas temperature were available prior to the simulations, making this an open exercise. While for *Part II* there were no experimental measurements, blind simulations were undertaken prior to the project meeting in October 2002, followed by further optional open simulations. Eleven organisations participated in *Part I*, collectively making simulations with three zone models, two lumped parameter models and four CFD models. For *Part II*, there were nine participating organisations, making simulations with three zone, one lumped parameter and four CFD models.

A description of the benchmark exercise is given, and the main results and findings are summarised. The report also includes a set of technical appendices written by the participants, where the individual contributions are described in more detail.

This document is not intended to provide guidance to users of fire models. Guidance on the use of fire models is currently being developed by several national and international standards organisations, industry groups, and utilities. This document is intended to be a source and reference for technical information and insights gained through the exercise. This information may be beneficial to users of fire models and developers of guidance documents or standards for the use of fire models in nuclear power plant applications.

ABSTRACT

This document is a panel report on the results and findings of the second benchmark exercise of the International Collaborative Project to Evaluate Fire Models for Nuclear Power Plant Applications. It forms part of an on-going international activity to assess the capability of current fire models for inclusion in fire risk assessments for nuclear power plants. Benchmark exercise # 2 was designed to challenge fire models in respect to their application to large enclosures, and to address complexities introduced by features such as horizontal (hatch) flows between compartments. The exercise was divided into *Part I* and *Part II*, each consisting of three separate scenario cases. Simulations were performed with zone, lumped parameter and CFD models. In *Part I* reasonable agreement between prediction and measurement was achieved with all class of fire model once the controlling mechanisms had been 'correctly' accounted for. Although for *Part II* there were no experimental measurements, the spread in the predicted values indicated that the modelling of large complex spaces such a turbine hall warrants further investigation.

ACRONYMS

BRE	Building Research Establishment
CFAST	Consolidated Model for Fire and Smoke Transport
CFD	Computational Fluid Dynamics
COCOSYS	Containment Code System
CTICM	Centre Technique Industriel de la Construction Métallique
EdF	Electricité de France
FDS	Fire Dynamics Simulator
GRS	Gesellschaft für Anlagen-und Reaktorsicherheit
HGL	Hot Gas Layer
HRR	Heat Release Rate
iBMB	Institut für Baustoffe, Massivbau und Brandschutz
IRSN	Institut de radioprotection et de sûreté nucléaire
JASMINE	Analysis of Smoke Movement in Enclosures
LC	Lower Compartment
LL	Lower Layer
NIST	National Institute of Standards and Technology
NFPA	National Fire Protection Association
NPP	Nuclear Power Plant
RF	Radiative Fraction
SFPE	Society of Fire Protection Engineers
UC	Upper Compartment
UL	Upper Layer
USNRC	United States Nuclear Regulatory Commission
WPI	Worcester Polytechnic Institute

EXECUTIVE SUMMARY

The traditional, prescriptive, approach to fire regulation is based on engineering judgement derived from operating experience, tests, codes and standards. Conversely, in a performance-based regulatory system the fundamental premise is that the operation of a fire safety system can be predicted by calculation or modelling. While this approach can be applied to nuclear power plants too, there are particular safety issues that necessitate an evaluation of these tools prior to their use as part of a fire risk assessment for a nuclear power plant.

An international collaborative project has been set up to share knowledge and resources from various organisations and to evaluate and improve the state of fire modelling for nuclear power plant fire safety. As part of this project, participants are undertaking a series of benchmark exercises. Predictions from a range of numerical fire models are being analysed by comparing the results from different models, and also against experimental measurements where available. Benchmark exercise # 1, comprising a set of fire scenarios inside a switchgear room, has been completed and reported. Due partly to the geometry of the room and the nature of the fire scenarios, the differences in the conclusions obtained using the various fire models were not judged significant. Target cable damage was predicted as unlikely in nearly all scenarios (by all participants).

This panel report covers the work of Benchmark exercise # 2, which was designed to challenge fire models in respect to their application to large enclosures, and to address complexities introduced by features such as horizontal (hatch) flows between compartments. The exercise was divided into *Part I* and *Part II*, each consisting of three separate scenario cases. Although most input parameters were defined in the problem specification, the benchmark exercise did involve user judgement in selecting physical sub-models and associated parameters.

Part I was based on a series of full-scale experiments inside the VTT Test Hall in Finland, for which the sloping roof provided a challenge to zone models in particular. Each case involved a single pool fire, in the range 2 to 4 MW, for which there were experimental measurements of gas temperature at three thermocouple trees and above the fire source. For two cases the hall was nominally sealed, and 'infiltration ventilation' was incorporated by including small openings. For the third case mechanical exhaust ventilation was employed, and two doorway openings were provided. *Part I* was conducted as an open exercise with the measured temperature data available to participants prior to the simulations. Eleven organisations participated in *Part I*, collectively making simulations with three zone models, two lumped parameter models and four CFD models.

Although for *Part II* there were no experimental measurements, it extended the scope of the exercise to examine the effect of a bigger fire, growing to approximately 70 MW, and a building with dimensions representative of a turbine hall. The building was divided into

a lower and an upper deck, connected by two open hatches. *Case 1* involved a nominally sealed building, for which small 'infiltration' openings were specified. The other cases included smoke exhaust ventilation using, in one case, purely natural ventilation and in the other a combination of natural and mechanical ventilation (i.e. natural wall vents combined with natural or mechanical roof vents respectively). For *Part II*, there were nine participating organisations, making simulations with three zone, one lumped parameter and four CFD models. Blind simulations were undertaken by eight organisations prior to the 6th meeting of the international collaborative project in October 2002, where predictions were presented and compared. This was followed by further optional open simulations.

This panel report includes a definition of the benchmark exercise, a summary of the results from the individual participants, an assessment of the main findings from the simulations and a set of technical appendices. For *Part I*, for which experimental measurements had been provided to the participants, a review of the main causes of discrepancy between prediction and measurement is provided. For *Part II*, for which there are no experimental measurements, a comparative review of the predictions from the various simulations is provided. While BRE has compiled the main body of the panel report, the technical appendices were provided by the individual participants, and describe in more detail the work undertaken with each of the fire models.

Benchmark exercise 2 has provided some valuable insights into the performance of fire models, extending the findings from the first benchmark exercise in a number of important respects. These include the modelling of large spaces, complex geometries and in comparing predictions against experimental measurement data. Confidence in the application of zone, lumped parameter and CFD models has been provided in the simulations of the test hall experiments in *Part I*, where reasonable agreement was obtained once the important, controlling mechanisms were accounted for. However, the simulations of the turbine hall in *Part II* identified a number of current weaknesses, and illustrated that quite varied predictions could be obtained with different models, including with those of the same type, e.g. zone or CFD.

The results for *Part I* were quite encouraging, with the general, qualitative, nature of the experiments being captured in the simulations by all types of model. Despite the 'complexity' of the roof structure the various models were able to predict the smoke layer formation process with reasonable reliability. Of particular note here was the justification in the zone models in assuming a flat ceiling such that the volume of the hall was conserved. The fact that zone models generally predicted lower layer heights than those derived from the experimental measurements might be attributed, in part at least, to the data reduction method used in calculating the layer height from the experimental temperature measurements.

There was, however, a tendency when using the original benchmark specification in *Part I* to predict higher smoke layer temperatures than those measured. Two principle mechanisms were identified, to which modifications were able to reduce the temperature of the smoke layer. The first of these was the proportion of heat attributed to the convective power of the fire plume, the value being dependent on the choice of heat of

combustion, combustion efficiency and radiative fraction. The second was the boundary heat loss, which was shown to play an important role in a number of studies. Some justification in increasing the boundary heat losses was provided by the probable error in the thermal properties specified for mineral wool, where more realistic values reduce the thermal inertia by about 50%.

In contrast to *Part I*, the predictions from different numerical models for *Part II* varied to a greater extent. This is perhaps not surprising given the complexity of the fluid dynamics and the fact that measurements were not available against which to compare predictions. While the size of the building was a challenge to CFD models, it was the fluid dynamics associated with two vertical compartments connected by two hatches that provided the greatest test to all models. This was true, in particular, to case 1 where the upper deck was completely sealed.

For case 2 and case 3 of *Part II* the predicted maximum lower and upper deck temperatures were, from an 'engineering perspective', broadly similar for the different models. To some extent the differences between the predicted temperatures could be attributed to the different assumptions for the convective power of the fire source. It was apparent that the CFD models, and to a lesser extent the lumped parameter model, identified three-dimensional effects not within the scope of a zone model.

For case 1 the variation between models was more marked, in particular in respect to the upper deck temperature. The main cause of this discrepancy seems to be the treatment of the hatch flows. This is known to be a complex phenomenon for the zone models, both for single vent and multiple vent scenarios. However, there were discrepancies between the CFD models too, with differences in the predicted hatch flow mechanisms. Further development and validation in respect to the ability of all types of fire models to predict flows through horizontal hatch type openings seems to be required. By contrast, in terms of the pressure and oxygen consumption predictions, the differences between the various models were judged not to be significant.

While the general consensus was that cable and beam target damage would not have occurred, the predicted level of thermal hazard varied quite significantly between different models. This was a consequence of differences in gas phase conditions and also the modelling of the incident flux. The flux predictions, in particular, were in some instances quite varied, which will have directly influenced the surface and centre-line target temperatures for those models including these calculations. Here the agreement was in some instances reasonably close, and in others quite varied. The variation in predicted conditions at the human target was also quite significant.

As in the first benchmark exercise, the issue of the radiative fraction and effective heat of combustion seems to require further clarification. The difference in the predicted temperatures for the various models in *Part II*, and discrepancies with measurements in *Part I*, seems to have been due, in part at least, to assumptions made here.

Further development of suitable sub-models for predicting the thermal damage to target elements, in particular cables, cable bundles and cable trays, seems to be required. This follows on from the findings from the first benchmark exercise, and is a general issue rather than one specific to turbine hall type scenarios. The calculation of incident fluxes

is particularly important in predicting cable damage, and highlights the need to address the radiative heat transfer, both from the flaming region and the smoke layer, more carefully.

The usefulness in applying a combination of zone and CFD modelling to practical problems akin to those represented by the benchmark exercise was apparent. In particular, the zone model approach, while obviously more limited in its geometrical and scientific capabilities, provides a very useful tool for an initial scoping study. CFD can then be used for selected scenarios.

INTRODUCTION

The traditional, prescriptive, approach to fire regulation is based on engineering judgement derived from operating experience, tests, codes and standards. In a performance-based regulatory system, however, the fundamental premise is that the performance of a fire safety system can be predicted by calculation or modelling. This gives the fire protection system designer the potential for greater flexibility to implement cost-effective and innovative systems and the ability to determine the safety levels likely to be achieved in the event of a fire.

The calculation methods and numerical models used in performance-based design can be applied to nuclear power plants too. However, there are particular safety issues here, and this necessitates an evaluation of these tools prior to their subsequent use as part of fire risk assessments for nuclear power plants. These fire risk assessments would then form part of the overall probabilistic risk assessment for a nuclear power plant.

In October 1999 the U.S. Nuclear Regulatory Commission and the Society of Fire Protection Engineers organised a planning meeting with international experts and practitioners of fire models to discuss evaluation of numerical fire models for nuclear power plant applications [1]. Following this meeting an international collaborative project was set up with a view to sharing knowledge and resources from various organisations and to evaluate and improve the state of the fire modelling methods and tools for use in nuclear power plant fire safety.

An important component of the collaborative project is the undertaking of a series of benchmark exercises. Here predictions from a range of numerical fire models are being analysed, by comparing the results from different models, and also against experimental measurements.

Benchmark exercise # 1, involving a series of hypothetical scenarios to predict cable damage inside an emergency switchgear room, has been completed. A panel report [2] has been produced, describing the first benchmark exercise and summarising the findings, and include technical appendices from the individual participants. Due partly to the geometry of the room and the nature of the fire scenarios, the differences in the conclusions obtained using the various fire models were not judged significant. Target cable damage was predicted to be unlikely in nearly all scenarios (by all participants).

Benchmark exercise # 2 was designed to challenge fire models in respect to issues not addressed in the first exercise, e.g. effects of fire in a large volume representative of, say, a turbine hall. The full problem definition [3] was distributed to participants following discussions at the 4th (GRS, 17-18 October 2001) [4] and 5th (NIST, 2-3 May, 2002) [5] meetings of the international collaborative project, and contained details of the scenarios to be modelled. The exercise was divided into two parts. For the first part (*Part I*) there were experimental measurements of temperature against which model predictions were

compared. The second part (*Part II*) extended the scope of the exercise to examine the consequence of larger fires, but for which there were no experimental measurements to compare against.

Part I included three cases, based on a series of full-scale experiments inside the VTT Test Hall, which has dimensions 19 m high by 27 m long by 14 m wide (i.e. floor area 378 m²). Each case involved a single fire (2 - 4 MW), for which there were experimental measurements of gas temperature at three thermocouple trees and above the fire source. Although the height of a nuclear turbine hall (c. 25 m) is similar to that of the test hall, the floor area of a turbine hall (c. 3500 m²) is much greater than that of the test hall. However, the test hall was one of the largest enclosures for which fire test data was available. *Part II* included three additional cases for which experimental measurements did not exist. However, it extended the scope of the exercise to examine the effect of a bigger fire and a floor area representative of a real turbine hall. Furthermore, the likelihood of beam and cable damage was addressed.

Although most input parameters were defined in the problem specification, Benchmark exercise # 2 did involve a greater degree of user judgement compared to the first benchmark exercise. This applied, for example, to the treatment of the sloping roof (with zone models) in *Part I*.

This panel report includes a definition of the benchmark exercise, a summary of the results from the individual participants, an assessment of the main findings from the simulations and a set of technical appendices. For *Part I*, for which experimental measurements had been provided to the participants, a review of the main causes of discrepancy between prediction and measurement is provided. For *Part II*, for which there are no experimental measurements, a comparative review of the predictions from the various simulations is provided. While BRE has compiled the main body of the panel report, the technical appendices were provided by the individual participants, and describe in more detail the work undertaken with each of the fire models.

While the main body of the report summarises the benchmark exercise, the reader is encouraged to look at the technical appendices for in-depth analyses from the individual participants.

DEFINITION OF BENCHMARK EXERCISE # 2

Benchmark Exercise # 2 was divided into two parts. For the first part there were experimental measurements of temperature against which model predictions could be compared. The second part extended the scope of the exercise to examine the consequence of larger fires, but for which there were no experimental measurements to compare against.

Part I included three cases, based on a series of full-scale experiments inside a test hall with dimensions 19 m high by 27 m long by 14 m wide (i.e. floor area 378 m²). Each case involved a single fire (2 - 4 MW), and for which there are experimental measurements of gas temperature and doorway velocity. The height of a turbine hall within an NPP (c. 25 m) is similar to that of the test hall although it is acknowledged that the area of a turbine hall (c. 3500 m²) is much greater. However, the test hall is one of the largest enclosures for which fire test data is available for comparison with model predictions.

Part II included three additional cases for which experimental measurements did not exist, but it extended the scope of the benchmark exercise to examine the effect of a bigger fire and larger floor area representative of a hydrocarbon pool fire in a real turbine hall.

Part I – Large Hall Tests

Introduction

The three cases were based on a series of full-scale fire tests inside a large hall. In each case a pool of heptane burned for approximately five minutes, during which time gas temperatures were measured at three thermocouple columns and at two thermocouple locations directly above the fire source. In two cases the hall was nominally closed, while for the third case a mechanical extract system was operational and two 'doorway' openings were provided.

For each case, two or three tests were performed under nominally identical conditions. Performing repeat tests allowed the variation in measured values due to changing ambient conditions (and other factors) to be investigated. In all three cases the repeatability of the measurements was reasonably good. The mass release rate of fuel for each of the three cases given below is the average from the repeated tests for that case.

Geometry

Figure 1 shows the geometry of the hall, comprising a rectangular space with a pitched roof structure above. A Cartesian axis system is defined, with the origin as indicated. All dimensions are in metres. The four walls are labelled as *west* ($x=0$), *east* ($x=27$ m), *south* ($y=0$) and *north* ($y=13.8$ m). Here the *west* and *east* walls known collectively as the end walls and the *south* and *north* walls as the side walls.

In case 3 there were two open doorways, 0.8 m wide by 4 m high, one located in each end wall. Both doorways opened to the external ambient environment, and were located such that the centre was 9.3 m from the *south* wall ($y=9.3\text{ m}$). The doorway openings are labelled as the *west* doorway (door 1) and the *east* doorway (door 2).

Figure 2 shows the internal geometry of the test hall for Part I, including the location of the fire source. A single mechanical exhaust duct was located in the roof space, running along the centre y -plane. It had a circular section with a diameter 1 m , and opened horizontally to the hall at a distance 12 m from the floor and 10.5 m from the *west* wall ($x=10.5\text{ m}$). Figure 2 also shows the location and dimensions of two obstructions that were present inside the hall during the experiments and may have influenced the internal air movement. If included in simulations, it was suggested that these should be treated as simple rectangular obstructions. The small circles indicate the location of the thermocouples and velocity probes, discussed below. Figures 3, 4 and 5 contain plan, side and end views of the hall respectively.

Participants were left to decide for themselves how to incorporate the roof geometry, and if appropriate were encouraged to undertake a series of simulations using alternate strategies, and to comment on the findings.

Material properties

The walls and ceiling consisted of a 1 mm (0.001 m) layer of sheet metal on top of a 0.05 m layer of mineral wool. The floor was constructed from concrete. Table 1 presents the thermal properties of the sheet metal, mineral wool and concrete materials.

Table 1 Material properties for *Part I*

Material	Thermal properties		
	conductivity ($J\text{ s}^{-1}\text{ m}^{-1}\text{ K}^{-1}$)	density ($kg\text{ m}^{-3}$)	specific heat ($J\text{ kg}^{-1}\text{ K}^{-1}$)
metal sheet	54	7850	425
mineral wool	0.2 *	500 *	150 *
concrete	2	2300	900

* See note in Results section

If included by the participant, the internal obstructions could be modelled as concrete (properties as given in Table 1). However, as the choice of material properties for the internal obstructions was not likely to have an important bearing on the numerical predictions, the obstructions could optionally be treated as adiabatic, i.e. no heat transfer.

All surfaces were assumed to have an emissivity of 0.95, i.e. almost black body, and a convective heat transfer coefficient of $10\text{ J s}^{-1}\text{ m}^{-2}\text{ K}^{-1}$.

Ambient conditions

Ambient pressure and temperature were 101300 N m^{-2} and $20\text{ }^{\circ}\text{C}$ respectively.

Ventilation conditions

Mechanical exhaust ventilation was operational for one case, with a constant volume flowrate of $11 \text{ m}^3 \text{ s}^{-1}$ drawn through the 1 m diameter exhaust duct. For this case there were two doorway openings as described above.

For the other two cases the mechanical exhaust system was not used, and the doors were closed. Ventilation was restricted to infiltration through the building envelope. Exact information on air infiltration during these tests was not available. However, following discussions with the scientists involved in the experiments, it was recommended that air infiltration be modelled by including four small, square openings to the outside ambient environment, each opening having an area 0.5 m^2 . For the purpose of the benchmark exercise it was suggested that two openings be located in the *east* wall, one at floor level and 12 m above the floor, and two at the opposite end of the hall in the *west* wall. Table 2 shows the co-ordinates of the centre of the four openings.

Note that air infiltration was to be ignored in the two cases with mechanical ventilation and doors open.

Table 2 Openings to simulate effect of air infiltration in *Part I*

Opening ($0.707\text{m} \times 0.707\text{m}$)	Co-ordinates of centre		
	x (m)	y (m)	z (m)
1	0	6.9	0.354
2	0	6.9	12
3	27	6.9	0.354
4	27	6.9	12

Fire Source

A single fire source was used in each test, its centre located 16 m from the *west* wall and 7.2 m from the south wall ($x=16 \text{ m}$, $y=7.2 \text{ m}$) as indicated in Figure 2. For all tests heptane was burned on top of water in a circular, steel tray. The fuel surface was 1 m above the floor. Two tray diameters were used, 1.17 m for *case 1* and 1.6 m for the other two. The trays were placed on load cells, and the mass release rate then calculated from the time derivative of the load cell weight readings.

For the three cases defined below the fuel mass release rate (dm_f/dt) was provided as an input parameter. The choice of combustion mechanism was left to the participant. However, it was suggested that the fuel rate of heat release be modelled as

$$\frac{dQ_f}{dt} = c \frac{dm_f}{dt} \Delta H_c \quad (1)$$

Here the heat of combustion (DH_c) was defined as $44.6 \times 10^6 \text{ J kg}^{-1}$. The benchmark specification suggested that the parameter c represent either a combustion efficiency or a radiative fraction, taking a recommended value of 0.8. Following the activities of the benchmark exercise, and discussions at the 7th meeting of the collaborative project [8], the terms effective heat of combustion, combustion efficiency, radiative fraction etc have been rationalised for purpose of the project. A summary is provided in a separate section later in this report.

For the purpose of the benchmark exercise, it was suggested that, as in the first benchmark exercise, a value of 12% be assigned to the lower oxygen limit parameter in those combustion models that make use of it. However, participants were encouraged to investigate other values if they believed this to be important.

Instrumentation

Data was obtained from the instrumentation described below, against which numerical predictions could be compared:

1. Three vertical thermocouple trees, located as shown in Figure 6, on the centre y -plane at distances 1.5 m , 6.5 m and 20.5 m from the west wall. The vertical distribution of thermocouples, the same for all three trees, is shown in Figure 7. Individual thermocouples are labelled as shown in Figure 7, where $T2.5$, for example, refers to the fifth thermocouple on tree number 2. Each thermocouple was a 0.1 mm K-type. Note that the readings from these thermocouples were used to calculate a layer height and upper layer temperature as described below.
2. Two horizontal thermocouple grids centred directly above the fire source at a height of 7 m and 13 m . Both grids consisted of nine 0.5 mm K-type thermocouples arranged in a 3 by 3 array. However, for the benchmark exercise attention is focussed only at the centre thermocouple at each height, directly above the centre of the fire tray. These are labelled as $TG.1$ and $TG.2$ in Figure 7.

Two-layer data reduction

A two-layer zone model will predict upper and lower layer properties, and the height of the interface separating the layers. Therefore, to make comparisons between experimental measurements and zone model predictions, the thermocouple data must be reduced in some way.

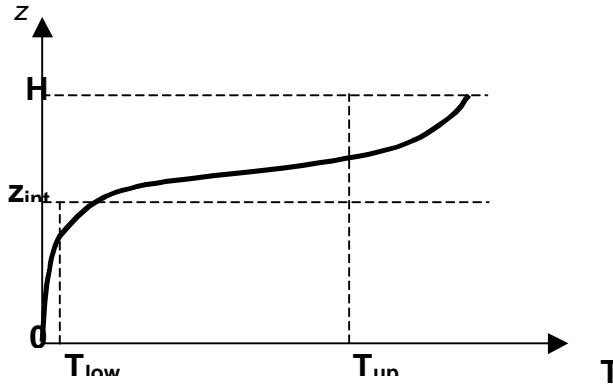
Participants were provided with the measurement data for all thermocouple locations, and were free to make their own data reduction to generate upper/lower layer and interface height 'measurements'. However, the method described below was provided as a 'baseline' method, and the resultant layer values were provided together with the 'raw' measurement data.

Furthermore, participants using CFD and network models were invited to calculate 'upper layer' and 'lower layer' temperatures and an 'interface height' for comparison against zone model predictions. For consistency, the method described below, based on predictions of temperature at the thermocouple tree locations, was recommended. However, if they wished, participants could use their own method for calculating 'upper layer' and 'lower layer' temperatures and an 'interface height'.

Layer temperature and interface calculation

The one-dimensional analytical method presented here allows an upper layer temperature (T_{up}), lower layer temperature (T_{low}) and interface height (z_{int}) to be calculated given a discrete set of temperatures (T_i) at heights above floor level (z_i), $i=1,N$.

Consider a continuous function $T(z)$ defining temperature as a function of height z , from 0 (floor level) to H (ceiling).



Then, from the zone model concept and the conservation of mass, we may write

$$(H - z_{int})T_{up} + z_{int}T_{low} = \int_0^H T(z)dz = I_1 \quad (2)$$

$$(H - z_{int})\frac{1}{T_{up}} + z_{int}\frac{1}{T_{low}} = \int_0^H \frac{1}{T(z)} dz = I_2 \quad (3)$$

Algebra then gives

$$z_{int} = \frac{T_{low}(I_1 I_2 - H^2)}{I_1 + I_2 T_{low}^2 - 2T_{low}H} \quad (4)$$

Here, T_{low} is taken as the temperature at the lowest discrete measurement location (T_1) and I_1, I_2 are calculated from the discrete data set using a quadrature rule, e.g. Simpsons Rule. T_{up} is then calculated by applying the mean value theorem over the interval $z=z_{int}$ to $z=H$

$$T_{up} = \frac{1}{H - z_{int}} \int_{z_{int}}^H T(z)dz \quad (5)$$

In reducing the thermocouple tree data it was proposed that the average of the three values (one from each tree) be taken at each distance above the floor.

Exercises

The three cases to be simulated are summarised below. Details of geometry, material properties, ambient conditions, ventilation rates and instrumentation are as defined above. The specifications given here represent the 'baseline' scenarios. Participants were invited to study variations on these cases in order to gain insight into the performance of the fire models used. However, the three 'baseline' cases were given priority, and furthermore *case 1* was given highest priority.

The fire source was to be taken as pure heptane, located as described above. For *case 1* the pool diameter was *1.17 m* while for *cases 2* and *3* it was *1.6 m*. Table 3 defines the fuel mass release rate for each case at discrete times in minutes. A piecewise linear polynomial was to be assumed, i.e. linear interpolation between the points.

Table 3 Fuel mass release rates for Part I

Case 1		Case 2		Case 3	
<i>t (min)</i>	<i>dm/dt (kg s⁻¹)</i>	<i>t (min)</i>	<i>dm/dt (kg s⁻¹)</i>	<i>t (min)</i>	<i>dm/dt (kg s⁻¹)</i>
0	0	0	0	0	0
0.22	0.033	0.23	0.057	0.22	0.064
1.5	0.045	0.5	0.067	1.05	0.084
4.8	0.049	1.52	0.081	2.77	0.095
5.45	0.047	3.22	0.086	4.27	0.096
6.82	0.036	4.7	0.083	4.87	0.091
7.3	0	5.67	0.072	5.5	0.07
		6.2	0.06	5.75	0
		6.58	0		

Table 4 summarises the ventilation conditions for the three cases. Natural leakage was to be modelled as described above. Each case was to be modelled for the duration of the fire, assuming the fire to have stopped after the last entry in Table 3, i.e. 7.5 minutes of *case 1*, 7 minutes for *case 2* and 6 minutes for *case 3*.

Table 4 Ventilation conditions for Part I

Case 1	Case 2	Case 3
doors closed	doors closed	doors open (0.8 m x 4m)
no mech. exhaust	no mech. exhaust	mech. exhaust ($11 \text{ m}^3 \text{ s}^{-1}$)
natural leakage	natural leakage	ignore natural leakage

Reporting procedure

Participants were requested to submit data in either a text file or Excel spreadsheet, and also summarise their findings and modelling assumptions. SI units were to be used throughout ($^{\circ}\text{C}$ or K for temperature).

It was suggested that results be reported at 10-second intervals. However, this was a guideline only and not a formal requirement (sufficient points to produce representative graphs is the minimum requirement).

Table 5 includes a list of suggested variables to be reported for zone and CFD models (acknowledging that for network models the number of reported variables will be somewhere in between). If a fire model did not output a particular variable, then the participant should ignore it. The number of variables to be reported depended in part on the fire model, with CFD models allowing for a greater number of outputs. Participants were free to include other variables that they considered important.

In addition to the tabulated results, participants were asked to summarise the main modelling assumptions and inputs used. This would include a short summary on the following topics at least (approximately one paragraph on each topic):

- § Heat release (combustion) mechanism. This could be a combustion model or a simple heat release source term. Issues such as the lower oxygen limit should be reported.
- § Radiation treatment (if included). Important issues may include the treatment radiation transfer to solid surfaces, the absorption/emission in the gas phase and radiation from soot in the plume.
- § The zonal approximations used and main empirical correlations (in the case of a zone model).
- § The number of control volumes or elements (in the case of a CFD model), or equivalently the number of network elements (in the case of a network model).
- § The turbulence model (in the case of a CFD model).
- § Roof geometry assumptions (this relates mainly to zone models).

Table 5 **Reported variables for *Part I***

Zone	CFD
<p>Heat release rate of fire</p> <p>Interface height</p> <p>Upper layer temperature</p> <p>Infiltration flow rate (cases 1 & 2)</p> <p>Mass flow rate in/out door 1 (case 3)</p> <p>Mass flow rate in/out door 2 (case 3)</p> <p>Total heat loss rate to solid boundaries</p> <p>Heat loss through mech. exhaust (case 3)</p> <p>Plume temperature</p>	<p>Temperatures at thermocouple trees (T1.1,...,T1.10,T2.1,...,T2.10,T3.1,...,T3.10)</p> <p>Temperatures at plume thermocouples (TG1.1 & TG.2)</p> <p>Infiltration flow rate (cases 1 & 2)</p> <p>Mass flow rate in/out door 1 (case 3)</p> <p>Mass flow rate in/out door 2 (case 3)</p> <p>Total heat loss rate to solid boundaries</p> <p>Heat loss through mech. exhaust (case 3)</p> <p>Interface height (using reduction of thermocouple tree data)</p> <p>Upper layer temperature (using reduction of thermocouple tree data)</p> <p>Total heat release rate (within whole hall)</p>

Part II – Extended NPP Scenarios

Introduction

Part II was added as an optional extension to the benchmark exercise. It included three scenario cases (*case 1, 2 & 3*) set inside a rectangular building with dimensions comparable to those of a real turbine hall. The fire size was chosen to produce temperatures that might be capable of damaging equipment or cables. Targets were added to *Part II* to allow the onset of damage to be studied.

Geometry

Figure 8 shows the dimensions of the building. As shown in Figure 9, the building was divided into two levels (decks) connected by two permanent openings (hatches). Although many turbine halls contain three decks, it was decided that modelling two decks was sufficient for the benchmark exercise. Figure 10 shows the exact location of the internal ceiling and the two open hatches (each 10 m by 5 m in size).

Material properties

The floor, lower walls (lower deck) and internal ceiling (separating the two decks) were constructed from concrete, with thermal properties as given in Table 1, and a thickness of 0.15 m . The upper walls (upper deck) and ceiling were constructed from steel, which for the benchmark exercise was to be modelled simply as sheet metal of thickness 0.002 m and with thermal properties as given in Table 1 ('metal sheet'). For both materials an emissivity of 0.95 and a convective heat transfer coefficient of $10\text{ J s}^{-1}\text{ m}^{-2}\text{ K}^{-1}$ were assumed.

Ambient conditions

As specified for *Part I*.

Ventilation conditions

Cases 1, 2, and 3 had different ventilation conditions, covering 'nearly-sealed' conditions, natural ventilation conditions and a combination of natural and mechanical ventilation.

For *case 1* the hall was 'nearly-sealed', with two 'infiltration' openings each of dimension $1\text{ m} \times 1\text{ m}$. Both openings were located at floor level on the lower deck. One was in the west wall, with its centre located at co-ordinates ($x = 0, y = 25, z = 0.5$), and the other was in the east wall at co-ordinates ($x = 100, y = 25, z = 0.5$).

Case 2 included natural ventilation. It was assumed for the benchmark exercise that the complete set of smoke exhaust vents at roof level was open for the full duration of the scenario. There were 36 smoke exhaust roof vents at roof level (upper deck), each with dimensions 3 m (x direction) by 1.5 m (y direction). The roof vents were arranged symmetrically in a 9 by 4 array in the x - y directions with a 10 m spacing between the centre of the vents (in each direction). There was thus a distance of 10 m between the centre of the outer vents and the edge of the roof.

For case 2 there was a complimentary set of 24 'make-up' vents in the side walls, each with dimensions of $2\text{ m} \times 2\text{ m}$, again assumed to be open for the full duration of the scenario. There were 12 vents located at floor level on the lower deck and 12 at floor level on the upper deck (just above the internal ceiling), i.e. the centre of the vents are located at $z = 1\text{ m}$ and $z = 11\text{ m}$ respectively. The 12 vents (at each deck) were distributed around the building with two vents in each of the *west* and *east* walls and four vents in each of the *south* and *north* walls. In each wall (at each deck) a distance of 20 m separated the centre of the vents. Hence there was a distance of 20 m from the centre of the outer most vents to the edge of the *south* and *north* walls, and a corresponding distance of 15 m to the edge of the *west* and *east* walls.

Case 3 was a variation on case 2, with the 36 roof level smoke exhaust vents replaced by a set of 36 mechanical vents, each with dimensions of $1\text{ m} \times 1\text{ m}$. The centres of the mechanical vents were at the same locations as those of the natural smoke exhaust vents in case 2. For case 3 it was assumed that a fixed total mechanical extraction rate of $194.4\text{ m}^3\text{ s}^{-1}$ was maintained for the full duration of the scenario (corresponding to 7 air-changes-per-hour). The individual mechanical extraction rate for each vent was $5.4\text{ m}^3\text{ s}^{-1}$. For the purpose of the benchmark exercise, it was assumed that the make-up air was supplied by natural ventilation openings in the four walls. For case 3 the same 24 natural ventilation wall openings were to be considered as for case 2.

Fire source

For all three cases, the fire source was assumed to be lube oil burning in a dike (tray) with dimension 7 m by 7 m , located at the centre of the lower deck. It was assumed that the surface of the fuel was 1 m above the floor.

The mass release rate of the pool fire (dm_f/dt) grows from zero to a steady value 1.66 kg s^{-1} as follows,

$$\frac{dm_f}{dt} = at^2 \quad (6)$$

Here t is the time in seconds from the start of the fire, and a is a constant with a value $4.611 \times 10^{-6}\text{ kg s}^{-3}$. This value gives a growth rate akin to an NFPA ultra fast t-squared growing fire. Equation (6) defined the mass release rate for the first 10 minutes, at which time it reaches the steady value 1.66 kg s^{-1} which was maintained for the next 10 minutes (giving 20 minutes total duration). It was assumed that the fuel surface covered the complete area of the 7 m by 7 m dyke for its full duration, i.e. the mass release rate per unit area increases according to the same function as in equation (6).

The chemical and thermal properties for the combustion of lube oil [6] are summarised in Table 6.

Table 6 Chemical properties for lube oil

Heat of combustion (DH_c) (J kg^{-1})	H/C mass ratio	Soot yield ($\text{kg soot}/\text{CO}_2/\text{CO per kg fuel burned}$)	CO_2 yield	CO yield
	(-)	(-)	(-)	(-)
4.235×10^7	0.17	0.059	2.64	0.019

Energy was released according to equation (7).

$$\frac{dQ}{dt} = \frac{dm_f}{dt} \Delta H_c \quad (7)$$

It could be assumed that the fraction of heat converted to radiation in the fire plume is 0.51 [6]. Furthermore, where appropriate, participants could assume a lower oxygen limit of 12%. However, participants were free to model radiation and oxygen limitation as they saw fit.

Targets

To make *Part II* relevant to practical applications, three cable targets were introduced, similar to the first benchmark exercise. Each cable was a 50 mm (0.05 m) diameter power cable, assumed to consist entirely of PVC. The thermal properties of the cable material were the same as in the first benchmark exercise, repeated below in Table 7. As for the first benchmark exercise, participants could assume the onset of cable damage when the centre-line temperature reached 200 °C.

Table 7 Material properties for cable targets

conductivity ($J s^{-1} m^{-1} K^{-1}$)	density ($kg m^{-3}$)	specific heat ($J kg^{-1} K^{-1}$)	emissivity	convective htc ($J s^{-1} m^{-2} K^{-1}$)
0.092	1710	1040	0.8	10

Two structural 'beam' targets were also included. To simplify the modelling, each 'beam' was approximated as a horizontally orientated rectangular slab of steel with cross-sectional dimensions of 0.15 m wide (x co-ordinate direction) and 0.006 m thick (z co-ordinate direction). Table 8 shows the material properties for the 'beam' targets, where the conductivity, density and specific heat correspond to steel (0.5% carbon) at 20°C. It was assumed for the purpose of this exercise that property values were temperature independent. A damage temperature of 538 °C was assumed.

Table 8 Material properties for 'beam' targets

conductivity ($J s^{-1} m^{-1} K^{-1}$)	density ($kg m^{-3}$)	specific heat ($J kg^{-1} K^{-1}$)	emissivity	convective htc ($J s^{-1} m^{-2} K^{-1}$)
54	7833	465	0.8	10

Figure 11 shows the locations of the three cable targets and the two 'beam' targets. The cables extended the full length of the hall (x direction), and the 'beam' targets extended the full width (y direction). The centre-lines of the three cables were 1 m from the south wall, and 9 m, 15 m and 19 m above the floor of the lower deck respectively. The 'beam' targets were located half-way along the length of the hall ($x = 50 m$). The centre-line of one 'beam' was 0.5 m below the ceiling of the lower deck (the internal ceiling), and the second 'beam' was 0.5 m below the ceiling of the upper deck (the roof).

Additionally, there was a 'human target', located 1.5 m above floor level (the internal ceiling) at the centre of the upper deck, i.e. at co-ordinates ($x = 50$, $y = 25$, $z = 11.5$). Only gas properties and incident heat fluxes were considered here.

Summary of exercise cases

The three cases to be simulated in *Part II* are summarised below in Table 9. Each case lasted for 20 minutes, or until the participant decided there was no need to proceed further, e.g. the cables and 'beams' are damaged. The full details of the location and size of the natural and mechanical ventilation openings are provided in the section on ventilation conditions above.

Table 9 Summary of cases for *Part II*

Case 1	Case 2
Nearly-sealed. Two 1 m x 1 m openings.	Natural ventilation. 36 roof vents. 24 make-up wall vents.
Case 3	
Mechanical (extract) and natural ventilation. $194.4 \text{ m}^3 \text{ s}^{-1}$ mechanical exhaust ventilation (divided evenly between 36 roof vents) 24 make-up wall vents.	

Reporting procedure

Table 10 summarises the main variables to be reported for zone and CFD models, where again for network (or lumped parameter) models the list would be somewhere between the two. As for *Part I*, participants were to exercise their own judgement whether to omit any variables or include additional ones. But as a core requirement, participants were to report gas layer temperatures for zone models and discrete location gas temperatures for CFD models.

Where zone models treated the hall as two compartments, participants were to report layer temperatures, heights etc. individually for the two decks.

CFD models were to report gas temperature and oxygen concentration at discrete locations at three columns of 'virtual thermocouples', shown in Figure 11 as $T1$, $T2$ and $T3$. The discrete locations at each column were separated by 1 m height intervals, labelled as $T1.1 - T1.19$, $T2.1 - T2.19$ and $T3.1 - T3.19$, where $T1.1$ was at a height of 1 m, $T1.2$ at 2 m etc. No values were required at locations $T1.10$ and $T2.10$ because of the presence of the internal ceiling. As for *Part I*, participants could optionally calculate layer heights and layer temperatures equivalent to those generated by zone models.

The maximum target values refer to the maximum along the length of the cable or 'beam'. If they wished, participants could provide the values simply at the mid-point (i.e. at $x=50\text{ m}$ for the cables and $y=25\text{ m}$ for the 'beams'). Oxygen concentration was to be expressed preferably as a volume fraction (however, mass fraction was acceptable). Soot concentration was to be expressed preferably as kg m^{-3} .

As for *Part I*, participants were asked to summarise the main modelling assumptions and inputs used.

Table 10 **Reported variables for *Part II***

Zone	CFD
Heat release rate of fire	Gas temperature at 'virtual thermocouple locations' (T1.1,...,T1.19,T2.1,...,T2.19,T3.1,...,T3.19)
Interface height	Oxygen concentration at 'virtual thermocouple locations'
Upper layer temperature	Mass flow rate in/out natural vents
Lower layer temperature	Mass flow rate through individual hatches
Upper layer oxygen concentration	Heat flow rate through individual hatches
Lower layer concentration	Total heat loss rate to solid boundaries
Upper layer 'smoke' concentration	Gas temperature above fire (x=50, y=25, z=9)
Lower level 'smoke' concentration	Mean pressure inside hall
Mass flow rate in/out natural vents	Maximum incident heat flux on targets
Mass flow rate through hatches	Maximum surface temperature of targets
Heat flow rate through hatches	Maximum centre-line temperature of targets
Total heat loss rate to solid boundaries	Incident heat flux at 'human target'
Plume temperature	Gas temperature at 'human target'
Mean pressure inside hall	Oxygen concentration at 'human target'
Maximum incident heat flux on targets	Smoke concentration at 'human target'
Maximum surface temperature of targets	
Maximum centre-line temperature of targets	
Incident heat flux at 'human target'	

RESULTS OF ANALYSES

Part I – Large Hall Tests

Summary of results

Table 11 lists the participants for *Part I*, showing the fire models used and the particular cases investigated. Also indicated is whether details of the work has been included in a separate appendix, supplied by the participant and included as part of this report. Where an appendix has not been supplied, information has been taken from presentation material provided at the 5th (NIST) [5] and 6th (BRE) [7] project meetings.

Table 11 Participant contributions for *Part I*

Participant	Fire model	Cases investigated	Appendix
K McGrattan (NIST)	FDS (CFD)	1, 2 & 3	A
D Roubineau (IRSN)	Flamme_S (zone)	1, 2 & 3	B
W Klein-Heßling (GRS)	COCOSYS (lumped parameter)	1, 2 & 3	C
M Heitsch (GRS)	CFX-4 (CFD)	1, 2 & 3	E
L Gay & B Gautier (EDF)	MAGIC (zone)	1, 2 & 3	D
D Joyeux & O Lecoq-Jammes (CTICM)	MAGIC (zone)	1, 2 & 3	G
S Miles (BRE)	CFAST (zone)	1, 2 & 3	H
	JASMINE (CFD)	1, 2 & 3	H
A Martin & D Coutts (WSMS)	CFAST (zone)	1, 2 & 3	-
B Malinovic & M Plys (Fauske)	HADCRT (lumped parameter)	1, 2 & 3	-
J Will (HPP Braunschweig)	Kobra3D (CFD)	1, 2 & 3	I
WPI class exercise	CFAST (zone)	1, 2 & 3	-
	JASMINE (CFD)	1	-
	FDS (CFD)	1	-

Measured temperatures, at each thermocouple location, were provided to participants at the start of the exercise. Derived upper and lower layer information, using the data reduction method presented in the specification, was provided also. Figure 12 shows the derived upper and lower layer temperature, and Figure 13 shows the interface height. Figure 14 shows the temperature measured at the two plume locations, 7 m and 13 m above the floor.

A short summary of each participant's individual work is provided below, followed by an overview of the findings of the collected studies and a discussion of the main issues raised. The reader is referred to the appendices for full details of each participant's work. Furthermore, technical descriptions of the fire models were provided previously in the report for the first benchmark exercise [2].

A note is made here to a probable 'error' in the thermal properties for mineral wool in Table 1 of the problem specification, which was not highlighted until May 2003. Rather than respective values of conductivity (k), density (ρ) and specific heat (c) of $0.2 \text{ J s}^{-1} \text{ m}^{-1} \text{ K}^{-1}$, 500 kg m^{-3} and $150 \text{ J kg}^{-1} \text{ K}^{-1}$, more realistic values may have been $0.04 \text{ J s}^{-1} \text{ m}^{-1} \text{ K}^{-1}$, 160 kg m^{-3} and $1150 \text{ J kg}^{-1} \text{ K}^{-1}$ respectively. The important point is that the thermal inertia ($k\rho c$) would then have been in the region $7400 \text{ J}^2 \text{ s}^{-1} \text{ m}^{-4} \text{ K}^{-2}$ compared to $15000 \text{ J}^2 \text{ s}^{-1} \text{ m}^{-4} \text{ K}^{-2}$ using the specified values, and the computed heat losses to the walls and ceiling would generally have been greater.

At the 7th meeting of the collaborative project the issue of the definition of effective heat of combustion, combustion efficiency and radiative fraction was discussed. Benchmark exercise 2 had re-iterated the conclusion that there was some confusion about the definition of these terms. At the meeting an agreed set of definitions was established for future use in the project, and this is summarised in a later section of this report.

K McGrattan (NIST) - using FDS (CFD)

Simulations of the three cases were made with FDS version 2 using the multiblock feature. A total of approximately 200,000 cells were used, with a finer grid at the fire plume (13 cm size). While heptane combustion was modelled using the mixture fraction method, radiation was included by reducing the fire heat release rate by 35%. Boundary heat loss was calculated using a one-dimensional heat conduction sub-model. As FDS uses a Cartesian grid, the sloping roof was approximated by a 'staircase' geometry, with the vorticity term deactivated at the bounding fluid cells.

Good agreement between predicted and measured temperatures was obtained for all three cases, with comparisons made at all thermocouple locations. This was attributed to the correct modelling of the air entrainment process. Figure 15 illustrates the comparison for case 2 at thermocouple tree 2.

D Roubineau (IRSN) - using Flamme S (zone)

Simulations were performed assuming a flat ceiling such that the volume of the hall was conserved. It was concluded that the obstructions were not important. Furthermore, results indicated that the presence, or absence, of the small infiltration openings was not

important in respect to the predicted layer temperature and height, but did have a significant bearing on pressure. At the temperatures found in the benchmark exercise, it was concluded that soot radiation was not important, and the use of a combustion efficiency of 80% was appropriate in determining the convective heat release.

A main observation of this work was that the choice of data reduction method (to obtain layer temperature and height from the measured profiles) was important, with different approaches yielding quite different results. Here, Flamme_S predictions were closer to the layer values derived using Quintiere's method (specified in the benchmark specification) than those derived by Audouin's method, although it is suggested that the latter provides a more realistic interpretation of the experiments. Figures 16 and 17 compare Flamme_S predictions against the measured data using the two data reduction methods.

W Klein-Heßling (GRS) - using COCOSYS (lumped parameter)

Using approximately 600 zones, it was possible to allocate an individual node to each thermocouple location. Figure 18 illustrates the nodalisation of the test hall. Satisfactory agreement between predicted and measured temperatures, at thermocouple trees T1 to T3, was achieved once the level combustion (heat release) at the source was reduced. This was implemented by reducing the combustion efficiency parameter to 60% at the source, while still allowing >60% of the fuel to burn in the whole domain. Figure 19 illustrates the results then achieved for case 2, at thermocouple column T2.

An investigation into the effect of varying the location of the infiltration openings for case 1 and case 2 showed that this had little effect on the results. Modifying the thermal properties of the boundaries had some influence, but not as much as the change to the effective heat of combustion. Predicted values for smoke layer height, using the data reduction method proposed in the benchmark specification, were lower than those derived from the measurement data.

M Heitsch (GRS) - using CFX-4 (CFD)

All three cases were modelled with CFX-4.4 using approximately 40,000 control volumes for most of the simulations (illustrated in Figure 20). A limited grid resolution study for case 1 indicated little change in the predicted values with the finer mesh. The main physical models employed in the simulations included an eddy break-up combustion model, a Monte Carlo radiation model and either the standard κ - ϵ or RNG κ - ϵ turbulence model.

Reasonable agreement between predicted and measured temperatures at the three thermocouple trees was achieved once the amount of heat lost to radiation inside the plume was increased. This was equivalent to decreasing the effective (convective) combustion efficiency from 80% to 66%. Figure 21 illustrates the results then obtained for case 2. There was still, however, a tendency to predict higher temperatures than those measured in the experiments. This was most pronounced at the fire plume.

For case 3, it was found to be necessary to extend the computational domain beyond the two doorways in order to obtain realistic behaviour.

L Gay & B Gautier (EDF) - MAGIC (zone)

Simulations of all three cases were made using MAGIC V3.4.8. Sub-models included the McCaffrey plume and Cooper ceiling jet correlations, and a one-dimensional heat conduction into multi-layer walls. The wall convective heat transfer coefficient was fixed at $15 \text{ W m}^{-2} \text{ K}^{-1}$. The geometry of the test hall was approximated by a parallelepiped with the same floor area and volume as the hall.

Using the fire source and solid boundary parameters as suggested in the benchmark specification, reasonable agreement between predicted and measured upper layer temperatures were obtained. Generally, the predicted upper layer temperature was modestly greater than the value derived from the measurement data, and the layer height lower. Figure 22 shows the predicted layer temperatures for case 2, and Figure 23 the layer height.

D Joyeux & O Lecoq-Jammes (CTICM) - using MAGIC (zone)

Simulations of all three cases were made using MAGIC V3.4.8. In addition to the combustion efficiency of 0.8, a radiative fraction of 0.2 was applied at the fire source (so that the overall convective component of the complete heat of combustion was reduced to 0.6). Consequently, the predicted upper layer temperatures are lower than those obtained by Gay and Gautier using the same fire model. Figures 24 and 25 present the predicted layer temperatures and height for case 2. While reducing the convective heat release rate of the fire has reduced the upper layer temperature, the influence on the layer height is minimal.

S Miles (BRE) - using CFAST (zone)

CFAST was used in conjunction with the FAST graphical user interface (version 3.1.6). As with other participants using zone models, the (flat) ceiling height was set to conserve the volume of the hall. A sensitivity study into the effect of varying the ceiling height was conducted. Other parameters varied as part of the sensitivity analysis included the radiative fraction, the thermal properties of the walls and ceiling, and the size and location (height) of the 'infiltration openings' for case 1 and case 2. A convective heat transfer coefficient of $10 \text{ W m}^{-2} \text{ K}^{-1}$ was used in all simulations.

Reasonable agreement between predicted and measured upper layer temperatures were achieved following a reduction in the convective power of the fire source, by increasing the radiative fraction from 0.2 to 0.4. Figure 26 shows results for case 2, which indicates also that the upper layer temperature is sensitive to the 'flat ceiling' height but not the details of the 'infiltration openings'. As indicated in Figure 27, agreement between measured and calculated layer height was not as close.

S Miles (BRE) - using JASMINE (CFD)

CFD simulations of all three cases were performed with JASMINE version 3.2.1. The geometry, including an extension beyond the wall openings, was modelled with approximately 130,000 Cartesian grid cells, with the sloping ceiling approximated as a staggered ('staircase') surface. The main sub-models included an eddy break-up combustion model, a six-flux radiation model and the standard κ - ϵ turbulence model. Radiative exchange from the fire plume and smoke layer due to CO₂ and H₂O was modelled, but not soot, for which the effect was included in the combustion efficiency term. A fixed convective heat transfer coefficient of 10 W m⁻² K⁻¹ was employed. Some parametric simulations were performed with increased heat losses to the boundaries.

Figure 28 illustrates the JASMINE predictions at three thermocouple locations in tree 2 for case 1. It was found that with the benchmark specification the predicted temperatures in the smoke layer were notably higher than those measured. By increasing the boundary heat losses a reasonable agreement could be attained. A detailed examination of the amount of heat transferred to the walls and ceiling showed that this was, in all cases, a significant proportion of the heat released by the fire. In the simulations with the increased boundary heat losses the proportion rose to approximately two-thirds in the later stages of the fire.

A Martin & D Coutts (WSMS) - using CFAST (zone)

This contribution was particularly useful as it was performed 'blind' without access to the experimental data. CFAST/FAST version 3.1.6 was used in simulating the three cases. As with other zone model applications, a flat ceiling approximation was used such that the volume of the hall was conserved. Predictions for upper layer temperature and layer height were in line with other zone modellers, i.e. a moderate 'over-prediction' of smoke layer temperature compared to measurement and a layer height closer to the floor.

B Malinovic & M Plys (Fauske) - HADCRT (lumped parameter)

In contrast to the COCOSYS simulations, relatively few 'junctions' were employed and so the modelling was perhaps more akin to that of a zone model. Consequently, simulations took only a few minutes. The upper layer temperature predictions were reasonably close to the experimental values (a 'modest' over-prediction in case 1 and case 2), but the layer was predicted to descend closer to the floor. Although radiation had been ignored in the simulations reported, about 20 to 25 % of the heat was transferred to the boundaries (by convection).

It was suggested that a parametric analysis of the effect of varying the size and location of the infiltration openings for case 1 and 2 be performed, as this may be important. In particular, it may influence the lower layer temperature.

J Will (HPP Braunschweig) - using Kobra3D (CFD)

Kobra3D versions 4.7e and 4.7.1 (demo version) were used in simulating all three cases. A fairly fine grid containing approximately 250,000 cells was employed. A volumetric heat

source represented the fire, where the height of the heat releasing volume was defined by an empirical correlation. For case 1 the combustion efficiency was varied between 0.8 and 1. In addition, the area of the fire source was extended to obtain a more realistic fire plume. The influence of boundary heat loss was investigated by assuming walls were made either of metal or mineral wool. Based on the results of case 1 the boundary conditions for case 2 and case 3 were chosen and the calculations were conducted without further parameter variations.

In all three cases the predicted hot gas layer temperatures were significantly larger than those measured. Furthermore, the predicted depth of the hot gas layer was smaller than that observed. These effects have been observed in applications of Kobra3D to comparable scenarios, and it is concluded that it seems to be difficult to get plausible results where there are small fires in large compartments. It is suggested that this problem might be due to the missing friction and turbulence terms in the equation set solved in Kobra3D.

WPI (class exercise) - using CFAST (zone), JASMINE (CFD) and FDS (CFD)

Nine students studying performance based fire design at Worcester Polytechnic Institute undertook simulations as part of a class exercise. Prior to the exercise they had only had limited experience of zone models, and none had any CFD experience. With all three models the students had found the sloping roof a challenge. For the zone model (CFAST) an equivalent flat ceiling had been specified. For both CFD models they had found setting up the sloping roof to be time consuming.

Two options had been investigated for setting the height of the equivalent flat ceiling in CFAST; conserving the enclosure volume and conserving the enclosure surface area. However, it was found that the choice had no significant effect on the results. The students had been unsuccessful in specifying mechanical exhaust ventilation for case 3.

Predictions for gas temperature were considered to appear reasonable for all models. Given that they had used the models with little, or no, prior fire modelling experience and were left in the main unsupervised, the outcome of the exercise was quite promising. However, the students had found the models quite difficult to use, and stressed the need for good guidance on their use.

Overview of findings and issues raised

Part 1 provided a challenge in a number of respects, in particular the following:

- Measured temperature data was available at discrete thermocouple locations, to which predictions could be compared. This provided a challenge in terms of understanding discrepancies, and making parametric simulation studies to identify the important mechanisms. Choices in respect to fuel heat of combustion, radiative losses and thermal boundary treatment were found, by various participants, to be significant.

- The sloping roof structure provided a test of the zone models, for which the smoke filling process is based on a Cartesian, two-layer concept.
- For *case 1* and *case 2*, where the hall was nominally closed, the ventilation was not known. A suggested prescription for air 'infiltration', by means of a set of small ventilation openings, was provided in the benchmark specification. However, the sensitivity of the predictions to the infiltration specification was an issue that warranted some attention.

The results for *Part I* were quite encouraging, with the general, qualitative, nature of the experiments being captured in the simulations by zone, lumped parameter and CFD models. Comparison between predictions and measurements was restricted to gas temperatures at three thermocouple trees and two locations directly above the fire source. However, this was sufficient to allow the above issues to be addressed with some degree of confidence.

The main findings may be summarised as follows:

- Despite the 'complexity' of the roof structure the various types of model were able to predict the smoke layer formation process with reasonable reliability. Of particular note here was the ability of zone models to make an assumption of a flat ceiling such that the volume of the hall was conserved.
- Zone models generally predicted lower layer heights than those derived from the experimental measurements using the suggested data reduction formula. This might possibly be attributed to the flat ceiling approximation. An alternative explanation may lie in the data reduction formula, where it was shown that the alternative method of Audouin yielded 'measured' layer heights lower than those predicted by the models.
- For *case 1* and *case 2* the precise specification of the 'infiltration' ventilation was not important in respect to the predicted temperatures inside the test hall. This provides some encouragement in modelling such scenarios.
- When using the original benchmark specification there was, in most studies, a tendency to predict higher smoke layer temperatures than those measured. Two principle mechanisms were identified, to which modifications were possible to reduce the temperature of the smoke layer.

The first of these is the proportion of heat attributed to the convective power of the fire plume, the value being dependent on the choice of heat of combustion, combustion efficiency and radiative fraction. It seems that the choice of 80% for the combined effect of combustion efficiency and radiative fraction was not ideal, resulting in too much heat being convected into the upper layer. This may have contributed to the predicted temperatures being higher than those measured.

The second is the boundary heat loss, which was shown to play an important role in a number of studies. Some justification in increasing the boundary heat losses is provided by the probable error in the thermal properties specified for mineral wool (Table 1 of the benchmark specification). More realistic values would reduce the

thermal inertia by perhaps 50%, which would in turn increase the calculated boundary heat loss.

Part II – Extended NPP Scenarios

Summary of results

Table 12 lists the participants for *Part II*, showing the fire models used and the particular cases investigated. Also indicated is whether details of the work is included in a separate appendix, supplied by the participant and included as part of this report. Where an appendix has not been supplied, information has been taken from presentation material provided at the 6th (BRE) project meeting. Apart from the Kobra3D simulations, which were undertaken after the 6th project meeting, the predictions were made 'blind' without knowledge of the work of the other participants.

Table 12 Participant contributions for *Part II*

Participant	Fire model	Cases investigated	Appendix
D Roubineau (IRSN)	Flamme_S (zone)	1	B
W Klein-Heßling (GRS)	COCOSYS (lumped parameter)	1, 2 & 3	C
M Heitsch (GRS)	CFX-4 (CFD) ¹	1	E
L Gay & B Gautier (EDF)	MAGIC (zone)	1, 2 & 3	D
M Dey (USNRC)	CFAST (zone) FDS (CFD)	1, 2 & 3 1, 2 & 3	F F
D Joyeux & O Lecoq-Jammes (CTICM)	MAGIC (zone)	1, 2 & 3	G
S Miles (BRE)	CFAST (zone) JASMINE (CFD)	1, 2 & 3 1, 2 & 3	H H
A Martin & D Coutts (WSMS)	CFAST (zone)	2 & 3	-
J Will (HPP Braunschweig)	Kobra3D (CFD)	1, 2 & 3	I

¹ first 864 s only

As for *Part I*, a short summary of each participant's individual work is provided below, followed by an overview of the findings of the collected studies and a discussion of the main issues raised. A model by model comparison of predictions for a number of key parameters, e.g. maximum gas temperature in the two decks and the maximum target temperatures, is included. Again, the reader is referred to the appendices for full details of each participant's work.

D Roubineau (IRSN) - using Flamme S (zone)

In common with other participants using zone models, *Part II* presented a challenge due to its geometry, in particular the combination of two decks connected by horizontal flow vents (hatches). In the absence of a horizontal vent flow model, the turbine hall was simplified into a single compartment. To assess, conservatively, the likelihood of damage to the cable and beam targets the height of the single compartment was set to match either the height of the lower deck ceiling (targets in the lower deck) or the upper deck ceiling (for targets in the upper deck). Simulations were performed for *case 1* only, for which the damage criteria were not reached for any of the targets.

W Klein-Heßling (GRS) - using COCOSYS (lumped parameter)

Approximately 600 zones were employed in the COCOSYS simulations for the three cases, with sufficient resolution to incorporate counter-flow at the hatches and to make predictions at the individual thermocouple locations.

Figure 31 illustrates the COCOSYS results, showing predicted temperatures at tree 2 for *case 1*. Figure 32 shows, for various parametric simulations of *case 1*, that COCOSYS predicts upward flow through hatch 1 and downward flow through hatch 2 throughout the simulation. Apart from the early stage of *case 2*, upward flow through both hatches is predicted in the other two cases.

No damage to the cable or beam targets is indicated in any of the cases. While quite high gas temperatures are predicted for cable 1 and beam 1 in the lower deck, the incident fluxes remain low. The maximum temperature at the human target, however, is hazardous in all cases, especially *case 1* where the maximum value is 129°C.

M Heitsch (GRS) - using CFX-4 (CFD)

Due to the time constraint imposed by the size of the simulations, predictions were made (using CFX-4.4) only for the first 864 s of *case 1*. However, this simulation yielded some interesting results, in particular in respect to the predicted flow through the hatches. Here there is upward flow through hatch 1, and a corresponding downward flow through hatch 2, followed by a flow reversal at both hatches at about 750 s. This is illustrated in Figure 33. During the simulated period, cable and beam target damage is not indicated. However, the incident flux to beam 1 reaches quite a high value (28 kW m⁻²). Figure 34 presents predicted temperatures at tree 2.

L Gay & B Gautier (EDF) - MAGIC (zone)

MAGIC V3.4.8 was used for simulating all three cases. It was noted that complex three-dimensional effects might not have been captured by the zone modelling approach. However, the results were seen as encouraging.

For *case 1* both upward and downward hatch flow was predicted, while for the other cases the flow was primarily from the lower to upper deck. Figure 35 shows the predicted layer temperatures for *case 1*. It was noted that the lower layer temperature climbed above the upper layer temperature (in the lower deck), but this was due to complexities

of the flow phenomena that were not included in this version of MAGIC. The 'problem' had been resolved in the next version of MAGIC (V3.4.9).

Figure 36 shows the layer heights predicted for the three cases. Complete destratification is predicted in the upper deck in case 1, while for case 3 (mechanical exhaust ventilation), the layer height remains quite high in both decks.

Target damage was not predicted in any of the cases, with the only notable heating occurring to cable 1, where the surface temperature rose to 155 °C in case 1 and approximately 130 °C in case 2 and case 3. Hazardous thermal conditions for the human target were predicted for case 2. (gas temperature and incident flux).

M Dey (USNRC) - using CFAST (zone)

CFAST 3.1.6 was used for modelling the three cases. The limitation in the ability of zone models such as CFAST to model horizontal flows was stressed, and that the algorithm employed had not been validated against experiment. Furthermore, the limitation imposed by treating multiple vents as a single combined vent was noted. Nevertheless, CFAST was seen as a useful tool for computationally quick bounding analyses.

Figures 37 and 38 show layer temperatures and heights for case 1. In all cases target damage was not predicted. Target cable 1 was subject to a moderate thermal hazard, with its surface temperature reaching of the order 160 °C in all cases. Due the layer height descending sufficiently, a severe hazard to the human target was suggested for case 1 and case 3, while in case 2 conditions remained relatively safe. Whereas for case 1 bi-directional hatch flow was predicted, for the other cases flow was from the lower to upper deck, for which greater confidence in the performance of the horizontal vent flow model can be assumed.

M Dey (USNRC) - using FDS (CFD)

FDS version 2 was used in the simulations of the three cases. The size of the geometry to be modelled posed a challenge, and consequently a coarser grid than would have been desired was employed, using cells of dimension 1 m rather than 10 cm. FDS version 3 overcomes this issue by utilising a multi-block structure whereby finer resolution grids, e.g. at the fire plume, can be embedded within a coarser 'background' grid. FDS employs a mixture fraction combustion model whereby a flamefront surface is computed from which the heat is released. A current limitation of this model is that oxygen depletion and temperature reduction effects are not included.

In line with other CFD models, FDS provides a detailed set of results that allows the complexities of the fluid dynamics to be examined closely. As an example, Figure 39 shows the predicted temperatures at thermocouple tree 2 in case 1. FDS allowed the details of the individual hatch and vent flows to be examined, and compared to those predicted by CFAST. Figure 40 shows the FDS predicted convected heat flows through the two hatches for case 1, which was characterised by an upward flow through hatch 1 and a downward flow through hatch 2. For case 2 and case 3 there was upward flow

through both hatches, accompanied by a significant heat flow from the lower to upper deck.

As with the CFAST simulations, cable and beam target damage was not predicted in any of the cases. However, the requirement for more advanced target heating sub-models was stressed, in particular to include radial heating and possibly the effect of cable bundles.

D Joyeux & O Lecoq-Jammes (CTICM) - using MAGIC (zone)

The three cases were simulated using MAGIC V3.4.8. The difficulty in modelling these scenarios with horizontal hatch flows was noted. This applied to case 1 in particular. Whereas for case 1 there was bi-directional flow at the horizontal vent, for case 2 and case 3 the flow was primarily from the lower to upper deck.

In terms of the gas phase properties, the predictions were very close to those of Gay and Gautier who had used the same version of MAGIC. Figures 41 and 42 show the predicted layer temperatures and heights for case 1. Whereas the layer height is seen to descend to the floor of the upper deck in case 1, it was maintained at over 3 m in both decks for case 2 and case 3. Although no target damage was again indicated, there were some discrepancies in target temperatures and fluxes compared to those from the other MAGIC study. In particular, higher surface and centre-line temperatures were predicted for target cable 1. Relatively safe thermal conditions were predicted for the human target in all three cases.

S Miles (BRE) - using CFAST (zone)

As for Part I, CFAST was used in conjunction with the FAST graphical user interface (version 3.1.6). For Part II, CFAST simulations were performed with two vertically connected compartments to represent the lower and upper decks. A two-layer (zone) treatment was applied to the lower deck in all simulations. For the upper deck, while a two-layer treatment was again used in most simulations, the sensitivity to the use of a one-layer ('shaft') treatment was investigated for case 1.

The fraction of heat converted to radiation in the plume was incorporated by reducing the heat of combustion to $0.75 \times 4.235 \times 10^7 \text{ J kg}^{-1}$ and specifying a radiative fraction of 0.33. For case 3, mechanical extraction was specified at a single HVAC diffuser. The targets specified in CFAST were generally at the mid-point of the actual beam or cable, and orientated such that maximum heating could be expected.

Figure 43 shows the predicted layer temperatures for case 1, and compares the consequence of using either a two-layer or one-layer treatment in the upper deck. Moderately higher temperatures, at the beam and cable targets, are predicted when using two-layers in the upper deck. Figure 44 compares the corresponding layer heights. For all three cases there was a greater temperature rise in the lower deck (the hot gas temperature reaching about 200°C), and only a modest one in the upper deck (the hot gas temperature reaching no more than 100°C). While a reasonable level of stratification is predicted in both decks for case 2 and case 3, for case 1 the layer descends towards

the floor in both decks (using here the two-layer treatment for the upper deck). No hazard as such was indicated for the upper deck targets in any of the three cases. While, in each case, there is a definite thermal hazard presented to the two lower deck targets, the predicted temperature rise is again insufficient to cause damage.

S Miles (BRE) - using JASMINE (CFD)

Simulations of all three cases were performed with JASMINE version 3.2.2 using between about 230,000 and 330,000 grid cells. As for *Part I*, the main sub-models included an eddy break-up combustion model, a six-flux radiation model and the standard κ - ϵ turbulence model. Again, a fixed convective heat transfer coefficient of $10 \text{ W m}^{-2} \text{ K}^{-1}$ was employed. An effective heat of combustion of $2.54 \times 10^7 \text{ J kg}^{-1}$ was specified, where this value incorporated a 40% reduction to account, approximately, for radiation losses from soot in the fire plume. Gas temperatures at the mid-points of the cable and beam targets were recorded in the simulations. Furthermore, incident target fluxes were estimated by taking the maximum of the three Cartesian components of the incident radiation flux field calculated by the six-flux model.

Figure 45 shows the predicted gas temperatures for *case 1* at thermocouple tree 2. Target damage is an issue for *case 1* only, where conditions for cable C1 and beam B1 indicate possible damage. The beam, in particular, is subject to local effects due to its proximity to the fire plume.

For *case 1* a complex flow pattern across the two hatches was predicted, with flow reversal and bi-directional flow occurring in both hatches. Figure 46 illustrates the flow reversal at both hatches, and Figure 47 plots the individual mass flow rates. Conversely, for *case 2* and *3* there is flow from the lower to upper decks only. For *case 1* and *3* the 'smoke layer' eventually fills the upper deck completely, while for *case 2* (with natural roof ventilation) a clear layer is maintained throughout the simulation. Boundary heat loss was shown to be a significant process, reaching over 90% of the fire heat release rate in *case 1*. In terms of the human target, *case 2* with natural roof vents, created significantly better conditions, in terms of both smoke and temperature

A Martin & D Coutts (WSMS) - using CFAST (zone)

CFAST/FAST version 3.1.6 was employed in simulating *case 2* and *case 3*. The interface height remained quite high in both cases. A parametric analysis into reducing the radiative fraction from 0.51 to 0.2 was performed, which resulted in increased maximum layer temperatures of the order 25 to 30 °C. Figure 48 illustrates this for *case 2*. An unexpected consequence of reducing the radiative fraction, however, was that the thermal hazard to beam 1 was reduced. However, the damage criteria were not reached for any of the targets with either setting of the radiative fraction.

J Will (HPP Braunschweig) - using Kobra3D (CFD)

Kobra3D version 4.71 was used to simulate the three cases using a grid of approximately 160,000 cells, with a maximum dimension of 1 m. The cases were modelled as suggested in the specification with no additional assumptions. In contrast to *Part I*, where

there had been some noted discrepancies, the predicted gas phase properties were here more in line with those predicted by the other CFD codes. Figure 49 shows the predicted gas temperatures for *case 1* at thermocouple tree 2.

While for *case 2* a stratified thermal layer in the upper deck is predicted, for *case 1* and *case 3* there is no layer structure in the upper deck. It is suggested in the appendix that the missing friction and turbulence terms in the equation set solved in Kobra3D, which might have been a cause of problems in *Part I*, were an advantage in *Part II*. However, this would require further investigation.

Overview of findings and issues raised

In contrast to *Part I*, the predictions from different numerical models varied to a significantly greater extent. This is perhaps not surprising given the complexity of the fluid dynamics and the fact that measurements were not available against which to compare simulations. While the size of the building was a challenge to CFD models, it was the fluid dynamics associated with two vertical compartments connected by two hatches that provided the greatest test to all models. This was true, in particular, to *case 1* where the upper deck was completely sealed.

While all models indicated that damage to the cable and beam targets was unlikely, there were notable variations in the predicted local gas and target temperatures, as well as the incident thermal fluxes. The figures and tables presented in this section illustrate some of the main areas of both agreement and discrepancy between the predictions made with the different fire models.

Figures 50 and 51 illustrate the inter-code predictions for upper and lower deck temperature conditions for *case 1* and *case 2* respectively. Here, for the zone models the upper gas layer temperature is plotted, and for the CFD and lumped parameter models the average gas temperatures at $T_{1.9}$ & $T_{2.9}$ (lower deck) and $T_{1.19}$ & $T_{2.19}$ (upper deck) are given. The rationale for selecting these measurement locations is that they are 1 m below the ceiling of the deck and are representative of locations where a fire model might be employed to predict the thermal hazard to a target such as a cable, and furthermore provide a 'measure' comparable to the hot gas layer temperature in a zone model.

Figure 51 supports the finding that the different fire models captured the same qualitative behaviour for *case 2*, although the 'hot layer temperature rise' (in °C) does vary within a factor of about two. Figure 50 indicates broad agreement for the 'hot layer temperature rise' in the lower deck for *case 1*, but a notable spread of values for the upper deck where the predicted gas temperatures range by a factor of about 5 between the different fire models. As suggested above, this can most likely be attributed to the fluid dynamic complexities of an upper deck sealed to the outside and connected to the lower deck by horizontal hatches.

A more detailed, comparative analysis of the range of predicted maximum hazard levels presented inside the two decks, and also to the individual targets, has been performed and is presented in the tables below.

Table 13 compares the predicted maximum (and minimum) values of various key variables for the three cases. The purpose of this table is to make a broad comparison of the general hazard level predicted by the various participants. In particular, maximum lower and upper deck temperature provides a rough estimate of the thermal hazard that ceiling level targets (cables etc) would be exposed to. For lumped parameter and CFD models the maximum temperature at each of the three thermocouple trees T1 to T3 is shown, which provides an indication of the lateral distribution of the thermal hazard, not available from a zone model. Some general findings are:

- For *case 2* and *case 3* the maximum lower and upper deck temperatures are, from an 'engineering perspective', broadly similar for the different models. To some extent the differences between the predicted temperatures can be attributed to different assumptions for the convective power of the fire source. For example, the FDS simulations have taken a greater convective power than the JASMINE ones, and the variation in the CFAST predictions seems to be due primarily to this also. It can be seen that the two CFD models, and to a lesser extent the lumped parameter model, have identified three-dimensional effects not within the scope of a zone model. For example, in the upper deck the local heating at T3 due to hatch 1 is clear. And the increased temperature at T2 in the lower deck due to the proximity of the fire plume is quite pronounced.
- For *case 1* the variation between models is more marked, particularly in respect to the upper deck temperature. The main cause of this discrepancy seems to be the treatment of the hatch flows. While it is understood that this is a complex phenomenon for the zone models, there is discrepancy between the CFD models too. In the case of FDS there is upward flow through hatch 1 and downward flow through hatch 2 throughout the simulation, whereas for JASMINE and CFX there is flow reversal.
- There is some discrepancy between models in terms of the relative level of thermal hazard predicted for the different cases. For example, the MAGIC simulations indicate that the smoke layer in *case 2* and *3* is markedly hotter compared to *case 1*, whereas for FDS the reverse is true.
- The CFD models have predicted higher maximum plume temperatures than the lumped parameter and zone models. This is most likely a consequence, in part at least, of the fact that the CFD models have resolved the plume structure, and will hence have identified the 'hot region'.
- In terms of the pressure and oxygen consumption predictions, the differences between the results is judged to be not that significant. Here it should be noted that a small variation in 'leakage ventilation' rates can give rise to large differences in compartment pressures, and so the difference between, say, 500 and 1000 Pa may not be too significant.

Table 13 Comparison of gas phase predictions for Part II

Case	Property	Zone	CFD and lumped parameter				
1	Max gas temp in lower deck (outside plume) (°C)	CFAST ^(BRE)	192	JASMINE ^(BRE)	T1	T2	T3
		CFAST ^(NRC)	229	FDS ^(NRC)	216	249	217
		MAGIC ^(EDF)	233	COCOSYS ^(GRS)	230	278	371
		MAGIC ^(CTICM)	233	CFX-4 ^(GRS) ⁵		238	
				Kobra-3D ^(HHP)	194	244	234
1	Max gas temp in upper deck (°C)	CFAST ^(BRE)	90	JASMINE ^(BRE)	T1	T2	T3
		CFAST ^(NRC)	98	FDS ^(NRC)	61	77	262
		MAGIC ^(EDF)	56	COCOSYS ^(GRS)	191	230	346
		MAGIC ^(CTICM)	56	CFX-4 ^(GRS) ⁵		64	134
				Kobra-3D ^(HHP)	130	160	177
1	Max plume temperature (°C) ⁶	MAGIC ^(EDF)	461	JASMINE ^(BRE)	963		
		MAGIC ^(CTICM)	460	FDS ^(NRC)	887		
				COCOSYS ^(GRS)	463		
1	Max (net) heat convected through hatches (MW)	MAGIC ^(EDF)	5	JASMINE ^(BRE)	9		
				FDS ^(NRC)	9		
				COCOSYS ^(GRS)	16		
1	Max heat lost to solid boundaries (MW)			JASMINE ^(BRE)	40		
				COCOSYS ^(GRS)	37		
1	Maximum relative static pressure (Pa)	CFAST ^(BRE)	599	JASMINE ^(BRE)	475		
		CFAST ^(NRC)	698	FDS ^(NRC)	1367		
		MAGIC ^(EDF)	1280	CFX-4 ^(GRS) ⁵	1051		
		MAGIC ^(CTICM)	1278	COCOSYS ^(GRS)	1580		
1	Minimum O ₂ concentration (%)	CFAST ^(BRE)	15.9 ¹	JASMINE ^(BRE)	13.6 ²		
		CFAST ^(NRC)	13.6 ¹	FDS ^(NRC)	11.8 ¹		
		MAGIC ^(EDF)	12.1 ¹	CFX-4 ^(GRS) ⁵	15.0 ¹		
		MAGIC ^(CTICM)	12.2 ¹	COCOSYS ^(GRS)	16.2 ¹		
2	Max gas temp in lower deck (outside plume) (°C)	CFAST ^(BRE)	194	JASMINE ^(BRE)	T1	T2	T3
		CFAST ^(NRC)	252	FDS ^(NRC)	148	157	104
		CFAST ^(WSMS)	215 ³ / 243 ⁴	COCOSYS ^(GRS)	191	236	167
		MAGIC ^(EDF)	195	Kobra-3D ^(HHP)	129	157	152
		MAGIC ^(CTICM)	193		132	130	64
2	Max gas temp in upper deck (°C)	CFAST ^(BRE)	68	JASMINE ^(BRE)	T1	T2	T3
		CFAST ^(NRC)	88	FDS ^(NRC)	58	61	120
		CFAST ^(WSMS)	96 ³ / 122 ⁴	COCOSYS ^(GRS)	72	80	163
		MAGIC ^(EDF)	105	Kobra-3D ^(HHP)	99	120	128
		MAGIC ^(CTICM)	95		65	64	90
2	Max plume temperature (°C) ⁶	MAGIC ^(EDF)	244	JASMINE ^(BRE)	947		
		MAGIC ^(CTICM)	238	FDS ^(NRC)	791		
				COCOSYS ^(GRS)	279		

2	Max (net) heat convected through hatches (MW)	MAGIC ^(EDF) 15	JASMINE ^(BRE) 37 FDS ^(NRC) 46 COCOSYS ^(GRS) 37																				
2	Max heat lost to solid boundaries (MW)		JASMINE ^(BRE) 18 COCOSYS ^(GRS) 22																				
3	Max gas temp in lower deck (outside plume) (°C)	CFAST ^(BRE) 196 CFAST ^(NRC) 266 CFAST ^(W/SMS) 216 ³ / 238 ⁴ MAGIC ^(EDF) 195 MAGIC ^(CTICM) 195	<table border="1"> <thead> <tr> <th></th> <th>T1</th> <th>T2</th> <th>T3</th> </tr> </thead> <tbody> <tr> <td>JASMINE^(BRE)</td> <td>147</td> <td>164</td> <td>113</td> </tr> <tr> <td>FDS^(NRC)</td> <td>197</td> <td>241</td> <td>172</td> </tr> <tr> <td>COCOSYS^(GRS)</td> <td>128</td> <td>155</td> <td>150</td> </tr> <tr> <td>Kobra-3D^(HHP)</td> <td>329</td> <td>315</td> <td>219</td> </tr> </tbody> </table>		T1	T2	T3	JASMINE ^(BRE)	147	164	113	FDS ^(NRC)	197	241	172	COCOSYS ^(GRS)	128	155	150	Kobra-3D ^(HHP)	329	315	219
	T1	T2	T3																				
JASMINE ^(BRE)	147	164	113																				
FDS ^(NRC)	197	241	172																				
COCOSYS ^(GRS)	128	155	150																				
Kobra-3D ^(HHP)	329	315	219																				
3	Max gas temp in upper deck (°C)	CFAST ^(BRE) 94 CFAST ^(NRC) 139 CFAST ^(W/SMS) 98 ³ / 132 ⁴ MAGIC ^(EDF) 100 MAGIC ^(CTICM) 98	<table border="1"> <thead> <tr> <th></th> <th>T1</th> <th>T2</th> <th>T3</th> </tr> </thead> <tbody> <tr> <td>JASMINE^(BRE)</td> <td>82</td> <td>91</td> <td>137</td> </tr> <tr> <td>FDS^(NRC)</td> <td>105</td> <td>120</td> <td>175</td> </tr> <tr> <td>COCOSYS^(GRS)</td> <td>101</td> <td>119</td> <td>128</td> </tr> <tr> <td>Kobra-3D^(HHP)</td> <td></td> <td></td> <td></td> </tr> </tbody> </table>		T1	T2	T3	JASMINE ^(BRE)	82	91	137	FDS ^(NRC)	105	120	175	COCOSYS ^(GRS)	101	119	128	Kobra-3D ^(HHP)			
	T1	T2	T3																				
JASMINE ^(BRE)	82	91	137																				
FDS ^(NRC)	105	120	175																				
COCOSYS ^(GRS)	101	119	128																				
Kobra-3D ^(HHP)																							
3	Max plume temperature (°C) ⁶	MAGIC ^(EDF) 245 MAGIC ^(CTICM) 248	JASMINE ^(BRE) 986 FDS ^(NRC) 820 COCOSYS ^(GRS) 277																				
3	Max heat convected through hatches (MW)	MAGIC ^(EDF) 14	JASMINE ^(BRE) 31 FDS ^(NRC) 44 COCOSYS ^(GRS) 37																				
3	Max heat lost to solid boundaries (MW)		JASMINE ^(BRE) 27 COCOSYS ^(GRS) 22																				

¹ volume % ² mass % ³ rad fraction = 0.51 ⁴ rad fraction = 0.2 ⁵ first 864 s ⁶ 8m above fire for CFD

Table 13 cont. Comparison of gas phase predictions for Part II

Tables 14, 15 and 16 compare, for the three cases, peak conditions at the targets for the different models, using the data that was available from the submitted results. The purpose of this analysis is to indicate the range of conclusions that might be drawn from an engineering analysis of the likelihood of damage to targets in these scenarios. It should be noted that in the case of zone models, the maximum gas temperature at the targets corresponds to the temperature in the layer in which the target is located.

While the general consensus was that cable and beam target damage would not have occurred, the level of thermal hazard posed was quite varied between the different models. This was a consequence of the variation in gas phase conditions, and also the modelling of the incident flux. The flux predictions, in particular, were in some instances quite varied, which will have directly influenced the predicted surface and centre-line target temperatures.

The JASMINE simulations indicated fairly severe conditions for beam 1 due to its proximity to the fire source, with high local gas temperature and incident flux levels, and provided conditions closest to those indicating damage. For the models that provided surface and centre-line temperature predictions the agreement was in some instances

quite close, and in others somewhat varied. Of particular note here is the variation in some of the target temperatures predicted in the two MAGIC contributions. The variation in predicted conditions at the human target was quite significant. In the case of zone models this can be explained, in part, by whether the human target was located in the upper or lower layer.

Summarising, it seems clear that further 'validation' of existing fire models is required for the type of scenario represented by *Part II*. Comparison against measurements would be useful here. Perhaps five main issues can be identified from *Part II* that warrant particular attention:

- The application of fire models to scenarios with single or multiple horizontal vents. This is known to be a 'difficult situation' for zone models, both for single vent and multiple vent scenarios. However, for CFD models further development and validation is perhaps required too, in particular with respect to the type of problem represented by *case 1*.
- The combined treatment of the fire source, combustion mechanism and radiation heat losses. As in the first benchmark exercise, issues such as the radiative fraction and effective heat of combustion seems to require further clarification. The difference in the predicted temperatures for the various models seems to have been due, in part, to the assumptions made here.
- Calculation of incident fluxes to targets. The variation in computed fluxes was large, both between different types of model and different models of the same type. Incident flux calculations are strongly influenced by the radiation treatment.
- Development of suitable sub-models for predicting the thermal damage to target elements, in particular cables, cable bundles and cable trays. This reiterates the conclusion from the first benchmark exercise. To some extent target damage sub-models can be considered separately to the gas phase zone or CFD model in that a particular target sub-model could be coupled to either a zone or CFD fire model, or used as part of a separate 'post-processing' calculation. In the latter case it would be assumed that the targets have only a minor influence on the fluid dynamics and heat transfer processes within the building so that during the gas phase (zone or CFD) simulation only the incident fluxes are recorded, and the solid phase calculations are then performed later.
- Very large geometries can pose problems for CFD models in terms of the computational requirement. Consequently, compromises may be necessary in respect to numerical grid resolution, or the range of scenarios that can be modelled may be limited.

Table 14 Comparison of target related predictions for Part II – case 1

Case	Property	Zone	CFD and lumped parameter
1	Max gas temp at cable target C1 (°C)	CFAST ^(BRE) 192 CFAST ^(NRC) 229 MAGIC ^(EDF) 233 MAGIC ^(CTICM) 233	JASMINE ^(BRE) 249 COCOSYS ^(GRS) 235
1	Max gas temp at cable target C3 (°C)	CFAST ^(BRE) 90 CFAST ^(NRC) 98 MAGIC ^(EDF) 56 MAGIC ^(CTICM) 56	JASMINE ^(BRE) 116 COCOSYS ^(GRS) 166
1	Max gas temp at beam target B1 (°C)	CFAST ^(BRE) 192 CFAST ^(NRC) 229 MAGIC ^(EDF) 233 MAGIC ^(CTICM) 233	JASMINE ^(BRE) 741 COCOSYS ^(GRS) 312
1	Max gas temp at beam target B2 (°C)	CFAST ^(BRE) 90 CFAST ^(NRC) 98 MAGIC ^(EDF) 56 MAGIC ^(CTICM) 56	JASMINE ^(BRE) 86 COCOSYS ^(GRS) 186
1	Max gas temp at human target (°C)	CFAST ^(BRE) 90 CFAST ^(NRC) 98 MAGIC ^(EDF) 56 MAGIC ^(CTICM) 56	JASMINE ^(BRE) 56 COCOSYS ^(GRS) 129
1	Max incident flux at cable target C1 (kW m ⁻²)	CFAST ^(BRE) 2.9 CFAST ^(NRC) 3.9	JASMINE ^(BRE) 7.0 FDS ^(NRC) 23.2 CFX-4 ^{(GRS) 1} 7.2 (COCOSYS ^(GRS) max net flux = 1.8)
1	Max incident flux at cable target C3 (kW m ⁻²)	CFAST ^(BRE) 1.1 CFAST ^(NRC) 1.3	JASMINE ^(BRE) 2.3 FDS ^(NRC) 3.4 CFX-4 ^{(GRS) 1} 7.2 (COCOSYS ^(GRS) max net flux = 1.2)
1	Max incident flux at beam target B1 (kW m ⁻²)	CFAST ^(BRE) 4.0 CFAST ^(NRC) 4.9	JASMINE ^(BRE) 81.7 FDS ^(NRC) 13.6 CFX-4 ^{(GRS) 1} 28.2 (COCOSYS ^(GRS) max net flux = 7.2)
1	Max incident flux at beam target B2 (kW m ⁻²)	CFAST ^(BRE) 0.9 CFAST ^(NRC) 1.3	JASMINE ^(BRE) 1.7 FDS ^(NRC) 5.6 CFX-4 ^{(GRS) 1} 8.2 (COCOSYS ^(GRS) max net flux = 1.5)
1	Max incident flux at human target (kW m ⁻²)	MAGIC ^(EDF) 0.8 MAGIC ^(CTICM) 0.8	JASMINE ^(BRE) 1.1 FDS ^(NRC)
1	Max surface temperature at cable target C1 (°C)	CFAST ^(BRE) 122 CFAST ^(NRC) 172 MAGIC ^(EDF) 155 MAGIC ^(CTICM) 197	FDS ^(NRC) 160 COCOSYS ^(GRS) 178 Kobra-3D ^(HHP) 253

1	Max surface temperature at cable target C3 (°C)	CFAST ^(BRE) 50 CFAST ^(NRC) 56 MAGIC ^(EDF) 35 MAGIC ^(CTICM) 40	FDS ^(NRC) 197 COCOSYS ^(GRS) 115 Kobra-3D ^(HHP) 199
1	Max surface temperature at beam target B1 (°C)	CFAST ^(BRE) 144 CFAST ^(NRC) 172 MAGIC ^(EDF) 21 Flamme_S ^(IRSN) 119	FDS ^(NRC) 271 COCOSYS ^(GRS) 298 Kobra-3D ^(HHP) 228
1	Max surface temperature at beam target B2 (°C)	CFAST ^(BRE) 51 CFAST ^(NRC) 55 MAGIC ^(EDF) 22 Flamme_S ^(IRSN) 51	FDS ^(NRC) 121 COCOSYS ^(GRS) 107 Kobra-3D ^(HHP) 47
1	Max centre-line temperature at cable target C1 (°C)	MAGIC ^(EDF) 38 MAGIC ^(CTICM) 129 Flamme_S ^(IRSN) 83	COCOSYS ^(GRS) 27
1	Max centre-line temperature at cable target C3 (°C)	MAGIC ^(EDF) 22 MAGIC ^(CTICM) 20 Flamme_S ^(IRSN) 84	COCOSYS ^(GRS) 23
1	Max centre-line temperature at beam target B1 (°C)	MAGIC ^(EDF) 20	COCOSYS ^(GRS) 298
1	Max centre-line temperature at beam target B2 (°C)	MAGIC ^(EDF) 21	COCOSYS ^(GRS) 107
1	Max 'smoke concentration' at human target (g m ⁻³)	CFAST ^(NRC) 0.74	JASMINE ^(BRE) 0.46 FDS ^(NRC) 0.56

¹ first 864 s only

Table 14 cont. Comparison of target related predictions for Part II – case 1

Table 15 Comparison of target related predictions for Part II – case 2

Case	Property	Zone	CFD and lumped parameter
2	Max gas temp at cable target C1 (°C)	CFAST ^(BRE) 194 CFAST ^(NRC) 252 CFAST ^(W'SMS) 215 ¹ / 243 ² MAGIC ^(EDF) 195 MAGIC ^(CTICM) 193	JASMINE ^(BRE) 144 COCOSYS ^(GRS) 154
2	Max gas temp at cable target C3 (°C)	CFAST ^(BRE) 68 CFAST ^(NRC) 88 CFAST ^(W'SMS) 96 ¹ / 122 ² MAGIC ^(EDF) 105 MAGIC ^(CTICM) 95	JASMINE ^(BRE) 66 COCOSYS ^(GRS) 124
2	Max gas temp at beam target B1 (°C)	CFAST ^(BRE) 194 CFAST ^(NRC) 252 CFAST ^(W'SMS) 215 ¹ / 243 ² MAGIC ^(EDF) 195 MAGIC ^(CTICM) 193	JASMINE ^(BRE) 268 COCOSYS ^(GRS) 198
2	Max gas temp at beam target B2 (°C)	CFAST ^(BRE) 68 CFAST ^(NRC) 88 CFAST ^(W'SMS) 96 ¹ / 122 ² MAGIC ^(EDF) 105 MAGIC ^(CTICM) 95	JASMINE ^(BRE) 84 COCOSYS ^(GRS) 138
2	Max gas temp at human target (°C)	CFAST ^(BRE) 20 CFAST ^(NRC) 21 CFAST ^(W'SMS) 22 ¹ / 22 ² MAGIC ^(EDF) 105 MAGIC ^(CTICM) 23	JASMINE ^(BRE) 30 COCOSYS ^(GRS) 102
2	Max incident flux at cable target C1 (kW m ⁻²)	CFAST ^(BRE) 3.0 CFAST ^(NRC) 4.1 CFAST ^(W'SMS) 3.5 ¹ / 3.9 ²	JASMINE ^(BRE) 3.3 FDS ^(NRC) 1.2 (COCOSYS ^(GRS) max net flux = 1.4)
2	Max incident flux at cable target C3 (kW m ⁻²)	CFAST ^(BRE) 0.6 CFAST ^(NRC) 1.2 CFAST ^(W'SMS) 1.2 ¹ / 1.5 ²	JASMINE ^(BRE) 1.4 FDS ^(NRC) 0.8 (COCOSYS ^(GRS) max net flux = 0.8)
2	Max incident flux at beam target B1 (kW m ⁻²)	CFAST ^(BRE) 10.1 CFAST ^(NRC) 16.9 CFAST ^(W'SMS) 13.1 ¹ / 6.7 ²	JASMINE ^(BRE) 21.2 FDS ^(NRC) 21.4 (COCOSYS ^(GRS) max net flux = 1.5)
2	Max incident flux at beam target B2 (kW m ⁻²)	CFAST ^(BRE) 0.9 CFAST ^(NRC) 1.1 CFAST ^(W'SMS) 1.2 ¹ / 1.6 ²	JASMINE ^(BRE) 1.6 FDS ^(NRC) 1.9 (COCOSYS ^(GRS) max net flux = 1.0)
2	Max incident flux at human target (kW m ⁻²)	MAGIC ^(EDF) 2.0 MAGIC ^(CTICM) 0.4	JASMINE ^(BRE) 0.7 FDS ^(NRC)

2	Max surface temperature at cable target C1 (°C)	CFAST ^(BRE) 130 CFAST ^(NRC) 167 CFAST ^(W'SMS) 148 ¹ / 163 ² MAGIC ^(EDF) 131 MAGIC ^(CTICM) 163	FDS ^(NRC) 92 COCOSYS ^(GRS) 127 Kobra-3D ^(HHP)
2	Max surface temperature at cable target C3 (°C)	CFAST ^(BRE) 39 CFAST ^(NRC) 50 CFAST ^(W'SMS) 54 ¹ / 70 ² MAGIC ^(EDF) 56 MAGIC ^(CTICM) 31	FDS ^(NRC) 67 COCOSYS ^(GRS) 91 Kobra-3D ^(HHP)
2	Max surface temperature at beam target B1 (°C)	CFAST ^(BRE) 249 CFAST ^(NRC) 359 CFAST ^(W'SMS) 299 ¹ / 224 ² MAGIC ^(EDF) 32	FDS ^(NRC) 392 COCOSYS ^(GRS) 244 Kobra-3D ^(HHP)
2	Max surface temperature at beam target B2 (°C)	CFAST ^(BRE) 42 CFAST ^(NRC) 56 CFAST ^(W'SMS) 56 ¹ / 74 ² MAGIC ^(EDF) 24	FDS ^(NRC) 58 COCOSYS ^(GRS) 85 Kobra-3D ^(HHP)
2	Max centre-line temperature at cable target C1 (°C)	MAGIC ^(EDF) 35 MAGIC ^(CTICM) 114	COCOSYS ^(GRS) 26
2	Max centre-line temperature at cable target C3 (°C)	MAGIC ^(EDF) 24 MAGIC ^(CTICM) 20	COCOSYS ^(GRS) 23
2	Max centre-line temperature at beam target B1 (°C)	MAGIC ^(EDF) 27	COCOSYS ^(GRS) 243
2	Max centre-line temperature at beam target B2 (°C)	MAGIC ^(EDF) 22	COCOSYS ^(GRS) 85
2	Max 'smoke concentration' at human target (g m ⁻³)	CFAST ^(NRC) 0. CFAST ^(W'SMS) 0. ¹ / 0. ²	JASMINE ^(BRE) 0.07 FDS ^(NRC)

¹ radiative fraction = 0.51 ² radiative fraction = 0.2

Table 15 cont. Comparison of target related predictions for *Part II – case 2*

Table 16 Comparison of target related predictions for Part II – case 3

Case	Property	Zone	CFD and lumped parameter
3	Max gas temp at cable target C1 (°C)	CFAST ^(BRE) 196 CFAST ^(NRC) 266 CFAST ^(W'SMS) 216 ¹ / 238 ² MAGIC ^(EDF) 195 MAGIC ^(CTICM) 195	JASMINE ^(BRE) 156 COCOSYS ^(GRS) 153
3	Max gas temp at cable target C3 (°C)	CFAST ^(BRE) 94 CFAST ^(NRC) 139 CFAST ^(W'SMS) 98 ¹ / 132 ² MAGIC ^(EDF) 100 MAGIC ^(CTICM) 98	JASMINE ^(BRE) 96 COCOSYS ^(GRS) 124
3	Max gas temp at beam target B1 (°C)	CFAST ^(BRE) 196 CFAST ^(NRC) 266 CFAST ^(W'SMS) 216 ¹ / 238 ² MAGIC ^(EDF) 195 MAGIC ^(CTICM) 195	JASMINE ^(BRE) 300 COCOSYS ^(GRS) 196
3	Max gas temp at beam target B2 (°C)	CFAST ^(BRE) 94 CFAST ^(NRC) 139 CFAST ^(W'SMS) 98 ¹ / 132 ² MAGIC ^(EDF) 100 MAGIC ^(CTICM) 98	JASMINE ^(BRE) 112 COCOSYS ^(GRS) 137
3	Max gas temp at human target (°C)	CFAST ^(BRE) 21 CFAST ^(NRC) 139 CFAST ^(W'SMS) 23 ¹ / 132 ² MAGIC ^(EDF) 24 MAGIC ^(CTICM) 22	JASMINE ^(BRE) 76 COCOSYS ^(GRS) 102
3	Max incident flux at cable target C1 (kW m ⁻²)	CFAST ^(BRE) 2.8 CFAST ^(NRC) 4.4 CFAST ^(W'SMS) 3.4 ¹ / 3.9 ²	JASMINE ^(BRE) 3.6 FDS ^(NRC) 1.2 (COCOSYS ^(GRS) max net flux = 1.4)
3	Max incident flux at cable target C3 (kW m ⁻²)	CFAST ^(BRE) 0.7 CFAST ^(NRC) 1.9 CFAST ^(W'SMS) 1.2 ¹ / 1.7 ²	JASMINE ^(BRE) 2.3 FDS ^(NRC) 1.5 (COCOSYS ^(GRS) max net flux = 0.9)
3	Max incident flux at beam target B1 (kW m ⁻²)	CFAST ^(BRE) 7.0 CFAST ^(NRC) 12.1 CFAST ^(W'SMS) 11.7 ¹ / 6.4 ²	JASMINE ^(BRE) 27.5 FDS ^(NRC) 15.8 (COCOSYS ^(GRS) max net flux = 0.7)
3	Max incident flux at beam target B2 (kW m ⁻²)	CFAST ^(BRE) 1.2 CFAST ^(NRC) 1.9 CFAST ^(W'SMS) 1.2 ¹ / 1.8 ²	JASMINE ^(BRE) 2.3 FDS ^(NRC) 2.5 (COCOSYS ^(GRS) max net flux = 1.1)
3	Max incident flux at human target (kW m ⁻²)	MAGIC ^(EDF) 0.14 MAGIC ^(CTICM) 0.4	JASMINE ^(BRE) 1.5 FDS ^(NRC)

3	Max surface temperature at cable target C1 (°C)	CFAST ^(BRE) 123 CFAST ^(NRC) 159 CFAST ^(W'SMS) 145 ¹ / 132 ² MAGIC ^(EDF) 130 MAGIC ^(CTICM) 165	FDS ^(NRC) 97 COCOSYS ^(GRS) 127 Kobra-3D ^(HHP)
3	Max surface temperature at cable target C3 (°C)	CFAST ^(BRE) 50 CFAST ^(NRC) 83 CFAST ^(W'SMS) 56 ¹ / 77 ² MAGIC ^(EDF) 57 MAGIC ^(CTICM) 58	FDS ^(NRC) 98 COCOSYS ^(GRS) 92 Kobra-3D ^(HHP)
3	Max surface temperature at beam target B1 (°C)	CFAST ^(BRE) 205 CFAST ^(NRC) 283 CFAST ^(W'SMS) 285 ¹ / 204 ² MAGIC ^(EDF) 34	FDS ^(NRC) 364 COCOSYS ^(GRS) 243 Kobra-3D ^(HHP)
3	Max surface temperature at beam target B2 (°C)	CFAST ^(BRE) 54 CFAST ^(NRC) 88 CFAST ^(W'SMS) 60 ¹ / 81 ² MAGIC ^(EDF) 24	FDS ^(NRC) 69 COCOSYS ^(GRS) 86 Kobra-3D ^(HHP)
3	Max centre-line temperature at cable target C1 (°C)	MAGIC ^(EDF) 35 MAGIC ^(CTICM) 112	COCOSYS ^(GRS) 26
3	Max centre-line temperature at cable target C3 (°C)	MAGIC ^(EDF) 24 MAGIC ^(CTICM) 20	COCOSYS ^(GRS) 23
3	Max centre-line temperature at beam target B1 (°C)	MAGIC ^(EDF) 29	COCOSYS ^(GRS) 243
3	Max centre-line temperature at beam target B2 (°C)	MAGIC ^(EDF) 22	COCOSYS ^(GRS) 86
3	Max 'smoke concentration' at human target (g m ⁻³)	CFAST ^(NRC) 0.50 CFAST ^(W'SMS) 0. ¹ / ²	JASMINE ^(BRE) 0.42 FDS ^(NRC)

¹ radiative fraction = 0.51 ² radiative fraction = 0.2

Table 16 cont. Comparison of target related predictions for *Part II – case 3*

GENERAL CONCLUSIONS AND RECOMMENDATIONS

Benchmark exercise 2 has provided some valuable insights into the performance of fire models, extending the findings from the first benchmark exercise in a number of important respects. These include the modelling of large spaces, complex geometries and in comparing predictions against experimental measurement data. Confidence in the application of zone, lumped parameter and CFD models has been provided in the simulations of the test hall experiments in *Part I*, where reasonable agreement was obtained once the important, controlling mechanisms were accounted for. However, the simulations of the turbine hall in *Part II* identified a number of current weaknesses, and illustrated that quite varied predictions could be obtained with different models, including with those of the same type, e.g. zone or CFD.

The results for *Part I* were quite encouraging, with the general, qualitative, nature of the experiments being captured in the simulations by zone, lumped parameter and CFD models. Despite the 'complexity' of the roof structure the various models were able to predict the smoke layer formation process with reasonable reliability. Of particular note here was the justification in assuming a flat ceiling with the zone models, with the height set such that the volume of the hall was conserved. The fact that zone models generally predicted lower layer heights than those derived from the experimental measurements might be attributed, in part at least, to the data reduction method used in calculating the layer height from the experimental temperature measurements.

When using the original benchmark specification, there was a tendency in *Part I* to predict higher smoke layer temperatures than those measured. Two principle mechanisms were identified, to which modifications were able to reduce the temperature of the smoke layer. The first of these was the proportion of heat attributed to the convective power of the fire plume, the value being dependent on the choice of heat of combustion, combustion efficiency and radiative fraction. The second was the boundary heat loss, which was shown to play an important role in a number of studies. Some justification in increasing the boundary heat losses was provided by the probable error in the thermal properties specified for mineral wool, where more realistic values reduce the thermal inertia by about 50%.

In contrast to *Part I*, the predictions from different numerical models for *Part II* varied to a greater extent. This is perhaps not surprising given the complexity of the fluid dynamics and the fact that measurements were not available against which to compare simulations. While the size of the building was a challenge to CFD models, it was the fluid dynamics associated with two vertical compartments connected by two hatches that provided the greatest test to all models. This was true, in particular, to *case 1* where the upper deck was completely sealed.

For case 2 and case 3 of *Part II* the maximum lower and upper deck temperatures were, from an 'engineering perspective', broadly similar for the different models. To some extent the differences between the predicted temperatures could be attributed to the different assumptions for the convective power of the fire source. It was apparent that the CFD models, and to a lesser extent the lumped parameter model, identified three-dimensional effects not within the scope of a zone model.

For case 1 the variation between models was more marked, in particular in respect to the upper deck temperature. The main cause of this discrepancy seems to be the treatment of the hatch flows. This is known to be a complex phenomenon for the zone models, both for single vent and multiple vent scenarios. However, there were discrepancies between the CFD models too, with differences in the predicted hatch flow mechanisms. Further development and validation in respect to the ability of all types of fire models to predict flows through horizontal hatch type openings seems to be required. By contrast, in terms of the pressure and oxygen consumption predictions, the differences between the various models was judged not to be significant.

While the general consensus was that cable and beam target damage would not have occurred, the predicted level of thermal hazard varied quite significantly between different models. This was a consequence of differences in gas phase conditions and also the modelling of the incident flux. The flux predictions, in particular, were in some instances quite varied, which will have directly influenced the surface and centre-line target temperatures for those models including these calculations. Here the agreement was in some instances reasonably close, and in others quite varied. The variation in predicted conditions at the human target was also quite significant.

As in the first benchmark exercise, the issue of the radiative fraction and effective heat of combustion seems to require further clarification. The difference in the predicted temperatures for the various models in *Part II*, and discrepancies with measurements in *Part I*, seems to have been due, in part at least, to assumptions made here.

Further development of suitable sub-models for predicting the thermal damage to target elements, in particular cables, cable bundles and cable trays, seems to be required. This follows on from the findings from the first benchmark exercise, and is a general issue rather than one specific to turbine hall type scenarios. The calculation of incident fluxes is particularly important in predicting cable damage, and highlights the need to address the radiative heat transfer, both from the flaming region and the smoke layer, more carefully.

The usefulness in applying a combination of simpler (e.g. zone) and more complex (e.g. CFD) models to practical problems akin to those represented by the benchmark exercise was apparent. In particular, the zone model approach, while obviously more limited in its geometrical and scientific capabilities, provides a very useful tool for an initial scoping study. CFD can then be used for selected scenarios as required in a particular safety study.

REVIEW OF HEAT RELEASE RATE AND COMBUSTION TERMS

At the 7th meeting of the international collaborative project, the issue of combustion efficiency and radiative fraction was discussed at length [8]. This is referred to on a number of occasions in the panel report. For *Part I* it is suggested that the appropriate choice of these parameters is a major factor in determining how close the predicted gas temperatures compare to those measured. For *Part II* it is again suggested that the choice of these parameters is a factor determining the level of agreement between the different fire models.

It was acknowledged at the 7th meeting that the terms are not well defined in the literature. Furthermore, the terms effective/total/net/complete/chemical heat of combustion are confusing, and the definitions used by different authors are not consistent. However, for the panel report, and the collaborative project in general, it has been proposed to follow the *SFPE Handbook of Fire Protection Engineering (third ed.)* as far as possible.

The following section draws upon the discussion held at the 7th meeting and follows the reasoning included within the meeting report [8]. While the terminology and definitions presented here are suggested for use within the collaborative project, the intention is not to suggest terminology for use within the wider fire community.

The 'effective heat of combustion' ($\Delta H_{c, \text{effective}}$) is related to the 'complete (or net) heat of combustion' ($\Delta H_{c, \text{complete}}$), as measured in a bomb calorimeter, as follows,

$$\Delta H_{c, \text{effective}} = c \Delta H_{c, \text{complete}} \quad (8)$$

where c is the 'combustion efficiency' which accounts for the formation of CO, soot etc. For fuels such as heptane, χ typically lies in the range 0.95 to 0.98, while for sooty fuels such as toluene it is of the order 0.8. However, some authors refer to $\Delta H_{c, \text{effective}}$ as the 'chemical heat of combustion' (e.g. [9]). There is further confusion in respect to the term 'gross heat of combustion', in which the reactants and products are in their standard states [10]. The 'net (complete) heat of combustion', where the product water is in the vapour state, is then slightly lower than the 'gross heat of combustion'.

For well ventilated conditions the total heat release rate of the fire ($\dot{Q}_{f, \text{total}}$) is,

$$\dot{Q}_{f, \text{total}} = \dot{m}_{\text{fuel}} \Delta H_{c, \text{effective}} \quad (9)$$

where $\dot{Q}_{f,total}$ is the total heat generated by the combustion process in the flaming region, and includes **both** the convective **and** radiative components, and \dot{m}_{fuel} is the pyrolysis rate of the fuel.

The radiative fraction is perhaps even less well defined. At the 7th meeting the following was proposed, and (at the time) accepted,

$$\dot{Q}_{f,total} = \dot{Q}_{f,convected} + \dot{Q}_{f,radiated} \quad (10)$$

$$\dot{Q}_{f,radiated} = \dot{Q}_{f,radiated,soot} + \dot{Q}_{f,radiated,gas} \quad (11)$$

where $\dot{Q}_{f,convected}$ and $\dot{Q}_{f,radiated}$ are the components of the total heat released that are convected from the top of the flaming region and radiated (in all directions) from the flaming region respectively, the split between the two then defining the radiative fraction. This concept applies only to cases where there is a well defined flaming (combustion) region above the fuel surface. For other scenarios, such as post flashover fires, the above description is not valid, making the concept of a radiative fraction then rather limited. Eqn. (11) emphasises the fact that radiation exchange is between gas species (principally CO_2 and H_2O) as well as soot particles. Note that Tewarson [9] introduces chemical (total), convective and radiative combustion efficiencies that are not in accord with the above definitions.

REFERENCES

1. U.S. Nuclear Regulatory Commission, "International Collaborative Project to Evaluate Fire Models for Nuclear Power Plant Applications: Summary of Planning Meeting (October 24-25 1999, University of Maryland)", NUREG/CP-0170, February 2000.
(http://techconf.llnl.gov/cgi-fire/downloader/fire_models_1/006-0002.pdf)
2. U.S. Nuclear Regulatory Commission, "Evaluation of Fire Models for Nuclear Power Plant Applications: Cable Tray Fires. International Panel Report", Compiled Dey, M., NUREG-1758, June 2002.
3.
 - i Miles, S.D., "International Collaborative Project to Evaluate Fire Models for Nuclear Power Plant Applications: Specification for Benchmark Exercise # 2 - Fire in a Large Hall", Issue 1, February 2002 (containing final specification for *Part I*).
(http://techconf.llnl.gov/cgi-fire/downloader/fire_models_4/006-0103.msw)
 - ii Miles, S.D., "International Collaborative Project to Evaluate Fire Models for Nuclear Power Plant Applications: Specification for Benchmark Exercise # 2 - Fire in a Large Hall", Issue 2, June 2002 (containing final specification for *Part II*).
(http://techconf.llnl.gov/cgi-fire/downloader/fire_models_5/006-0134.pdf)
4. "International Collaborative Project to Evaluate Fire Models for NPP Applications: Proceedings of the 4th Meeting (17-18 October 2001, GRS, Berlin)", GRS-A-3106, December 2002.
5. Dey, M. Hamins, A. & Miles, S., "International Collaborative Project to Evaluate Fire Models for Nuclear Power Plant Applications: Summary of 5th Meeting (National Institute of Standards and Technology Gaithersburg, MD 20899, May 2-3, 2002)", NISTIR 6986, September 2003.
(See also NUREG/CP-0181, October 2003)
6. Dey, M. International Collaborative Project to Evaluate Fire Models for Nuclear Power Plant Applications – Thread ID: 90.2, 2002.
(http://techconf.llnl.gov/cgi-fire/replyto?fire_models/90.2)
7. Miles, S. & Dey, M., " 6th meeting of the International Collaborative Project to Evaluate Fire Models for NPP Applications: meeting minutes (10-11 October 2002, BRE, UK)".
(http://techconf.llnl.gov/cgi-fire/downloader/fire_models_7/015-0242.pdf)

8. "7th meeting of the International Collaborative Fire Model Project – Summary (30 Jul - 1 Aug 2003, WPI, USA).
(http://techconf.llnl.gov/cgi-fire/downloader/fire_models_7/015-0250.pdf)
9. Tewarson, A, "Generation of heat and chemical compounds in fires". Chapter 3-4, SFPE Handbook of Fire Protection Engineering, 3rd ed., 2002.
10. Drysdale, D, "Thermochemistry". Chapter 1-5, SFPE Handbook of Fire Protection Engineering, 3rd ed., 2002.

ACKNOWLEDGEMENTS

The experimental measurements for *Part I* were collected by VTT as part of the European Coal and Steel Community project *NFSC₂*, and are used by permission of the executive committee, SERDEC.

FIGURES

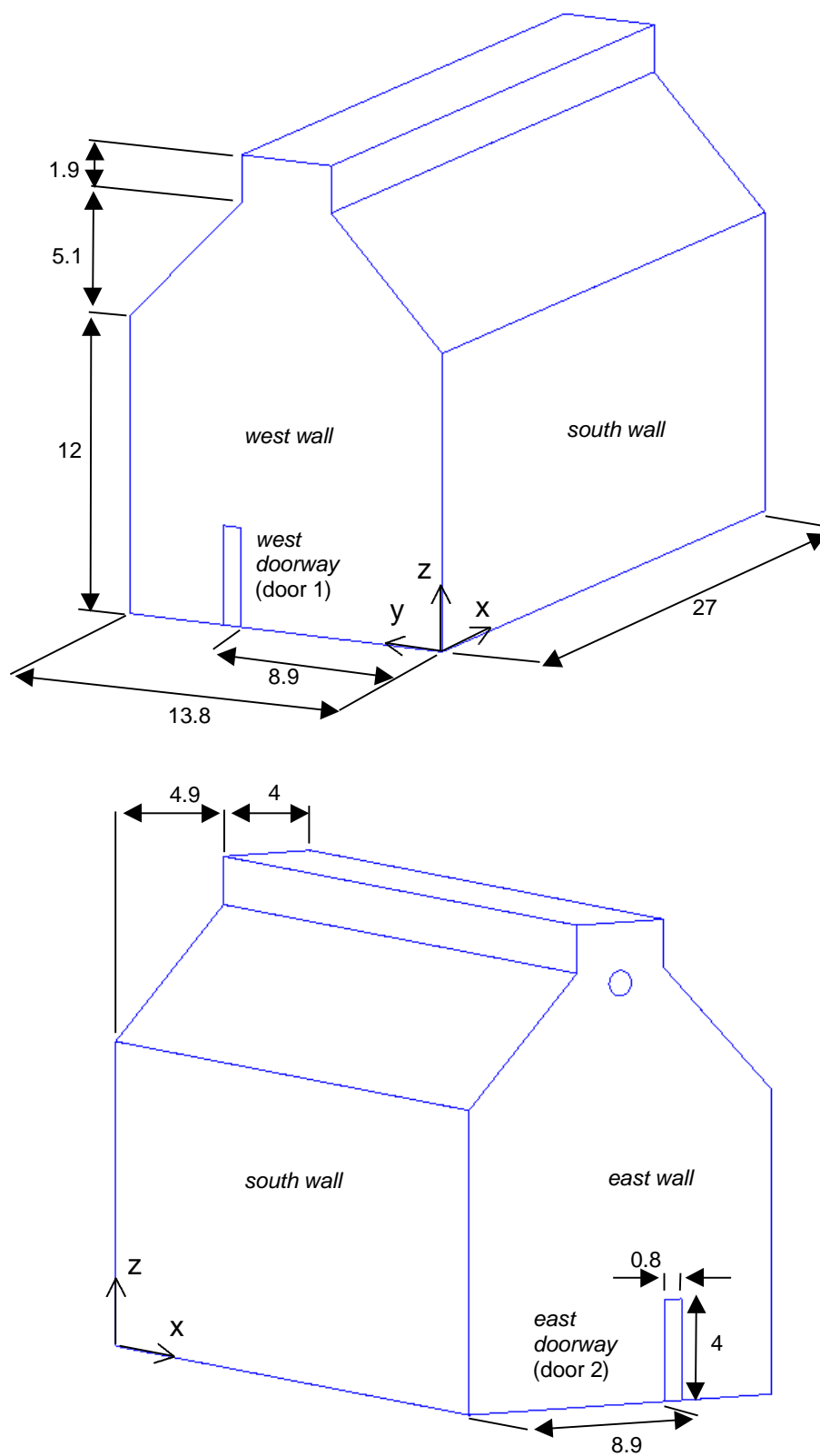


Figure 1 Hall and doorway dimensions for *Part I*

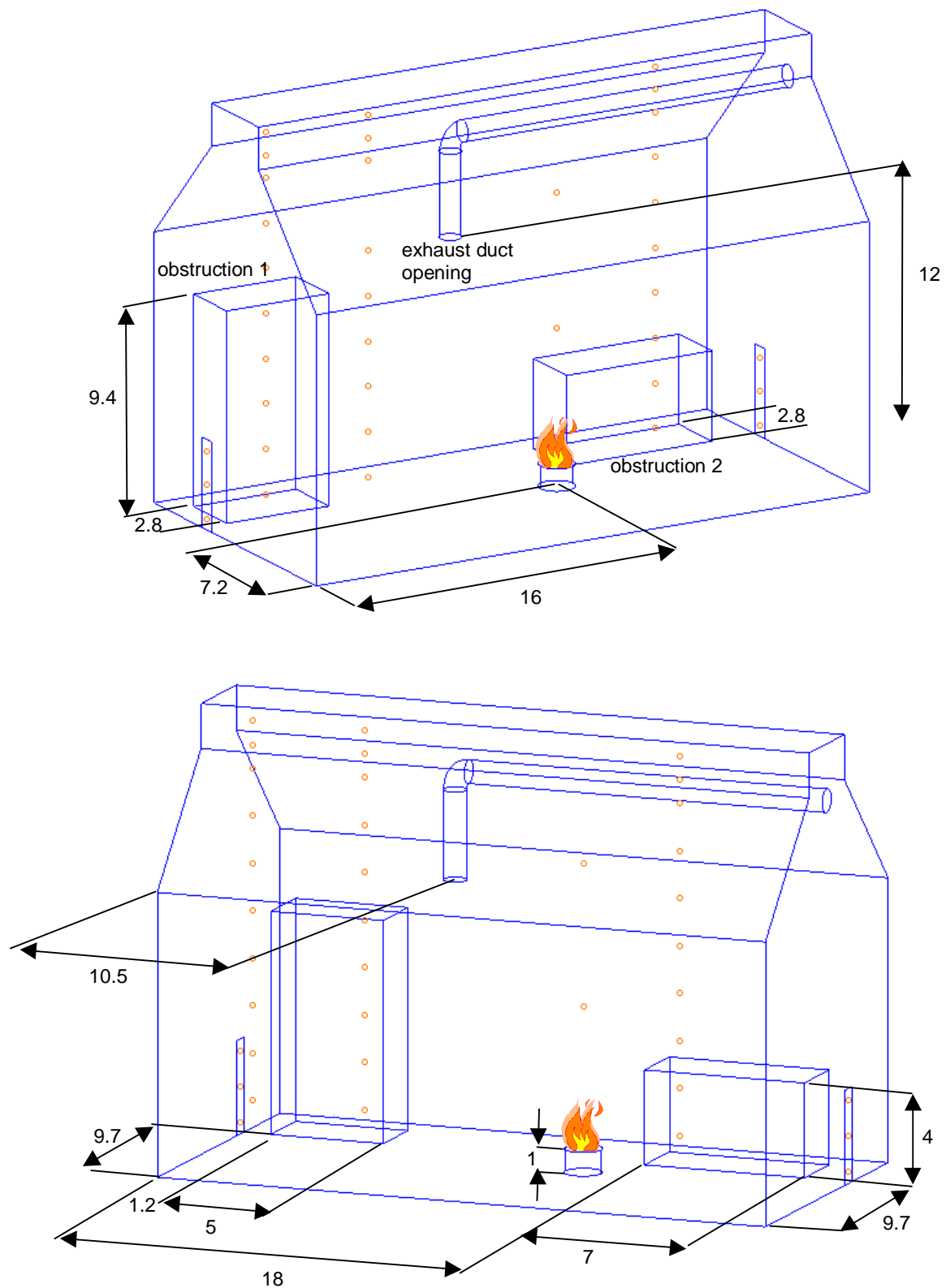


Figure 2 Internal geometry for *Part I*

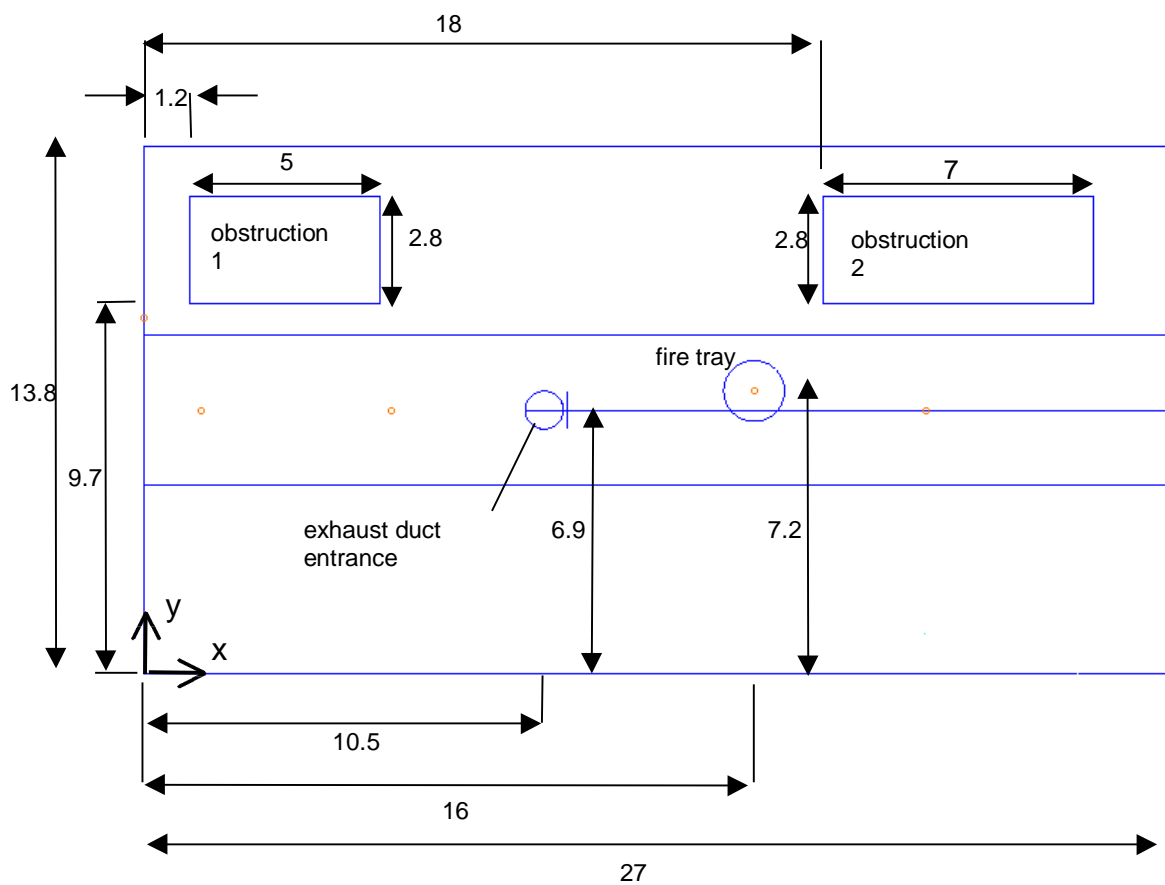


Figure 3 Plan view for *Part I*

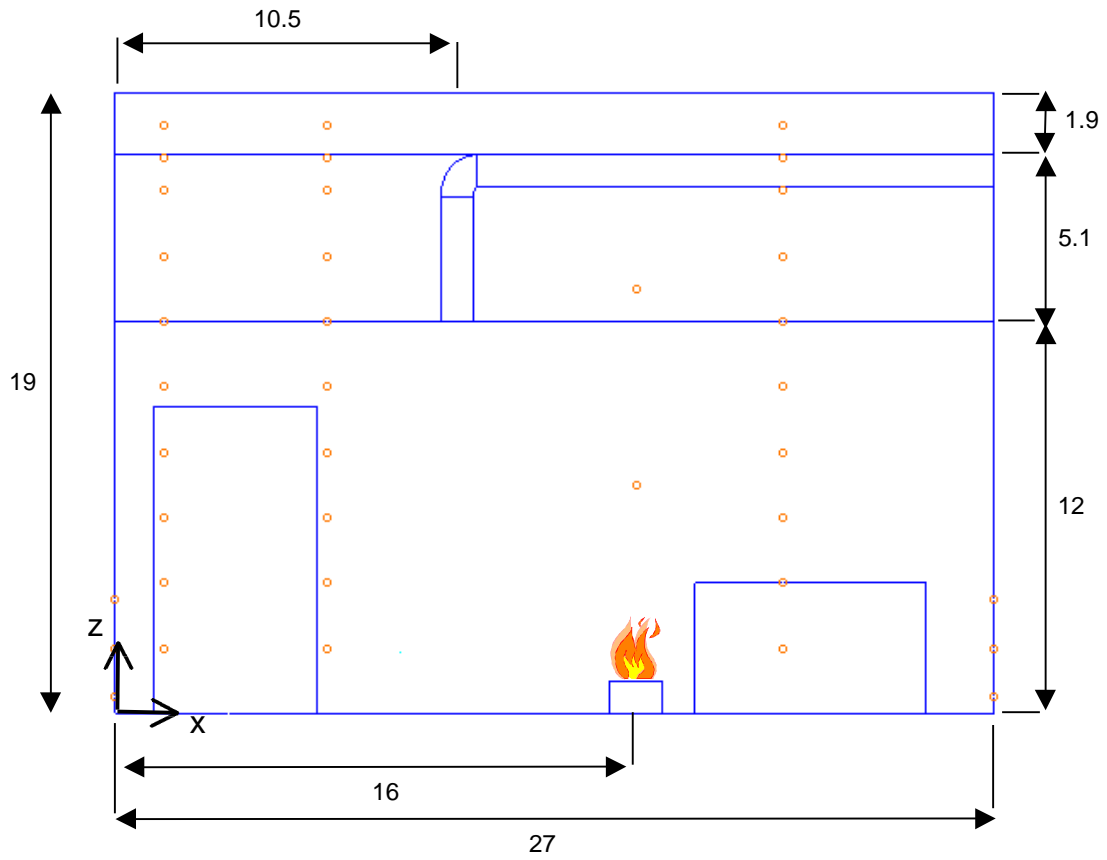


Figure 4 Side view for *Part I*

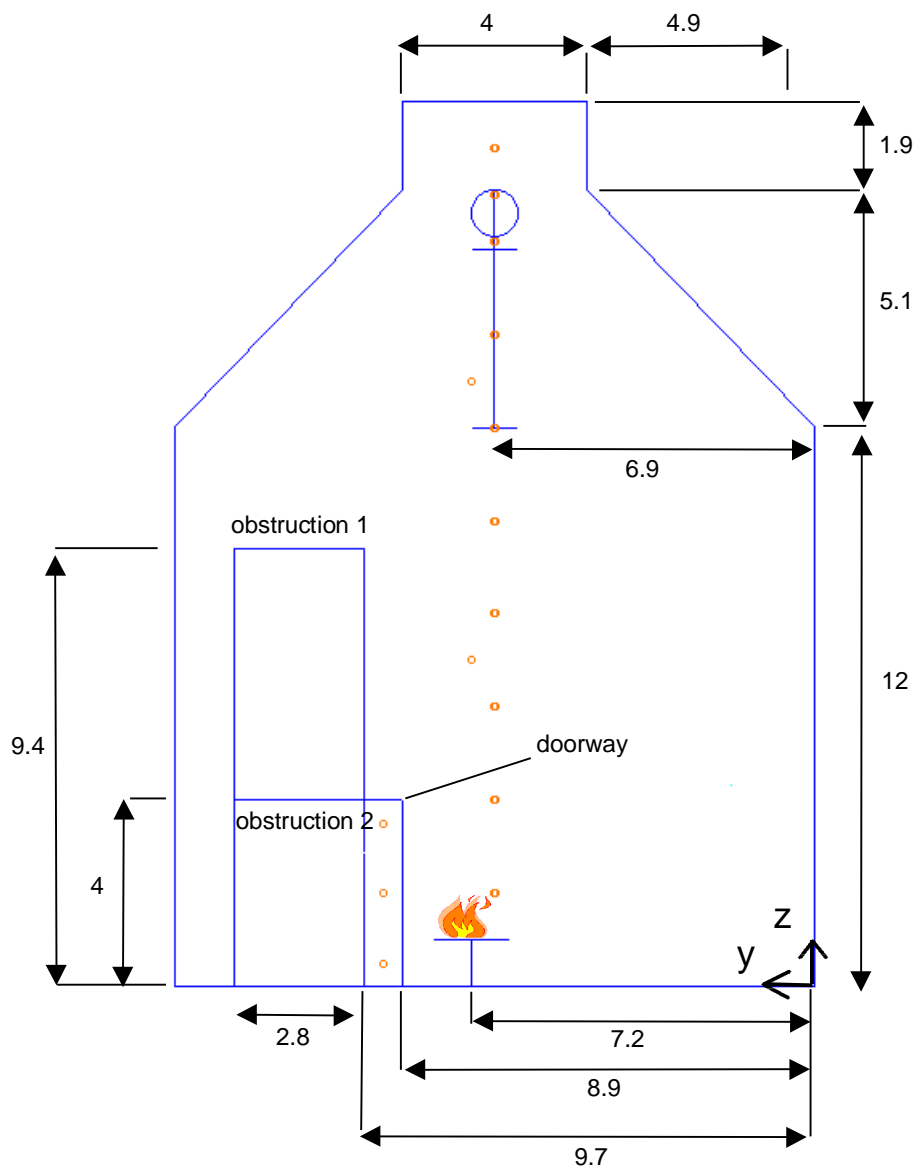


Figure 5 End view for *Part I*

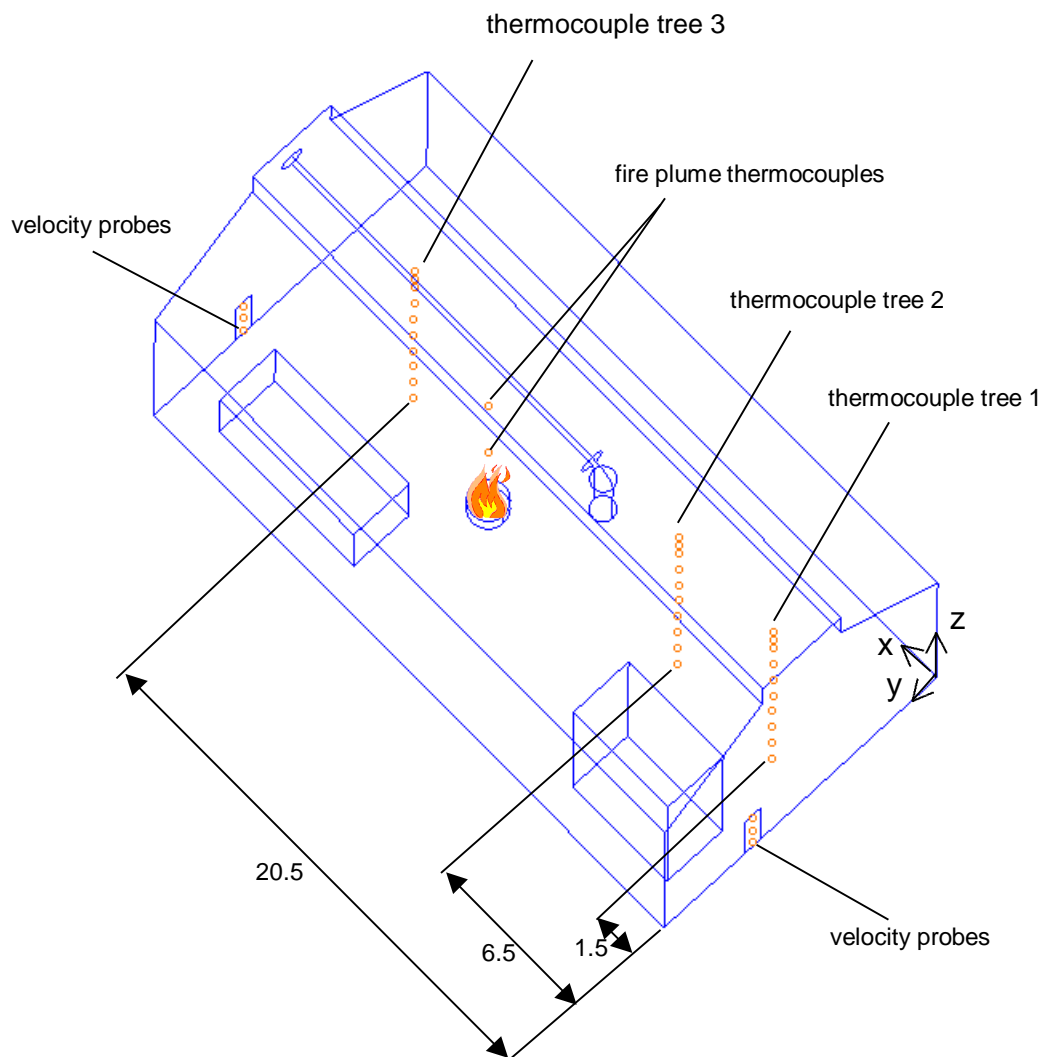


Figure 6 Experimental instrumentation for *Part I*

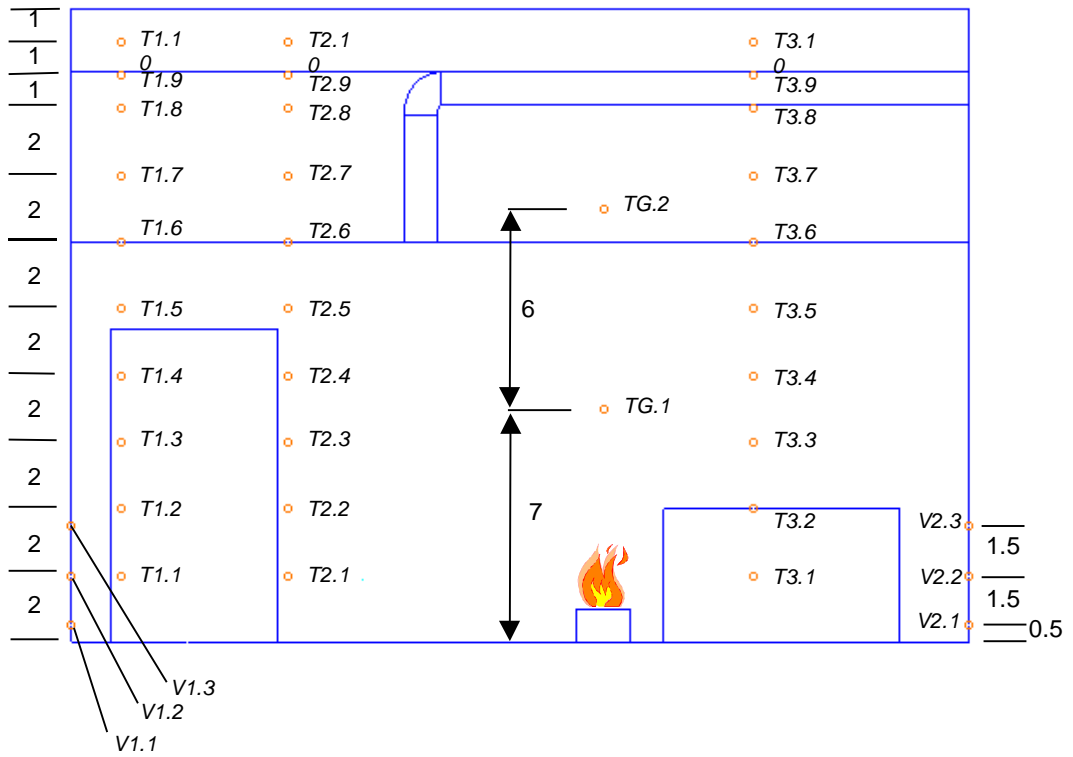


Figure 7 Individual thermocouples and velocity probes for Part I

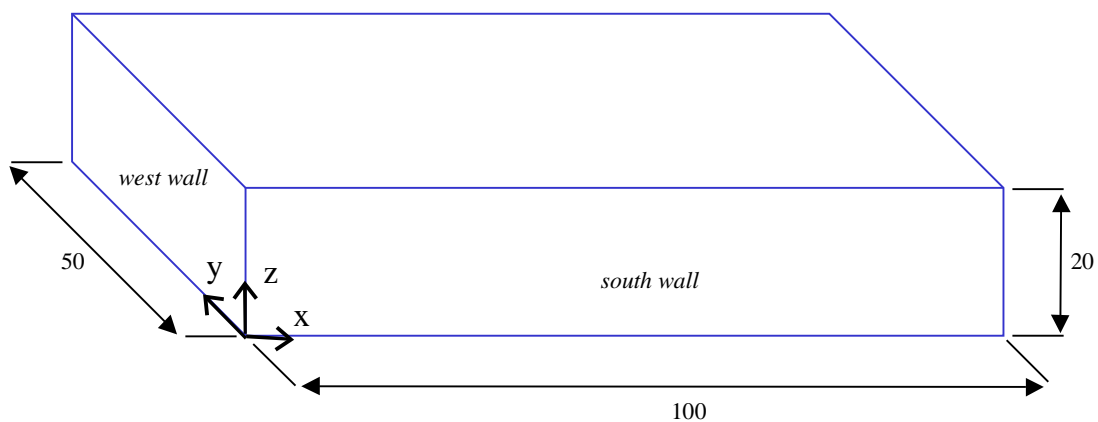


Figure 8 External dimensions for *Part II*

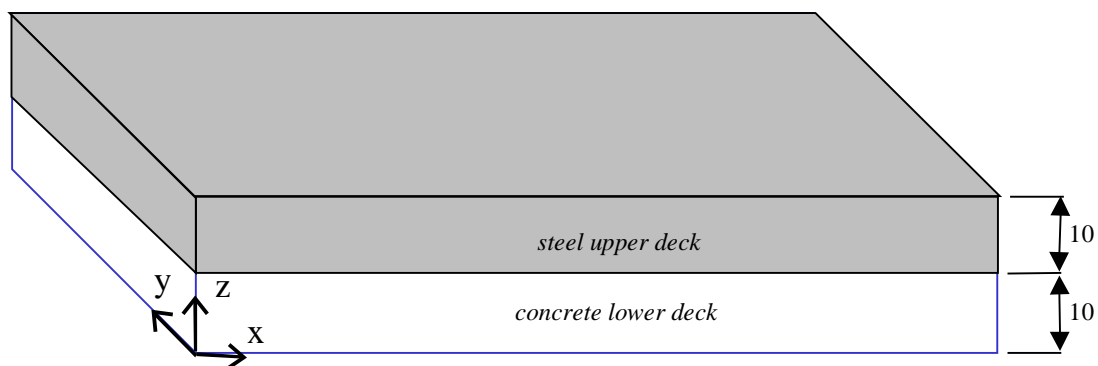


Figure 9 Upper and lower decks for *Part II*

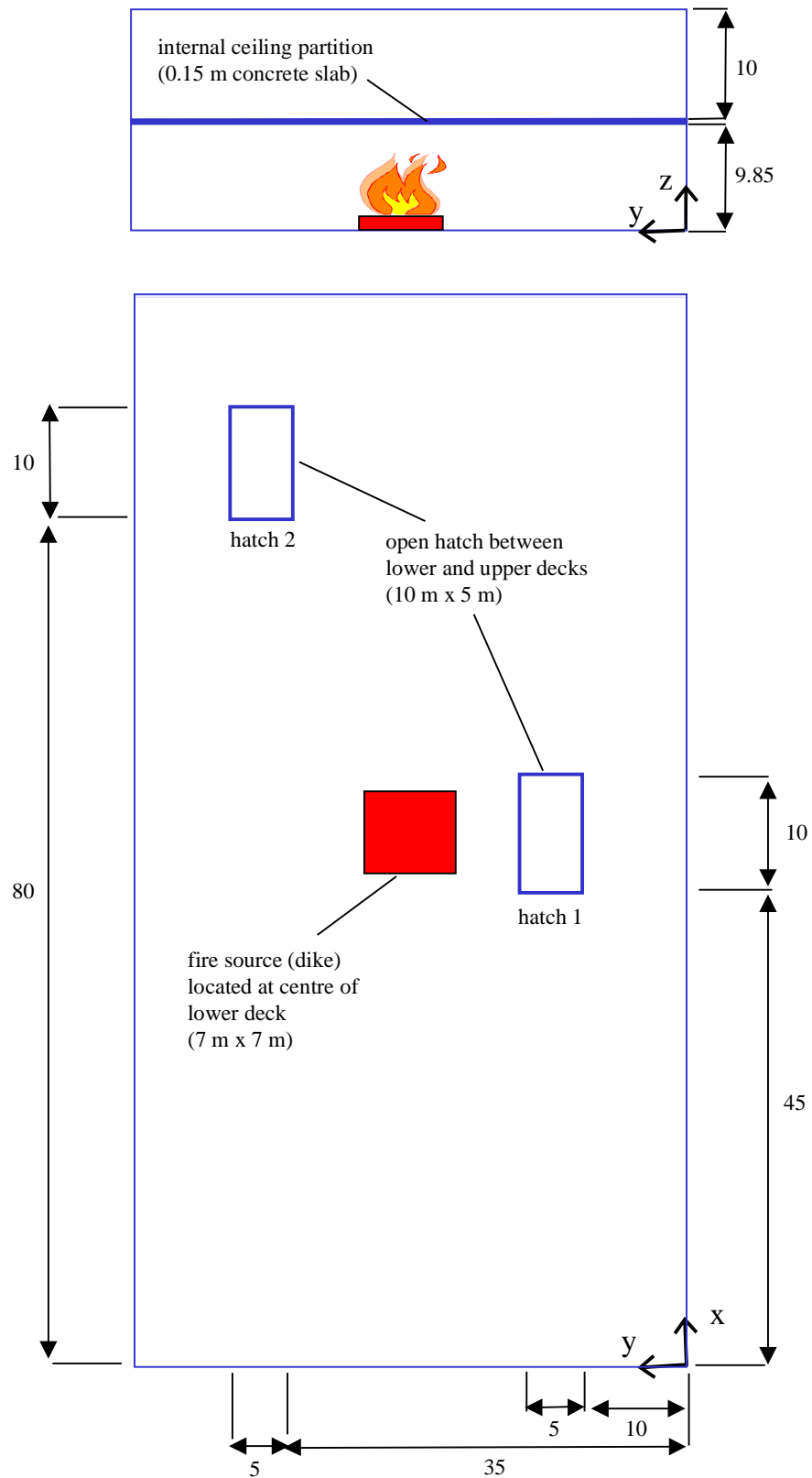


Figure 10 Internal dimensions for *Part II*

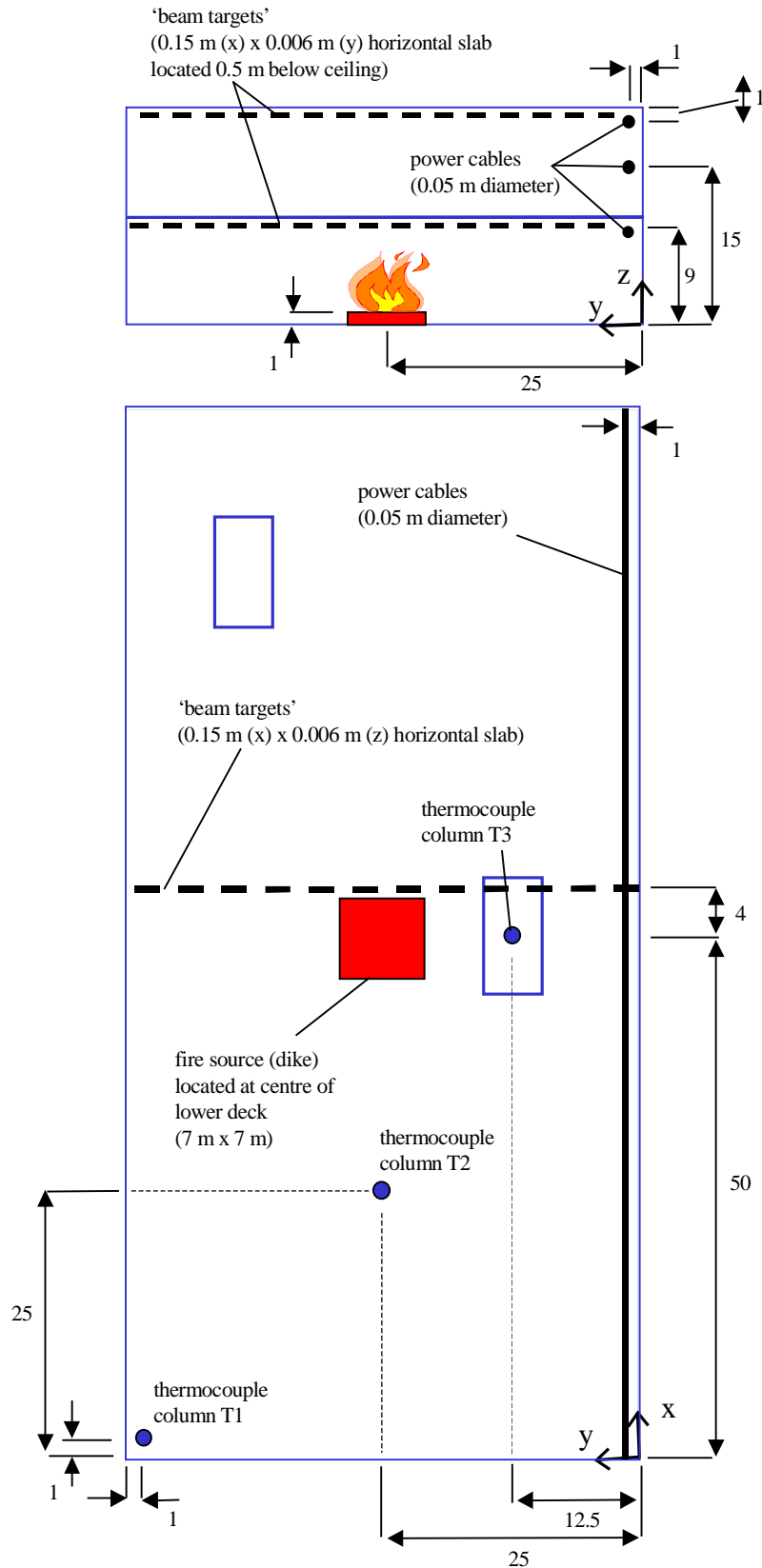


Figure 11 Location of thermocouple trees and 'targets' for Part II

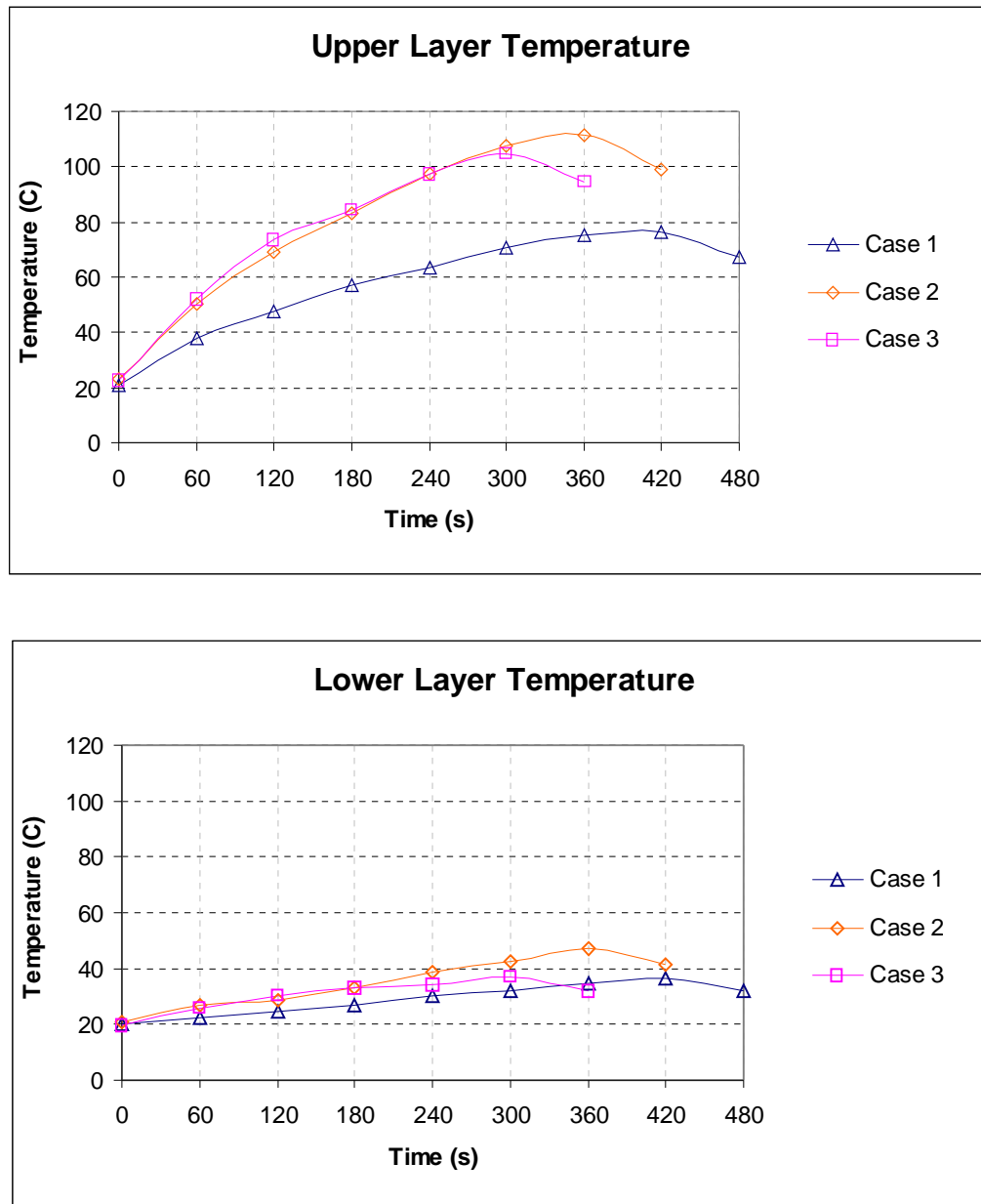


Figure 12 Derived upper and lower layer temperatures for *Part I*

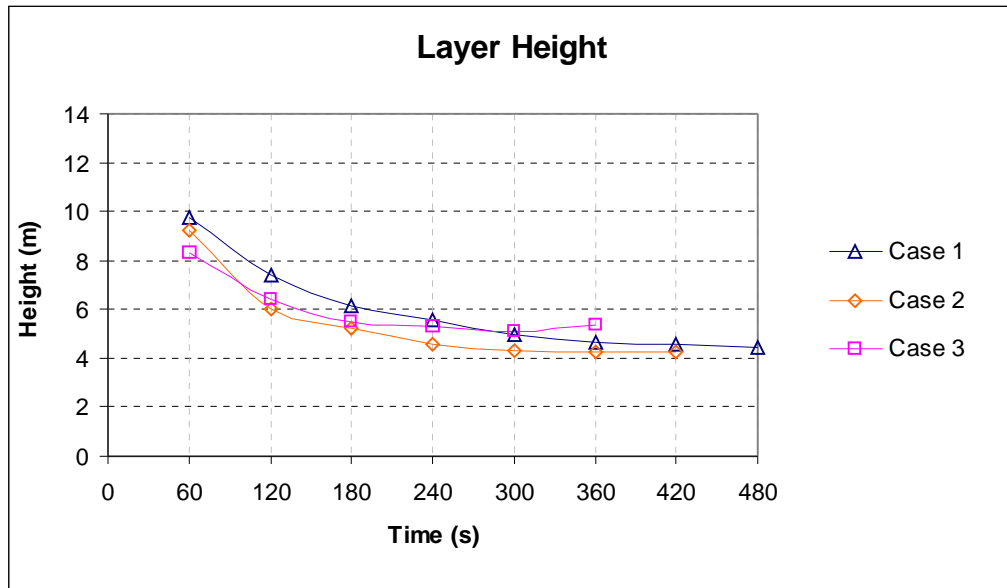


Figure 13 Derived layer height for *Part I*

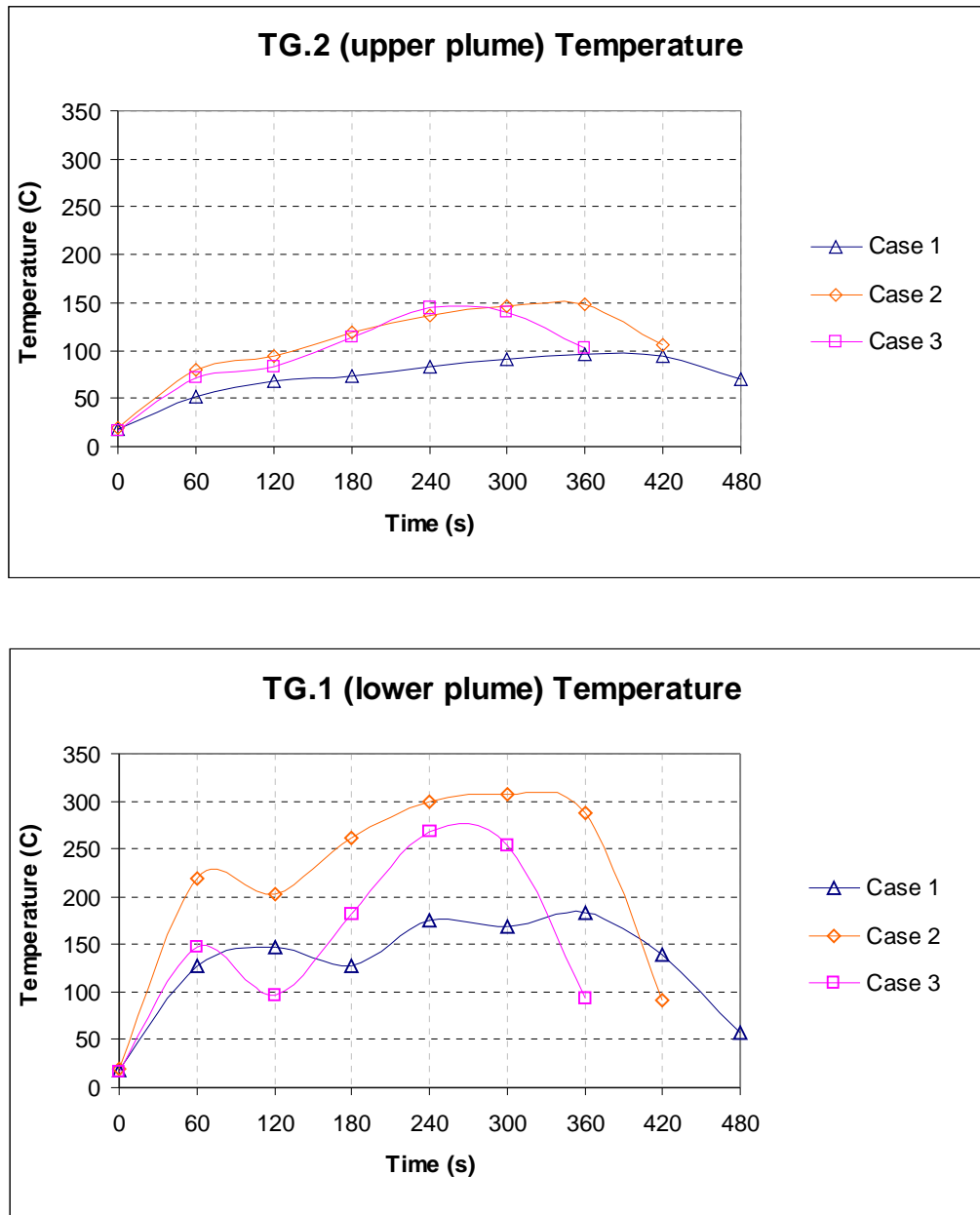


Figure 14 Fire plume temperatures for *Part I*

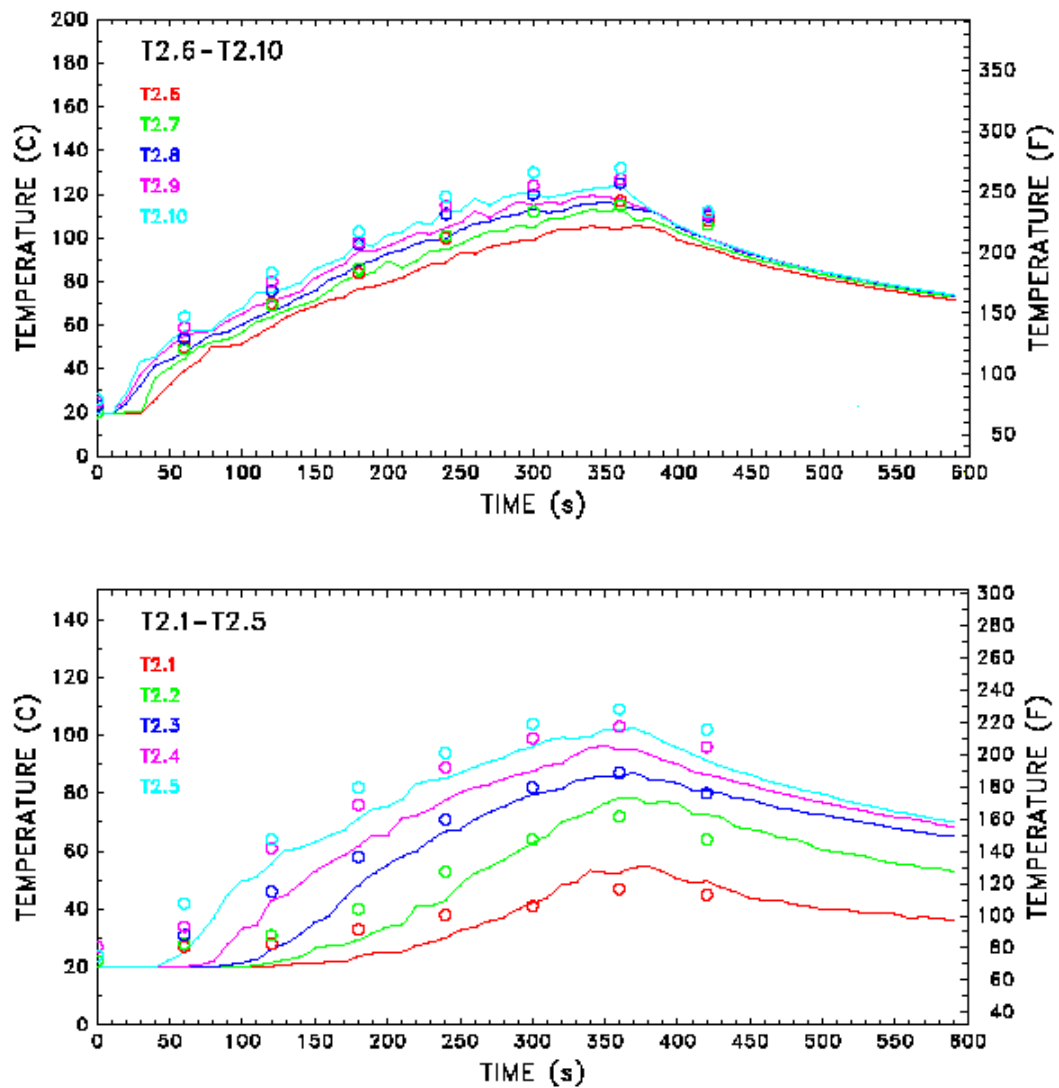


Figure 15 Comparison of predicted (FDS - solid lines) and measured temperatures for *Part I case 2* (taken from Appendix A - K. McGrattan)

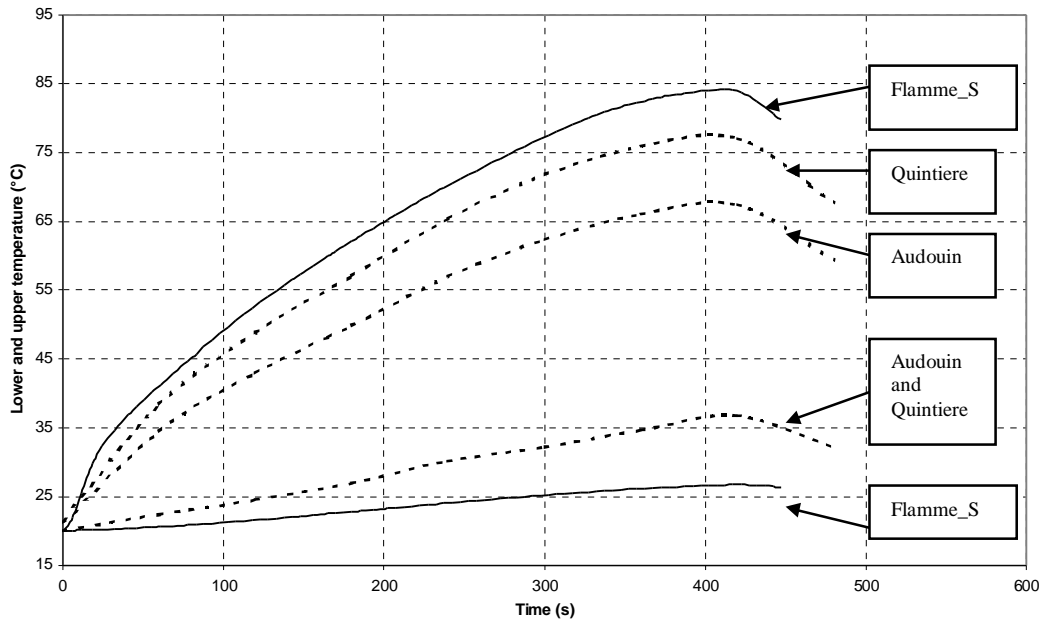


Figure 16 Comparison of predicted (Flamme_S) and measured temperatures for Part I case 1, using two data reduction methods (taken from Appendix B - D. Roubineau)

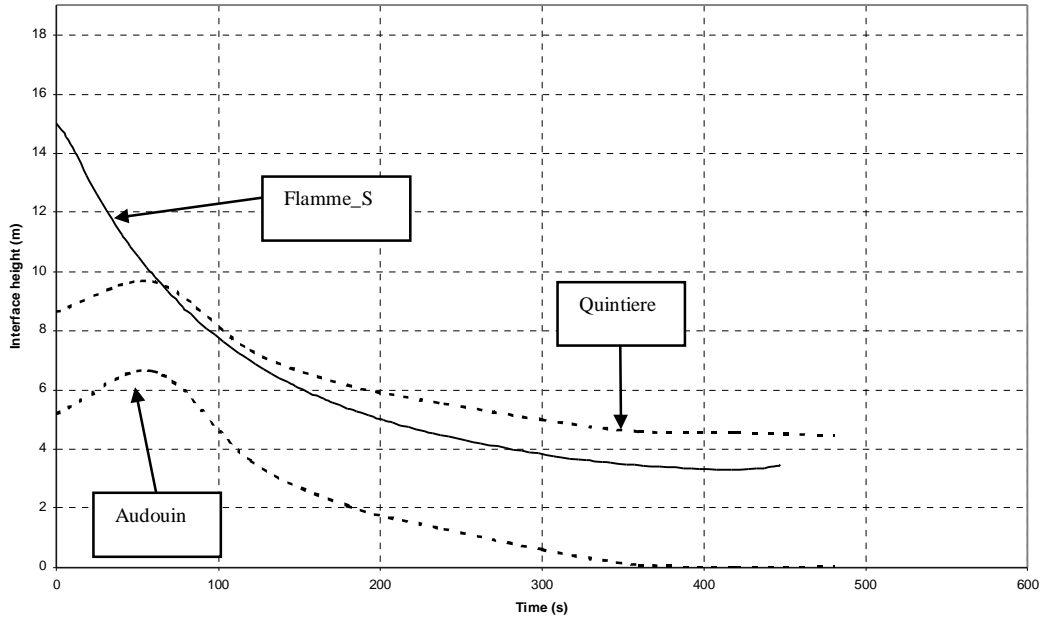


Figure 17 Comparison of predicted (Flamme_S) and measured layer heights for Part I case 1, using two data reduction methods (taken from Appendix B - D. Roubineau)

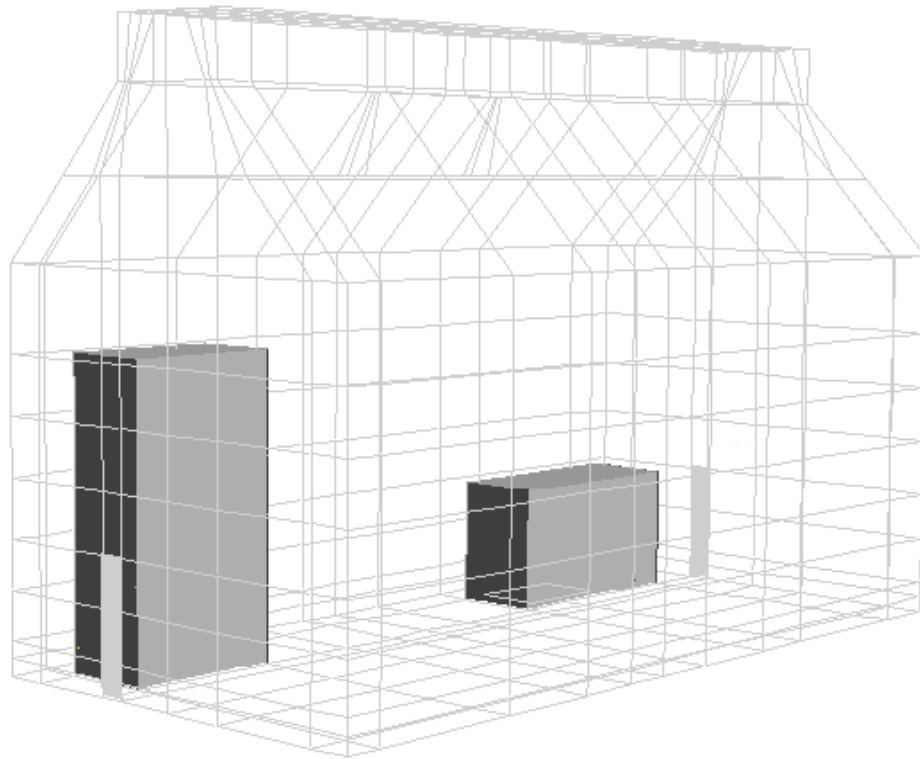


Figure 18 COCOSYS nodalisation for *Part I* (taken from Appendix C - W. Klein-Hebling)

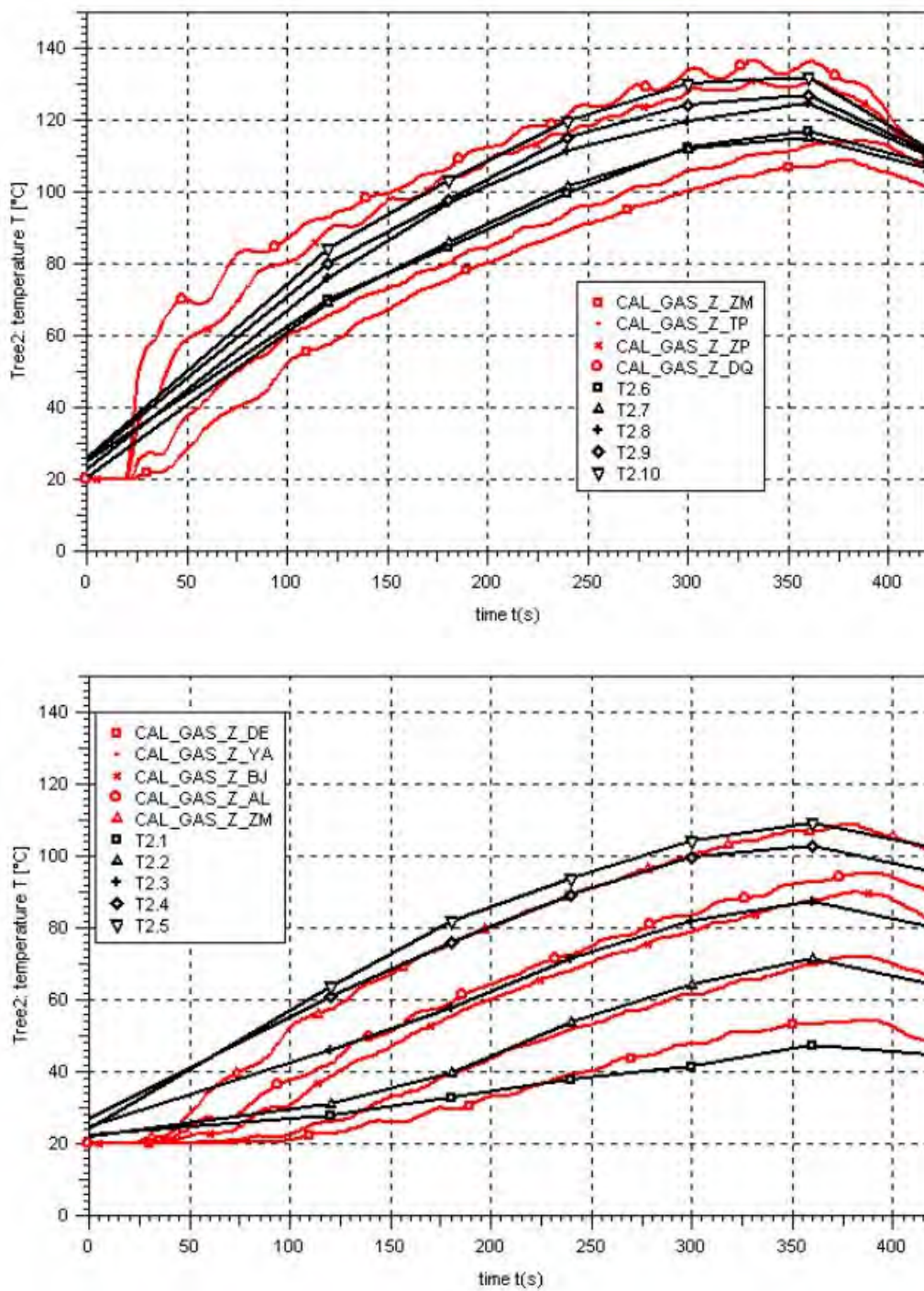


Figure 19 Comparison of predicted (COCOSYS - red lines) and measured temperatures for *Part I case 2* (taken from Appendix C - W. Klein-Hebling)

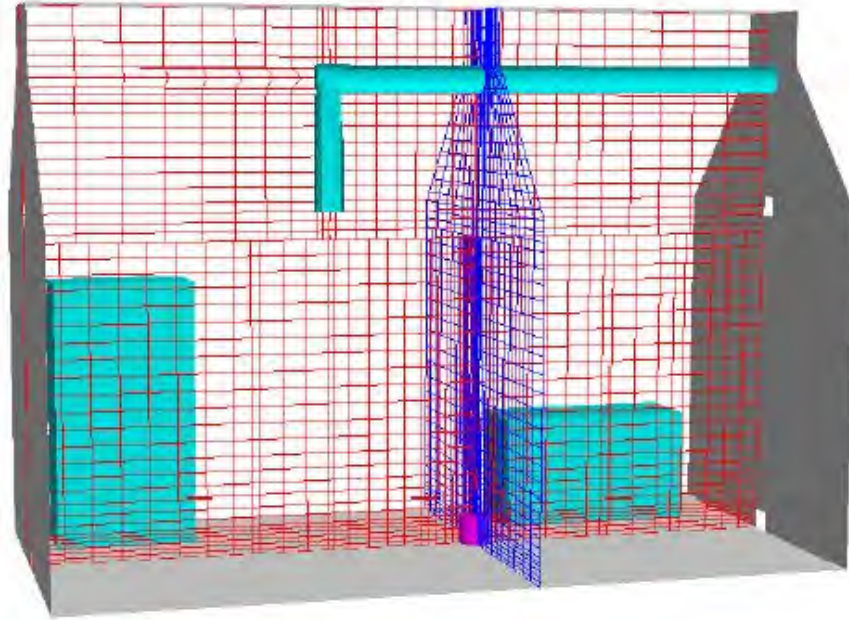


Figure 20 CFX-4 numerical mesh (standard grid) for *Part I* (taken from Appendix E - M. Heitsch)

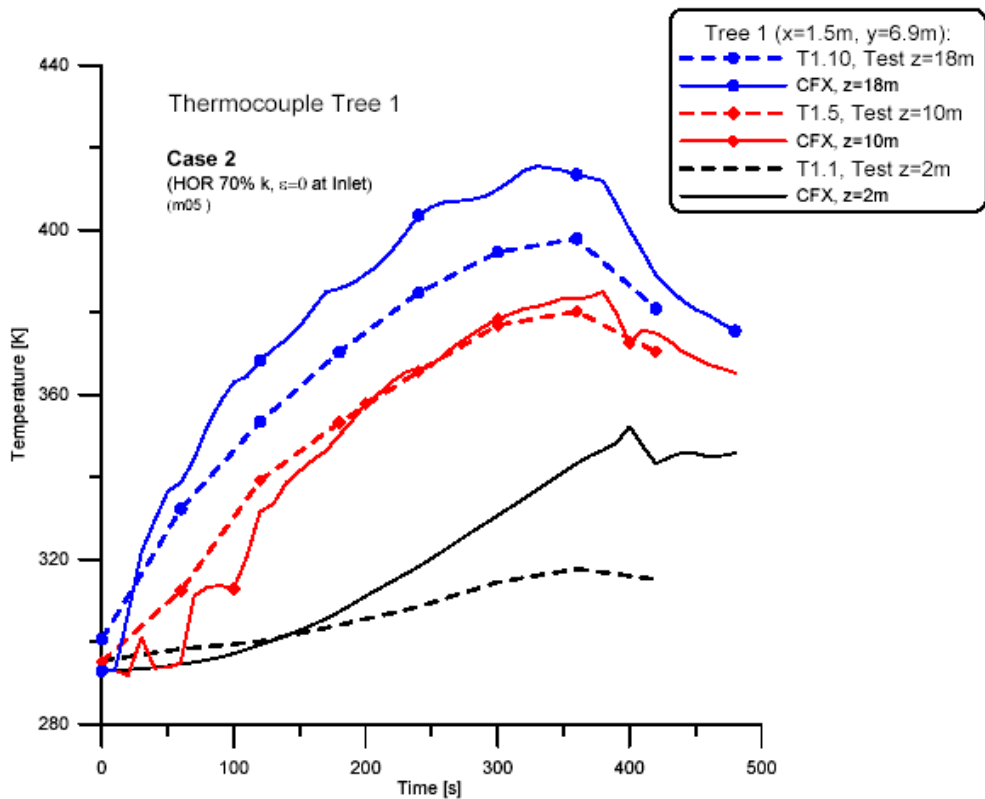


Figure 21 Comparison of predicted (CFX-4 - solid lines) and measured temperatures for *Part I* case 2 (taken from Appendix E - M. Heitsch)

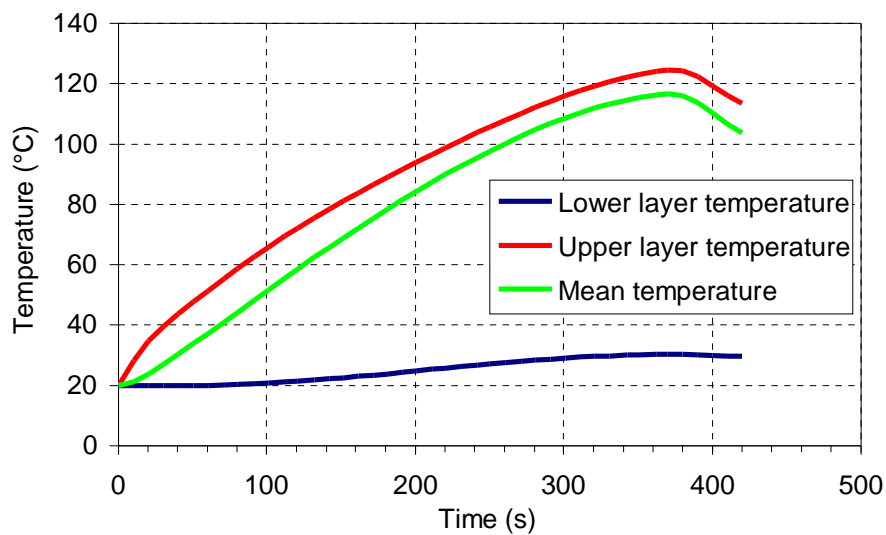


Figure 22 Predicted (MAGIC) layer temperatures for *Part I case 2* (taken from Appendix D - L. Gay & B. Gautier)

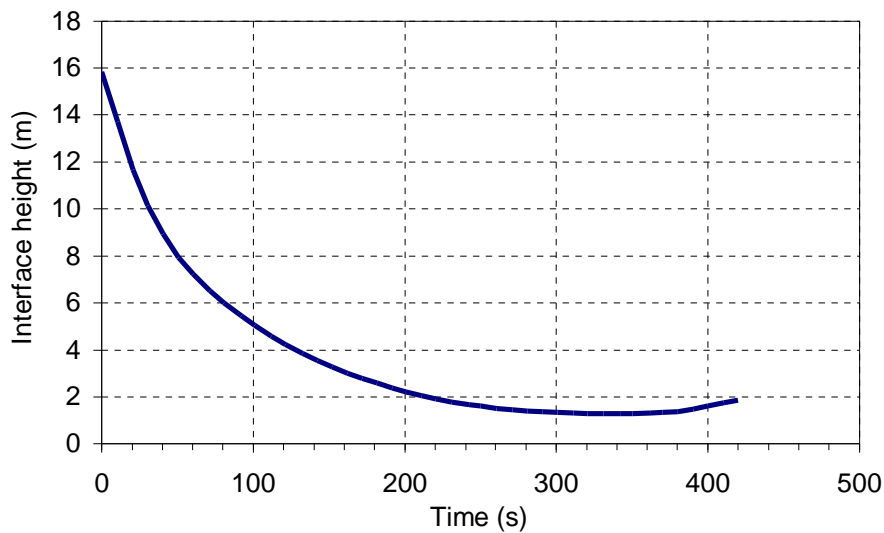


Figure 23 Predicted (MAGIC) layer height for *Part I case 2* (taken from Appendix D - L. Gay & B. Gautier)

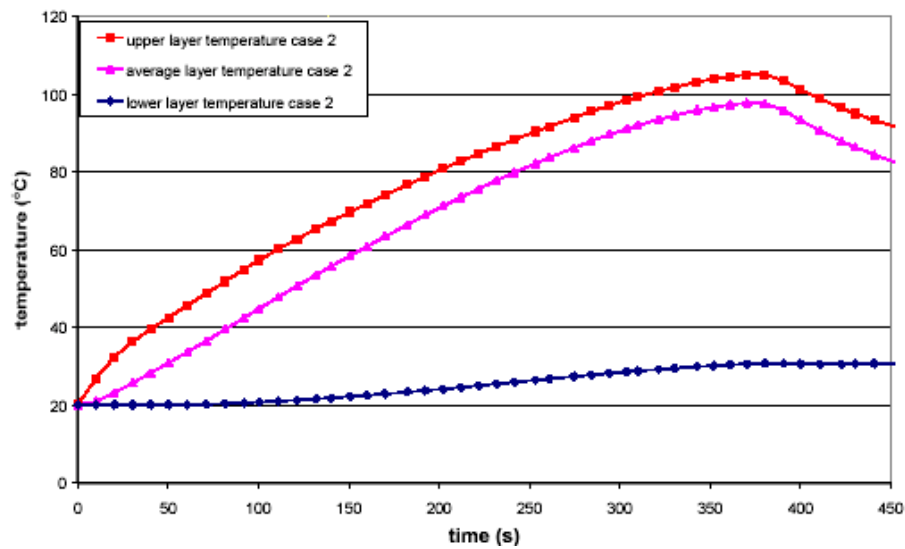


Figure 24 Predicted (MAGIC) layer temperatures for *Part I* case 2 (taken from Appendix G - D. Joyeux & O. Lecoq-Jammes)

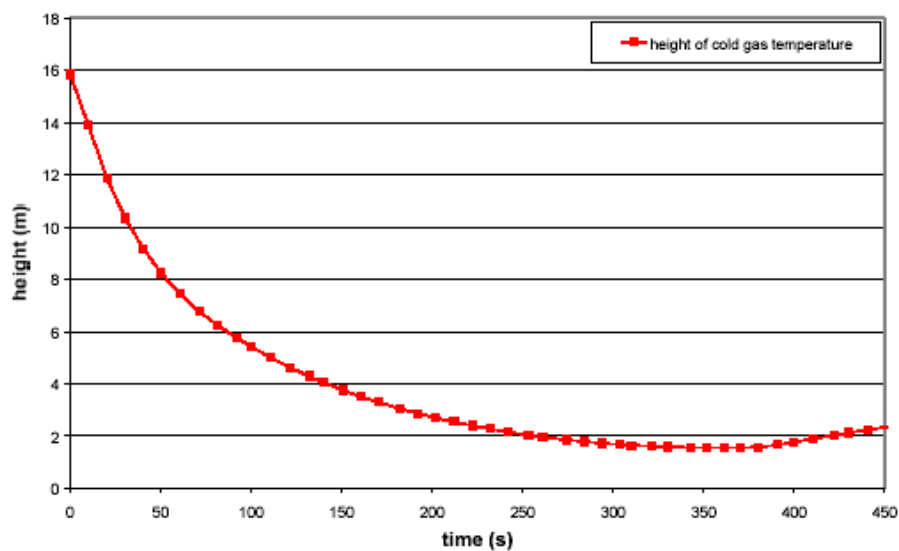


Figure 25 Predicted (MAGIC) layer height for *Part I* case 2 (taken from Appendix G - D. Joyeux & O. Lecoq-Jammes)

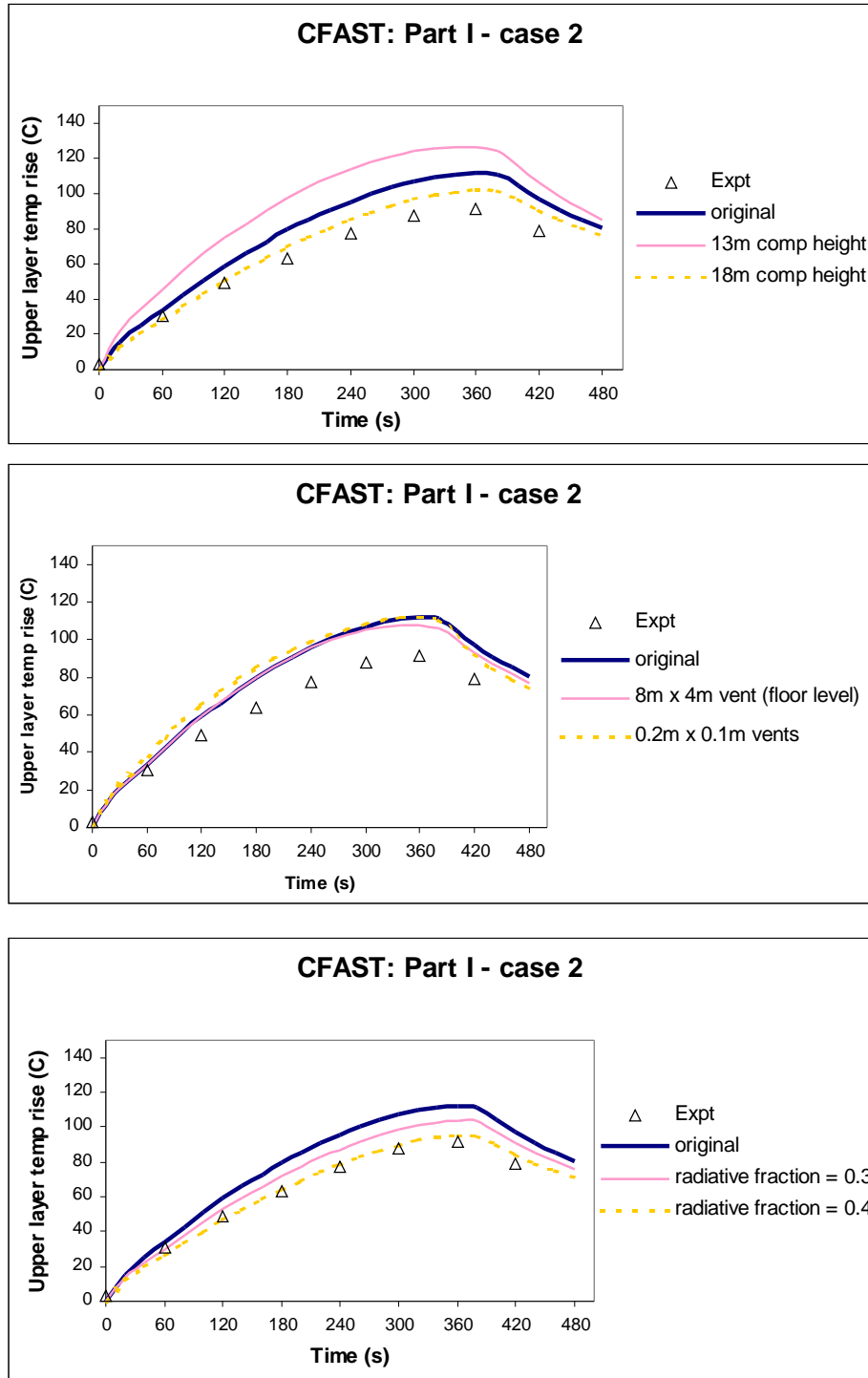


Figure 26 Comparison of predicted (CFAST) and measured layer temperatures (triangles) for *Part I case 2* (taken from Appendix H - S. Miles)

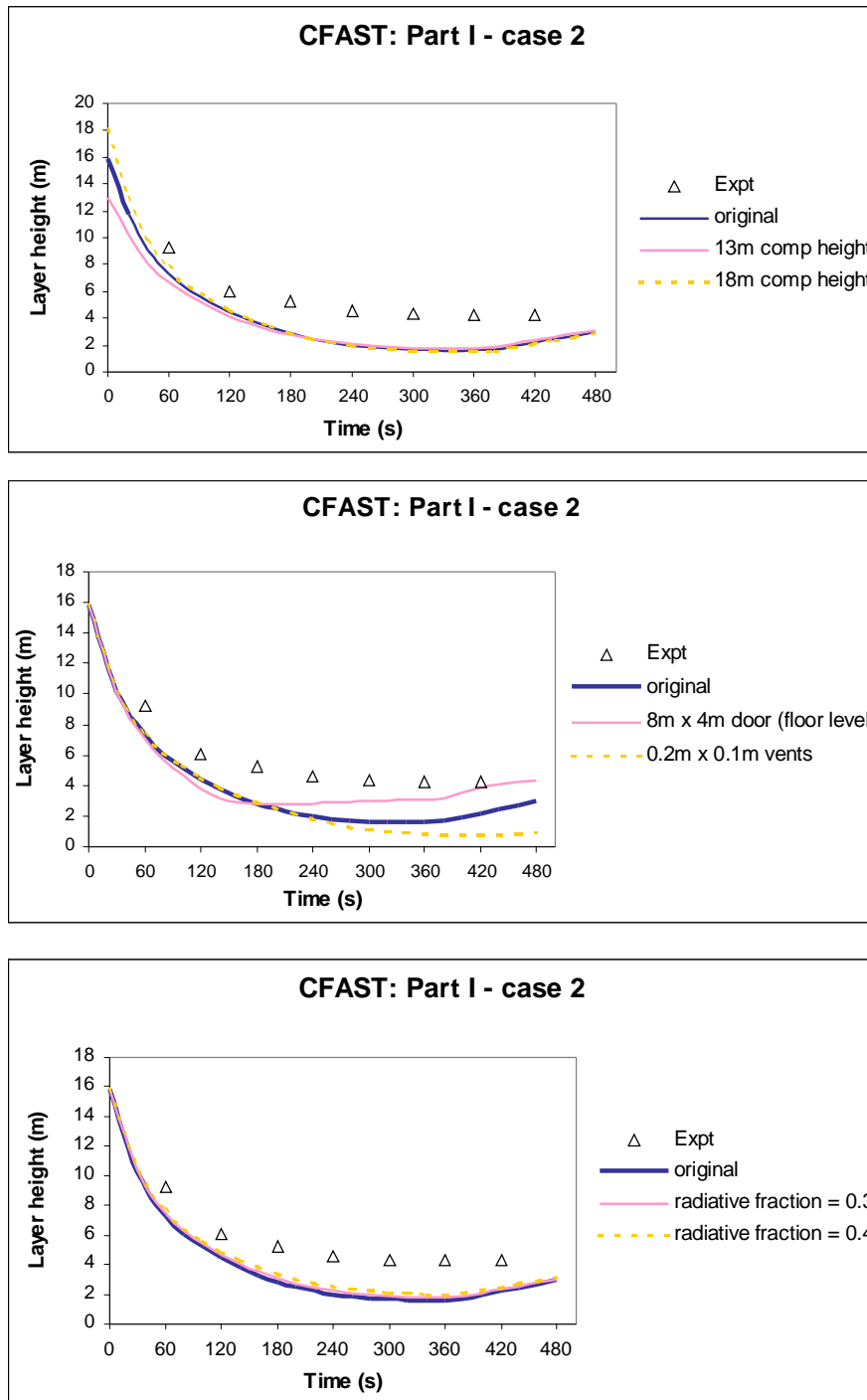


Figure 27 Comparison of predicted (CFAST) and measured layer height (triangles) for Part I case 2 (taken from Appendix H - S. Miles)

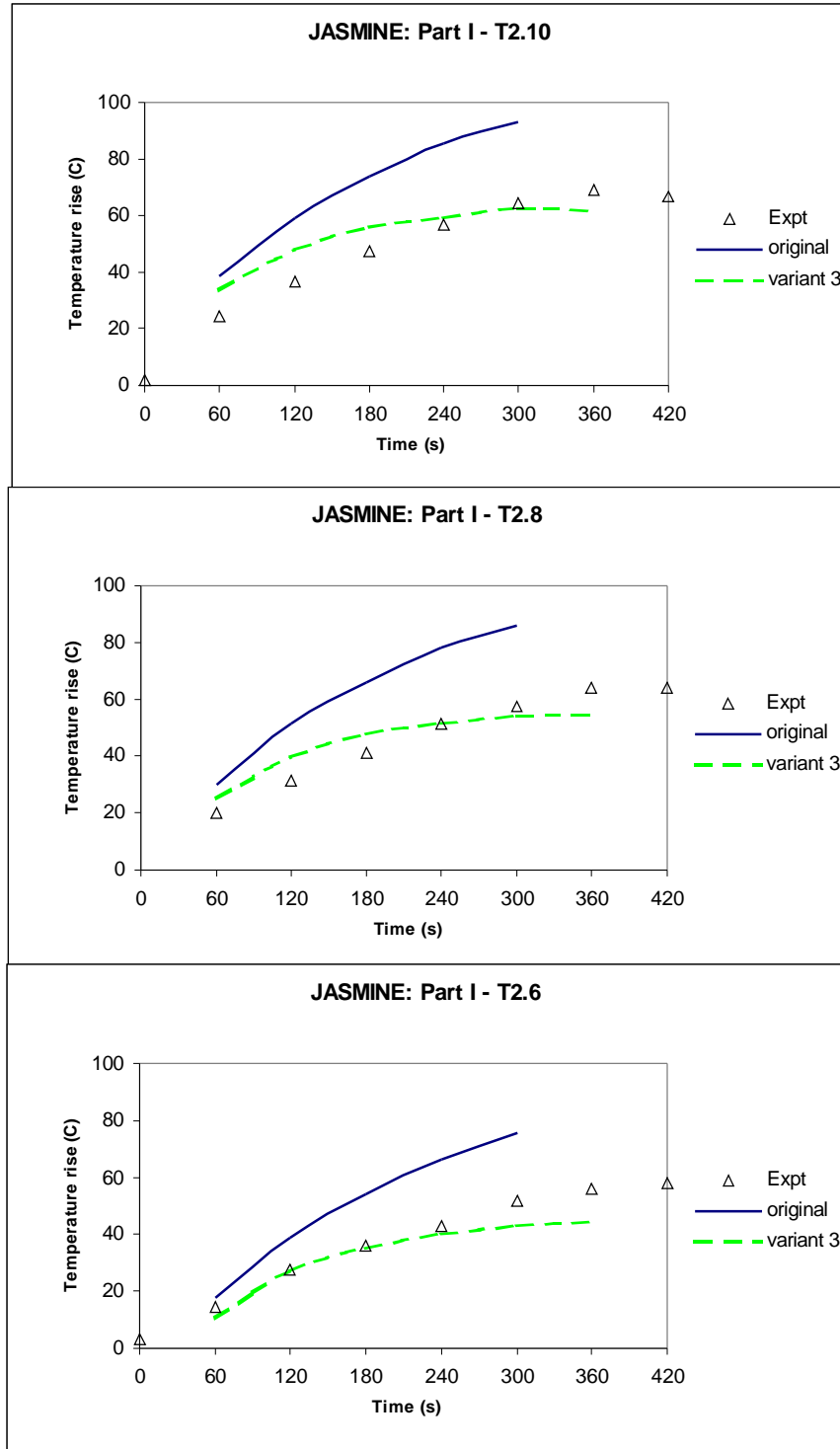


Figure 28 Comparison of predicted (JASMINE) and measured temperatures (triangles) for selected locations in Part I case 1 (taken from Appendix H - S. Miles)

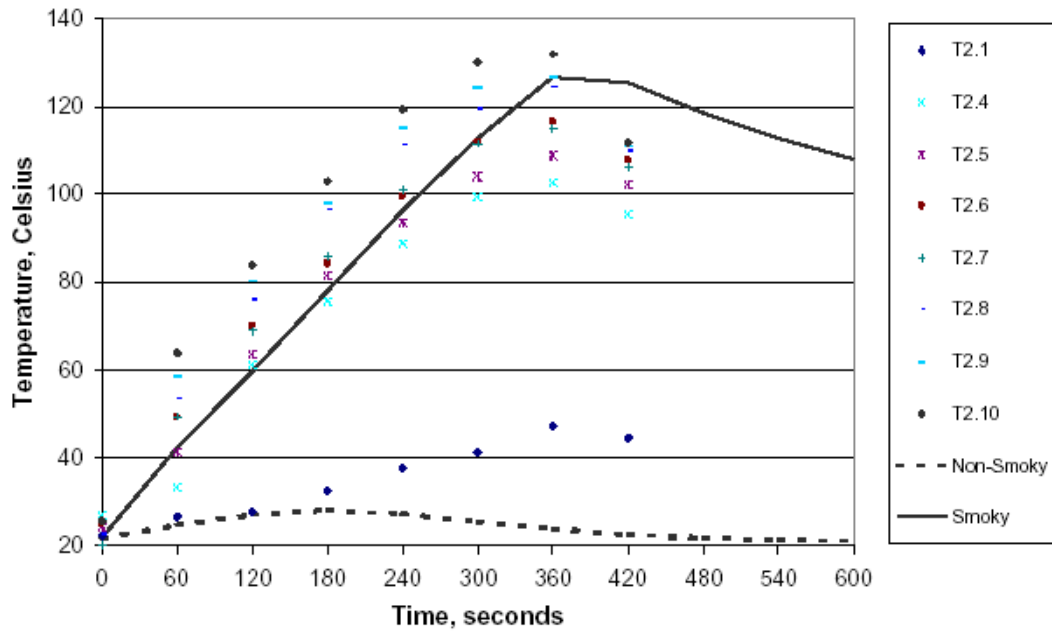


Figure 29 Predicted (HADCRT) temperatures for *Part I case 2* (taken from presentation at 5th meeting - B. Malinovic & M. Plys)

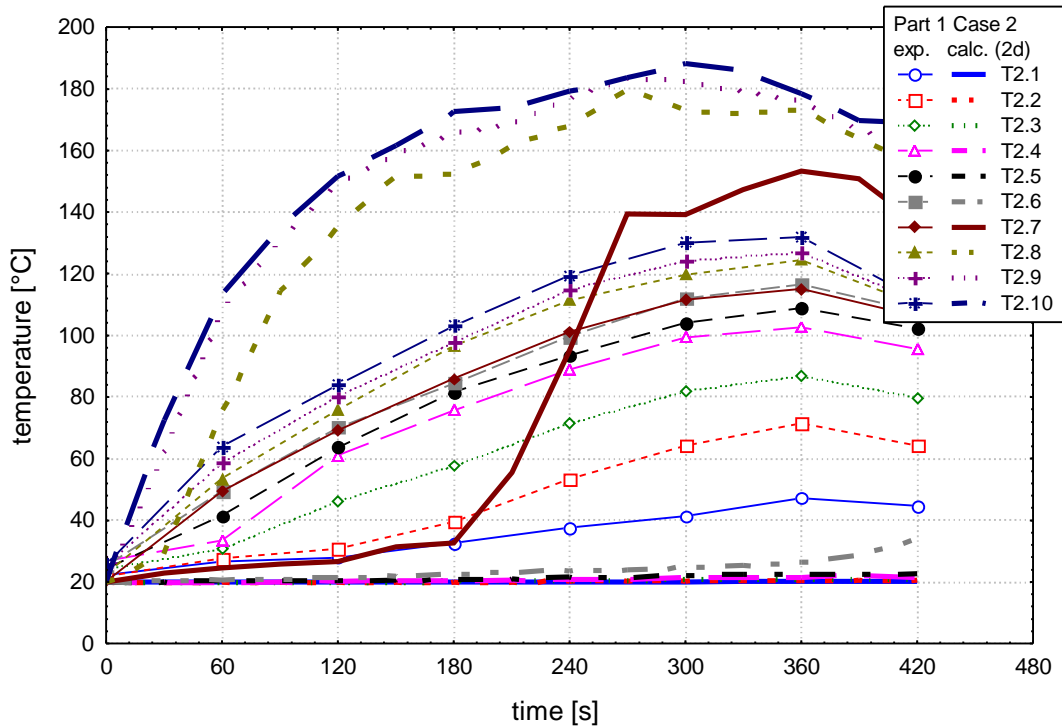


Figure 30 Predicted (Kobra3D) temperatures for *Part I case 2 - tree 2* (taken from Appendix I - J. Will)

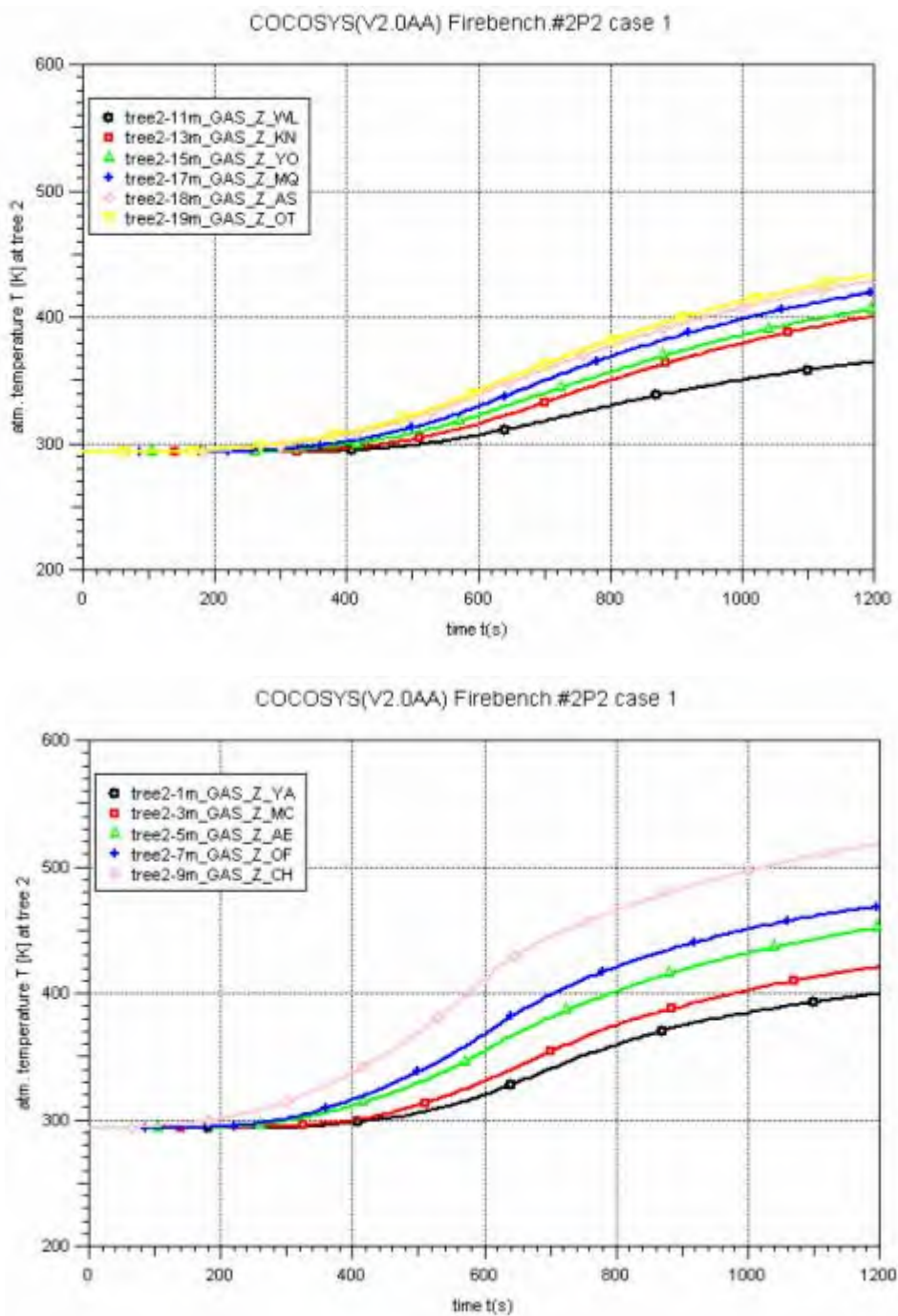


Figure 31 Predicted (COCOSYS) temperatures for *Part II case 1* – tree 2 (taken from Appendix C - W. Klein-Hebling)

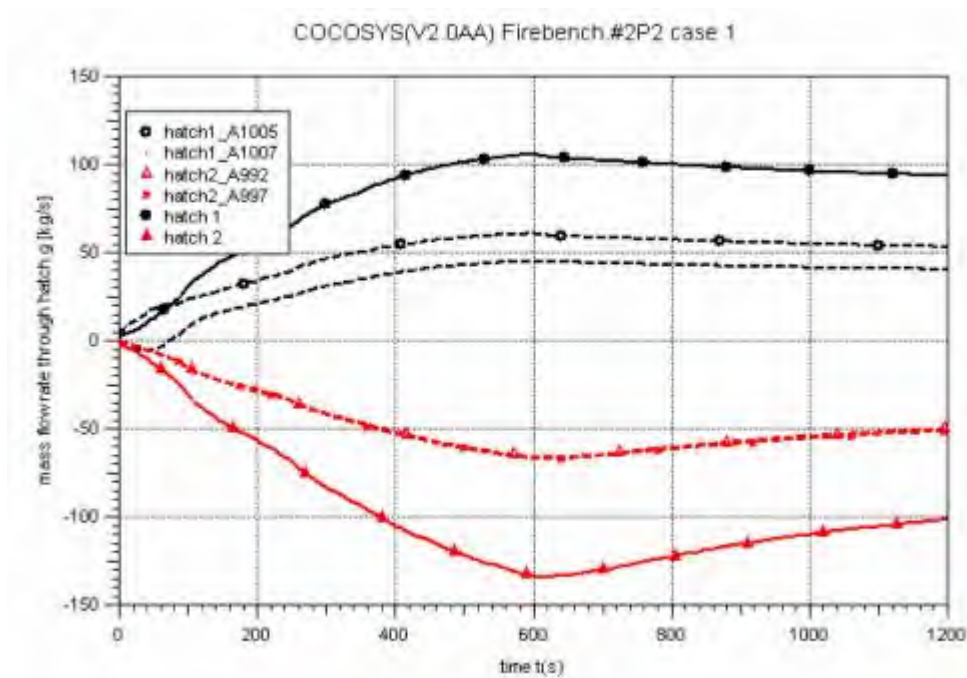


Figure 32 Predicted (COCOSYS) hatch mass flows for *Part II case 1* (taken from Appendix C - W. Klein-Hebling)

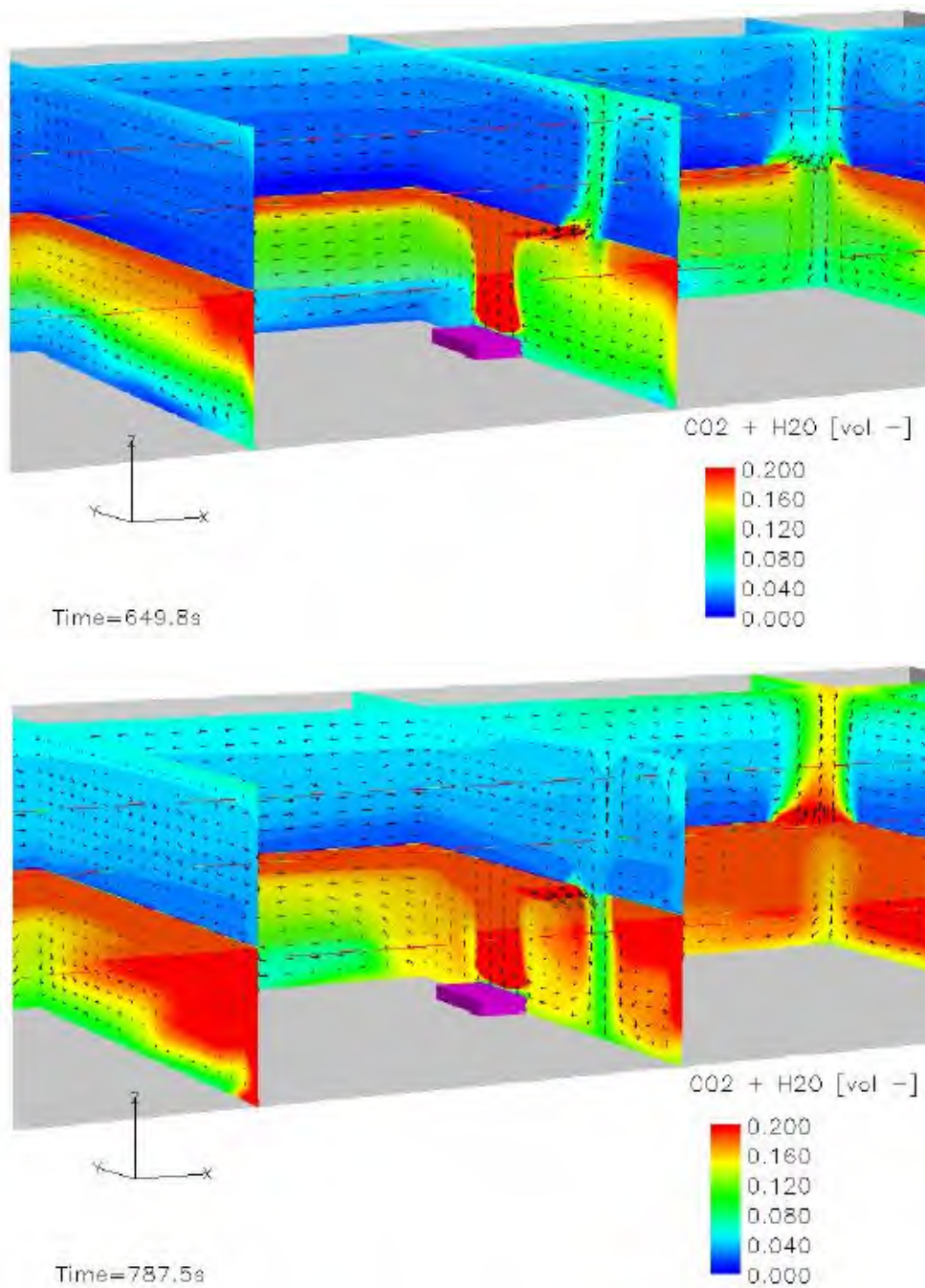


Figure 33 Flow reversal at hatches predicted by CFX-4 for *Part II case 1* (taken from Appendix E - M. Heitsch)

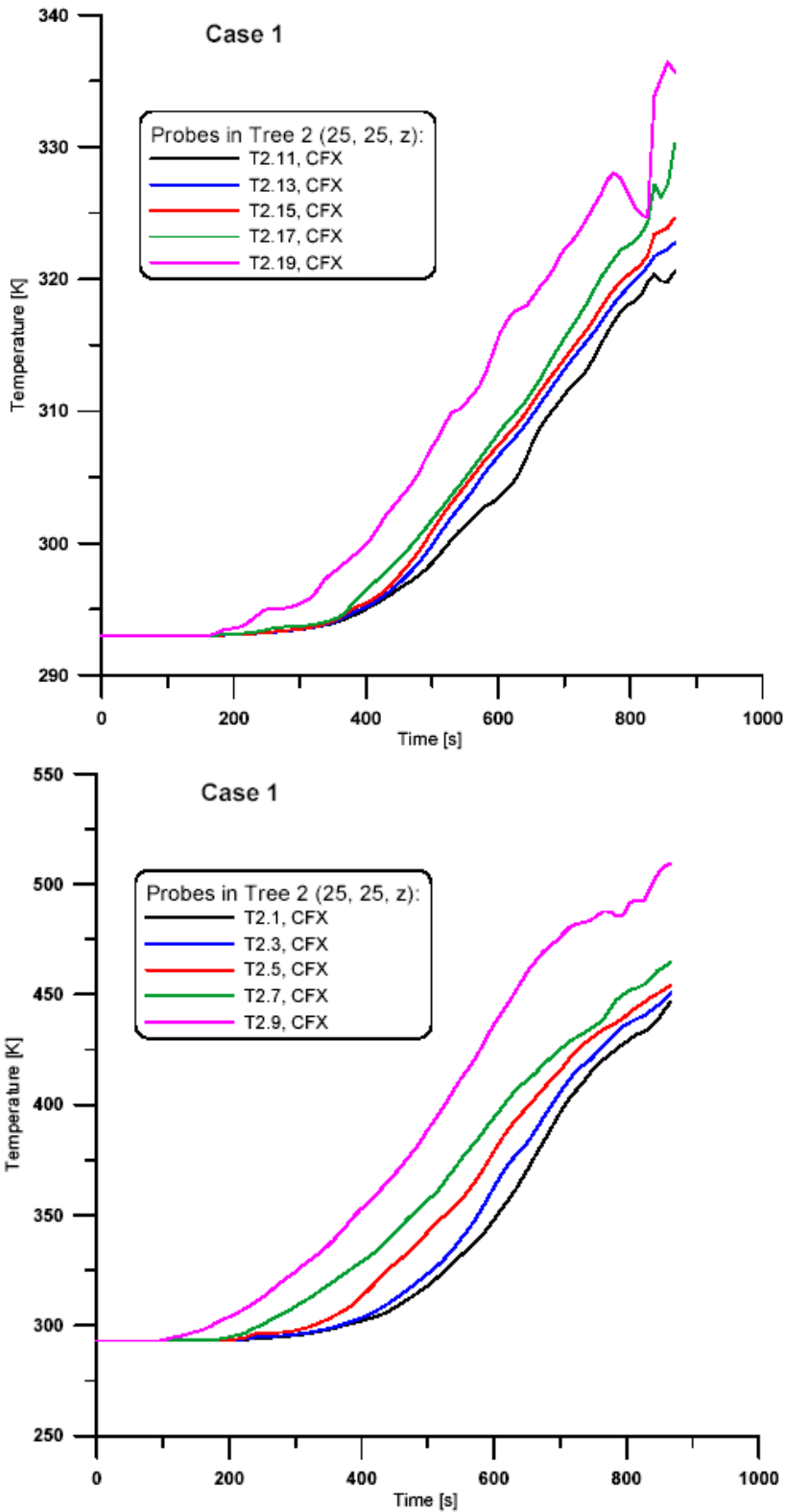


Figure 34 Predicted (CFX-4) temperatures for *Part II case 1 – tree 2* (taken from Appendix E - M. Heitsch)

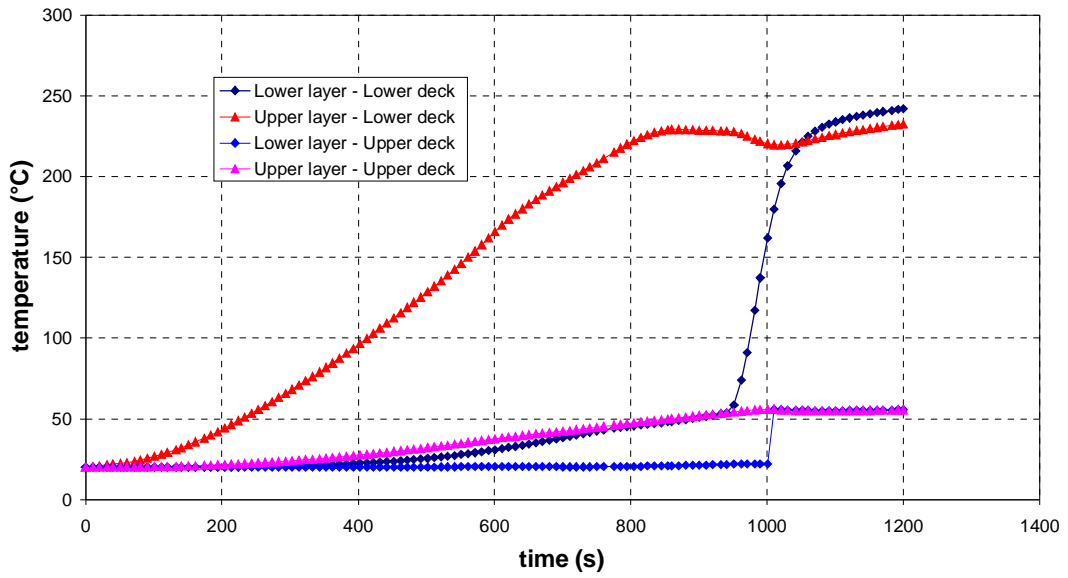


Figure 35 Predicted (MAGIC) layer temperatures for *Part II* case 1 (taken from supplied results - L. Gay & B. Gautier)

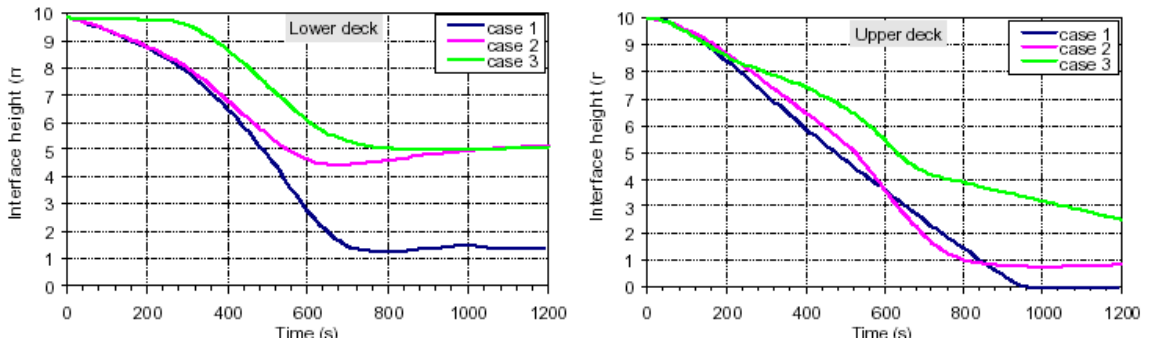


Figure 36 Predicted (MAGIC) layer heights for *Part II* (taken from Appendix D - L. Gay & B. Gautier)

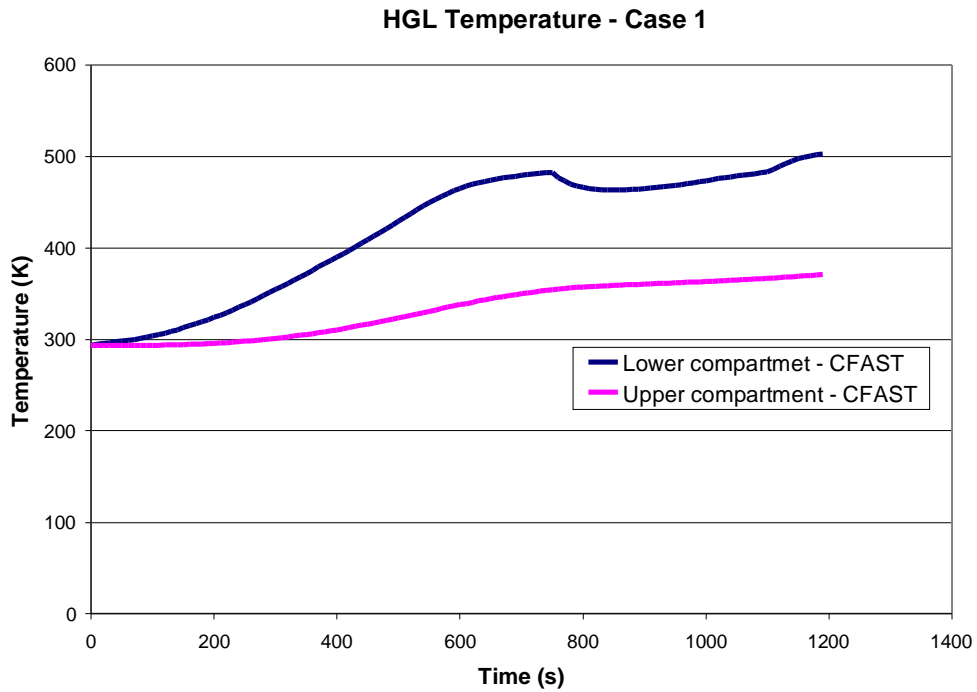


Figure 37 Predicted (CFAST) layer temperatures for *Part II case 1* (taken from supplied results - M. Dey)

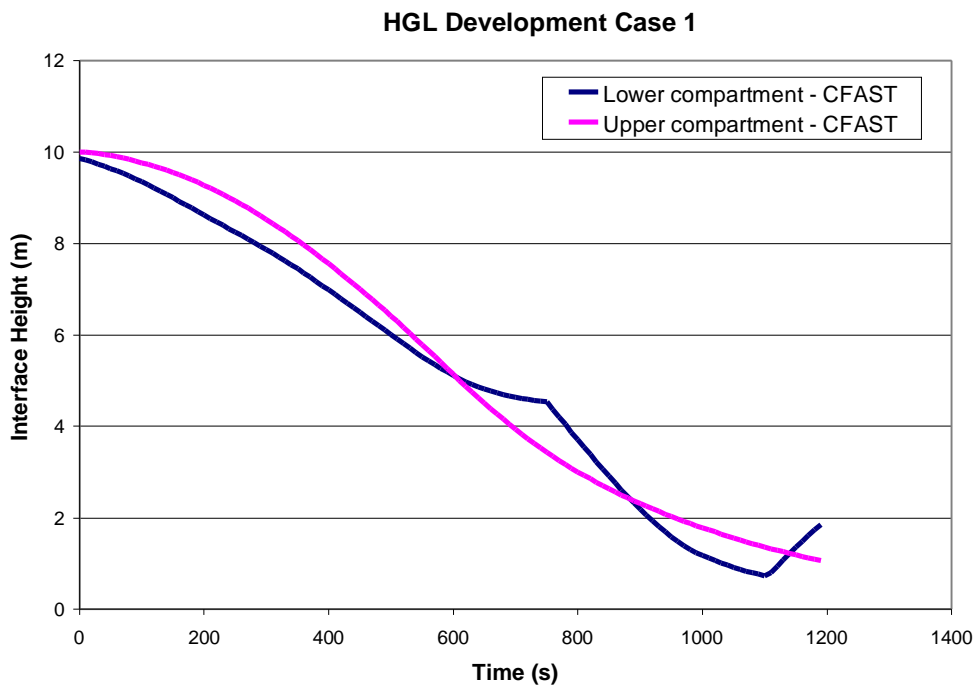


Figure 38 Predicted (CFAST) layer heights for *Part II case 1* (taken from supplied results - M. Dey)

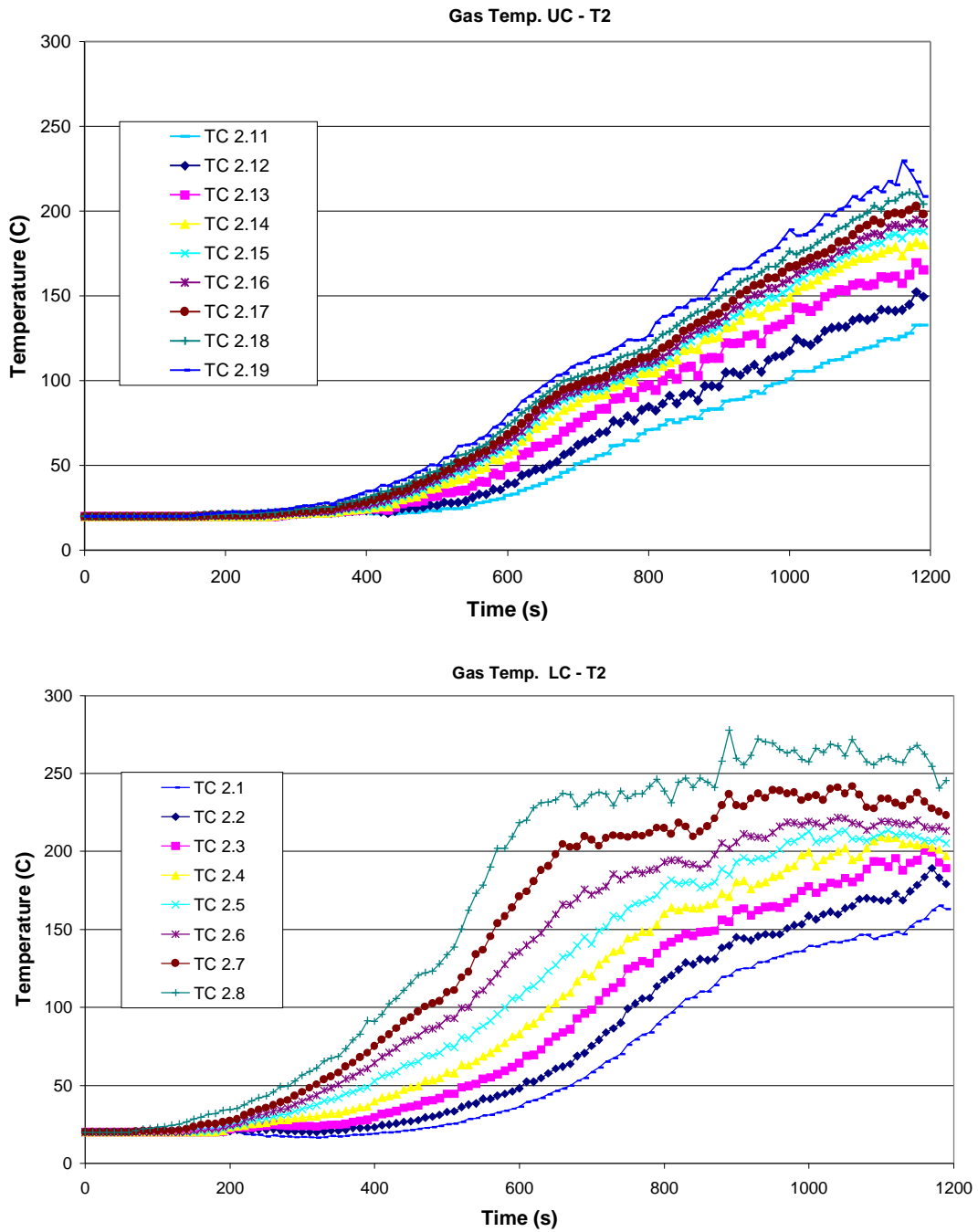


Figure 39 Predicted (FDS) temperatures for *Part II case 1 – tree 2* (taken from supplied results - M. Dey)

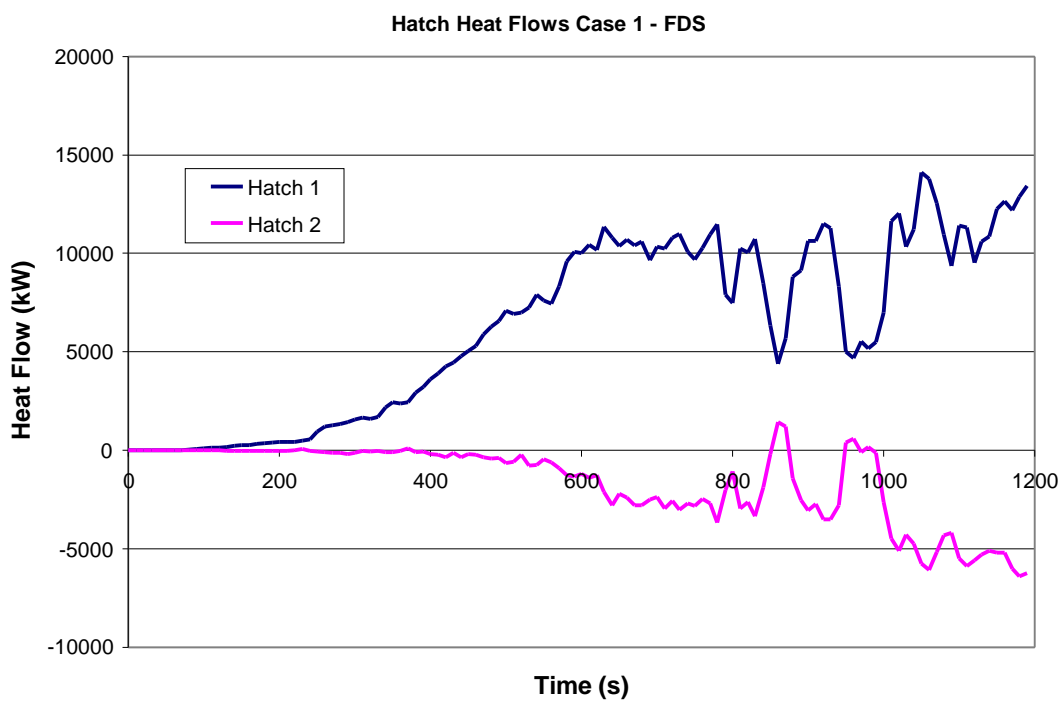


Figure 40 Predicted (FDS) hatch heat flows for *Part II case 1* (taken from Appendix F - M. Dey)

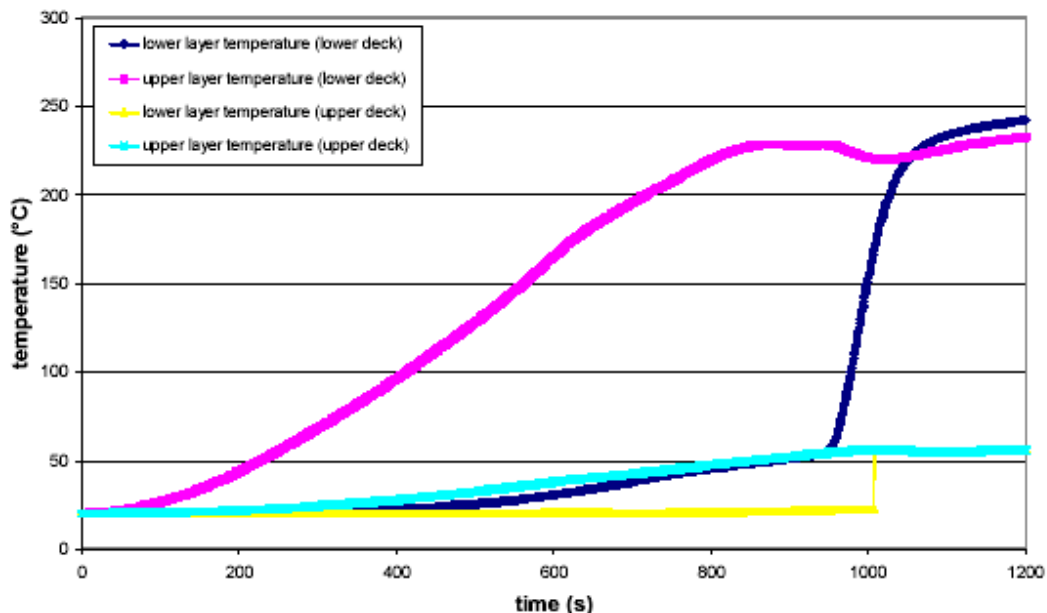


Figure 41 Predicted (MAGIC) layer temperatures for *Part II case 1* (taken from Appendix G - D. Joyeux & O. Lecoq-Jammes)

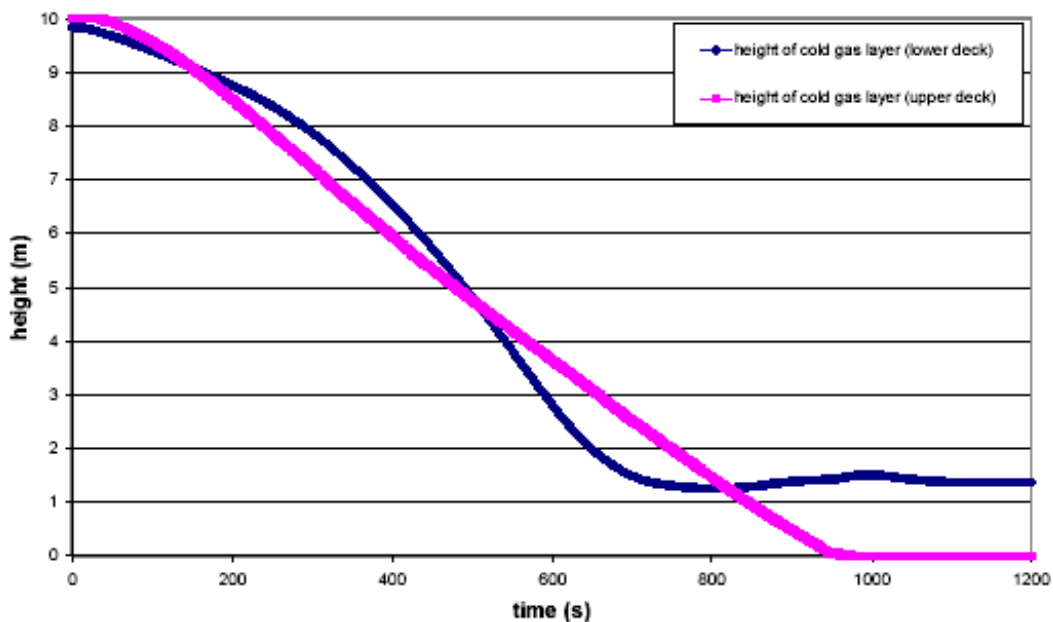


Figure 42 Predicted (MAGIC) layer heights for *Part II case 1* (taken from Appendix G - D. Joyeux & O. Lecoq-Jammes)

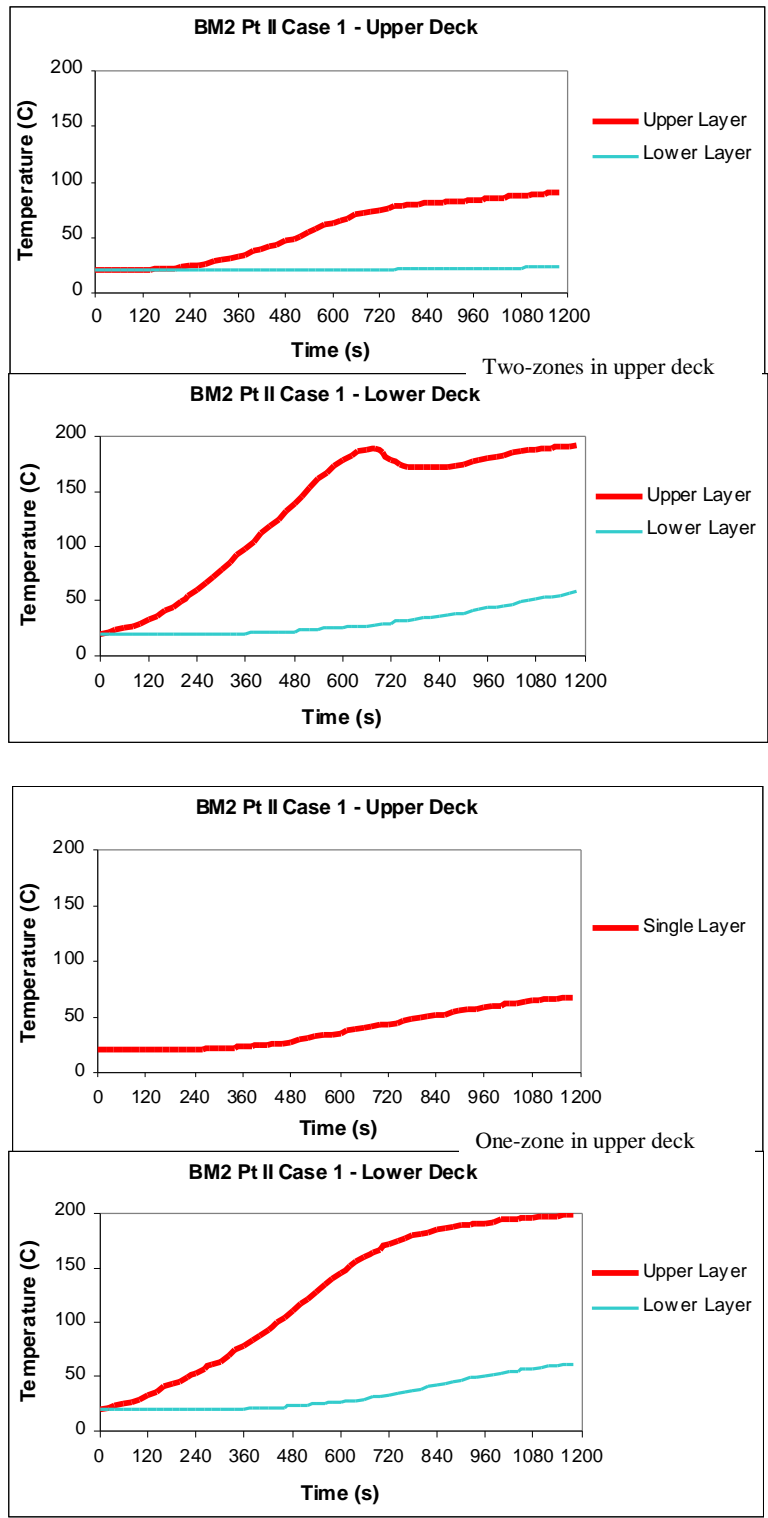


Figure 43 Predicted (CFAST) layer temperatures for *Part II case 1* (taken from Appendix H - S. Miles)

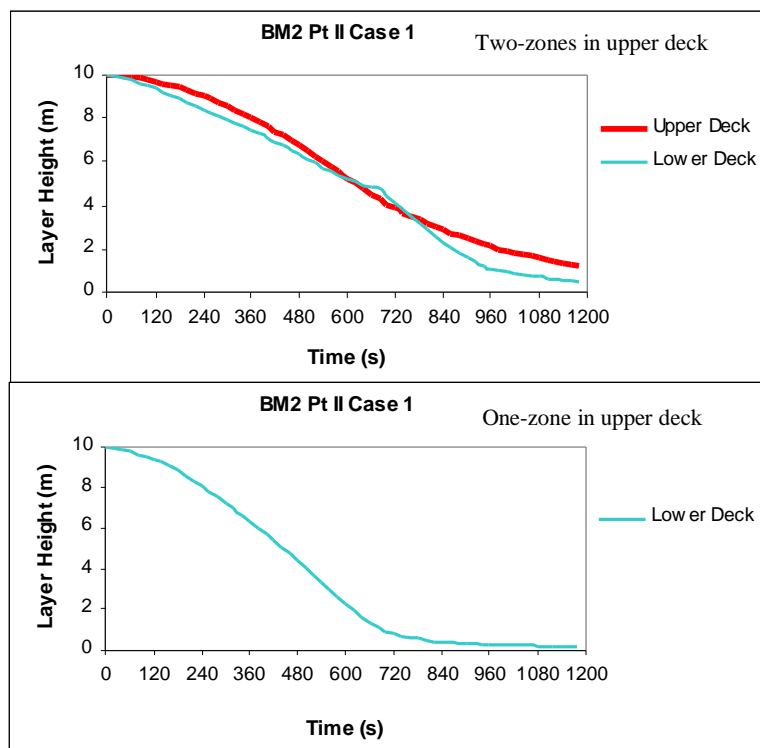


Figure 44 Predicted (CFAST) layer heights for *Part II case 1* (taken from Appendix H - S. Miles)

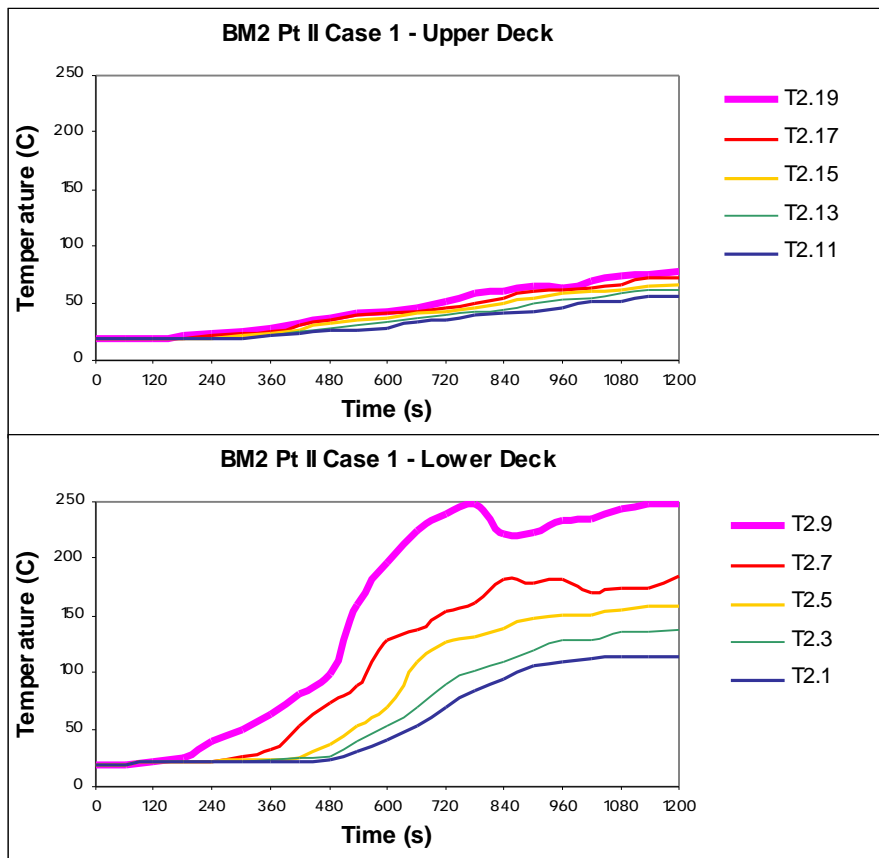


Figure 45 Predicted (JASMINE) temperatures for *Part II case 1 - tree 2* (taken from Appendix H - S. Miles)

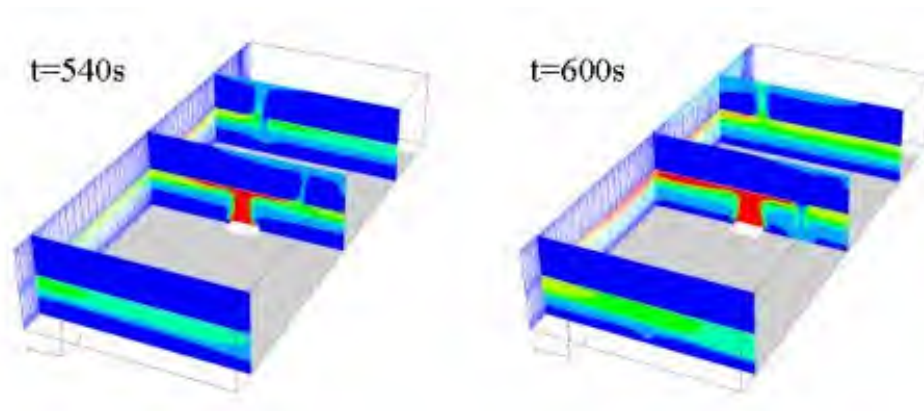


Figure 46 Flow reversal at hatches predicted by JASMINE for *Part II case 1* (taken from Appendix H - S. Miles)

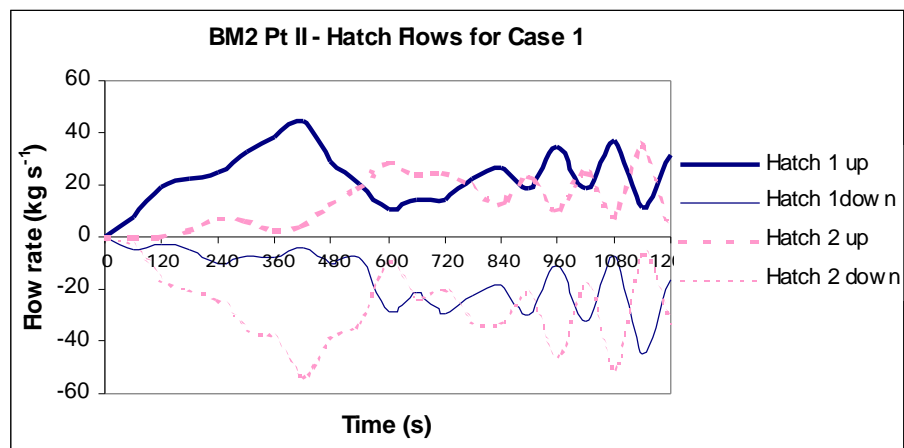


Figure 47 Predicted (JASMINE) hatch mass flows for *Part II case 1* (taken from Appendix H - S. Miles)

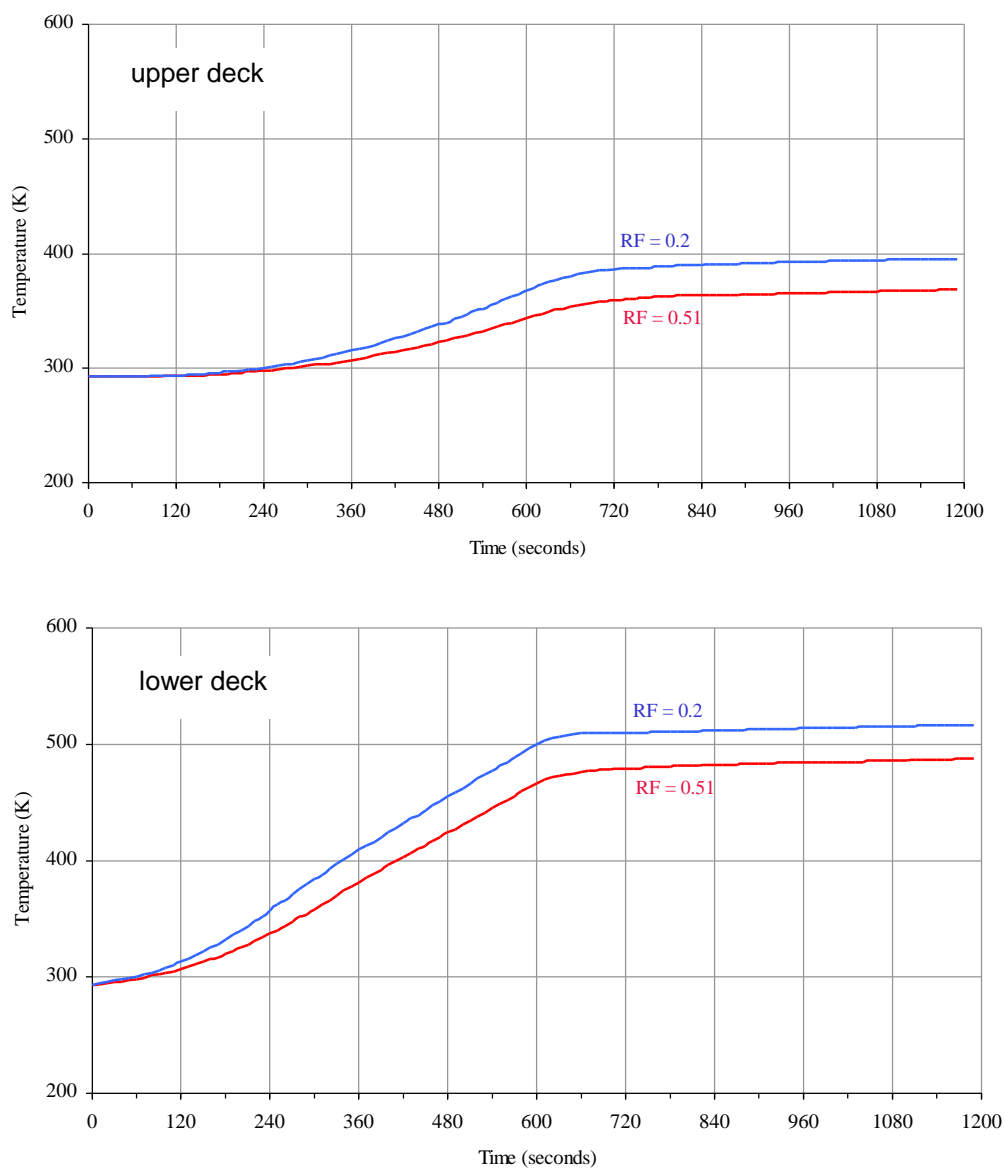


Figure 48 Predicted (CFAST) layer temperatures for *Part II case 2* (taken from 6th meeting presentation - A. Martin & D. Coutts)

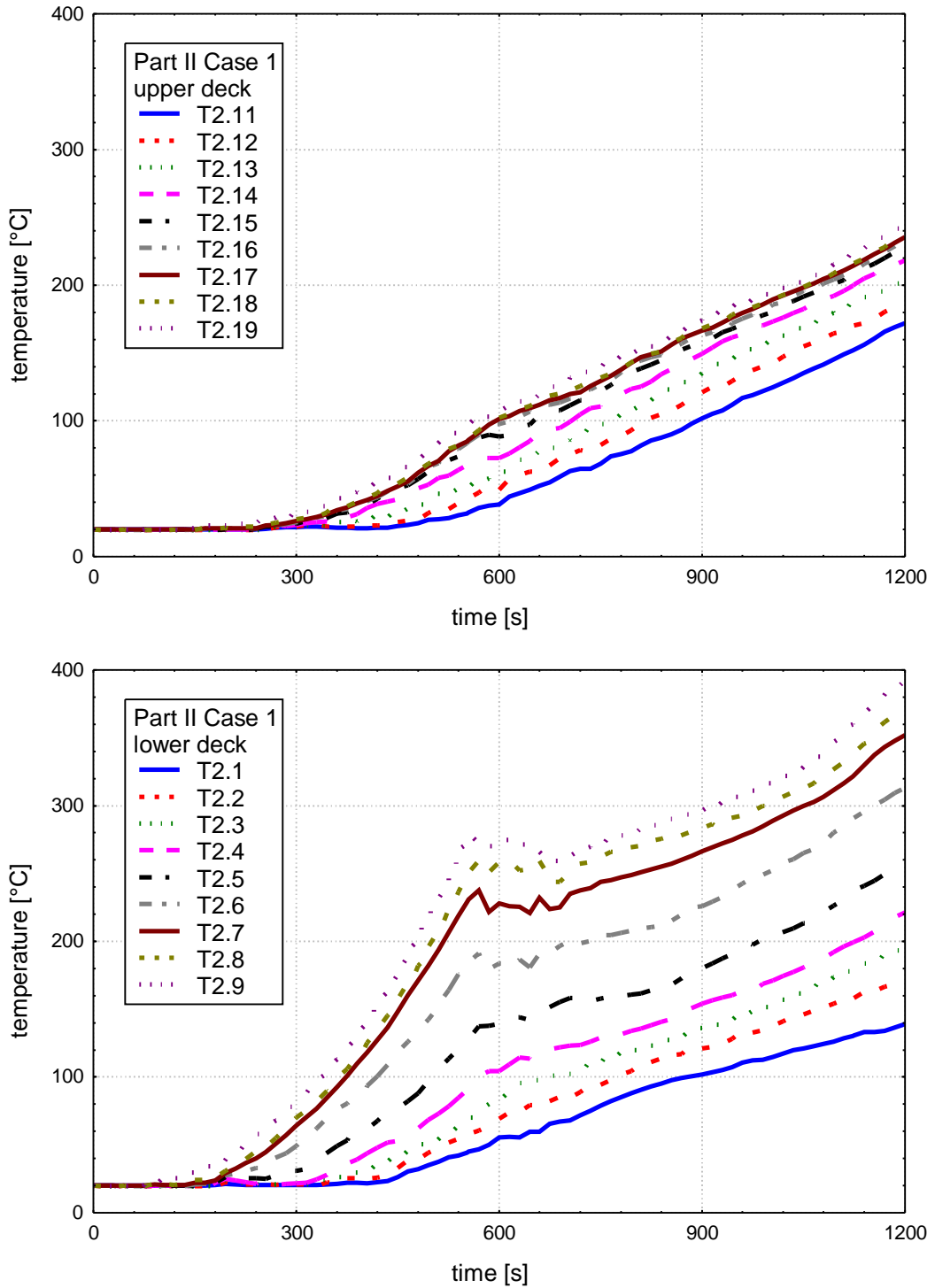
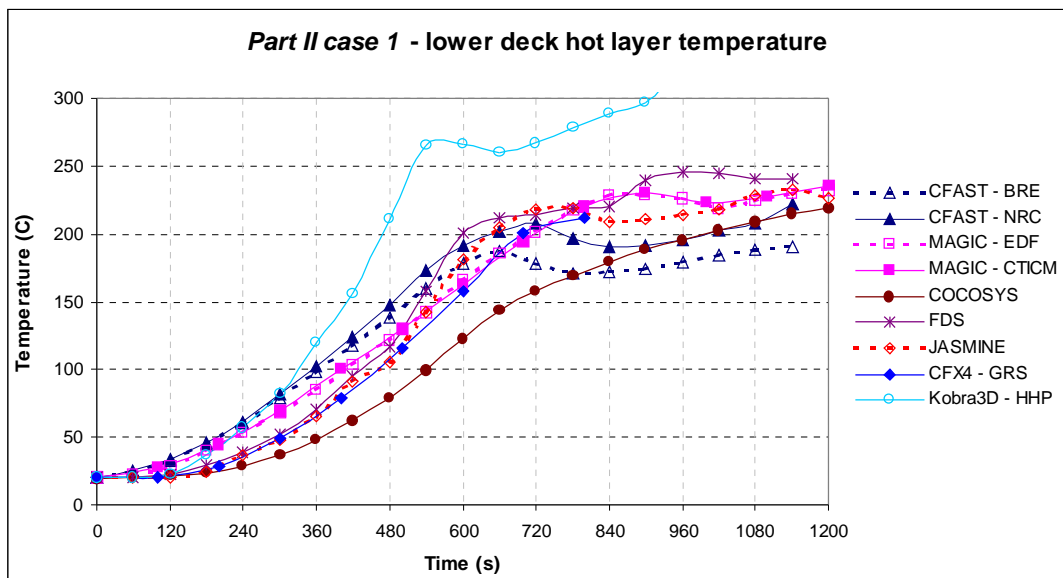
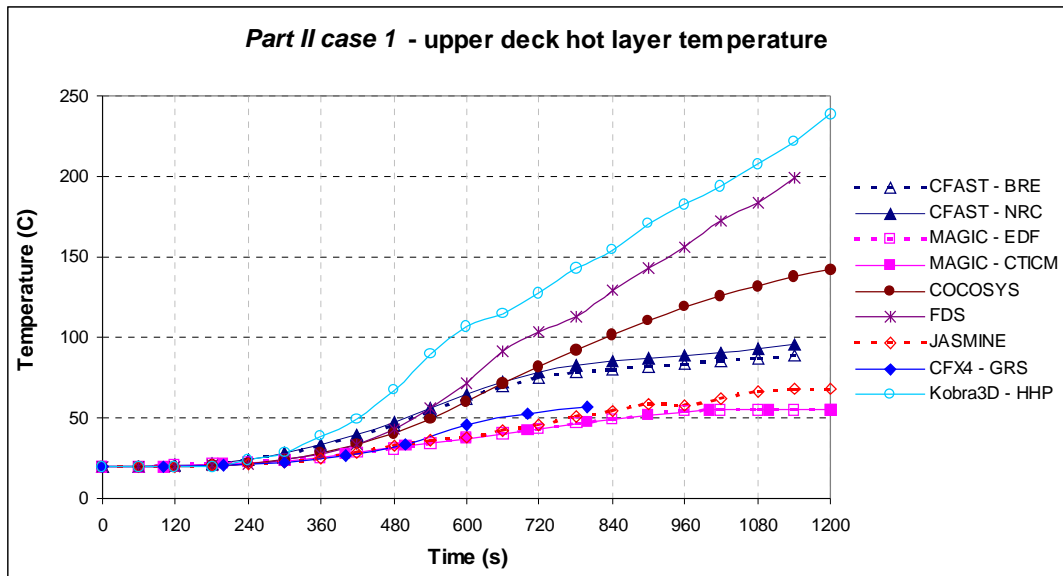
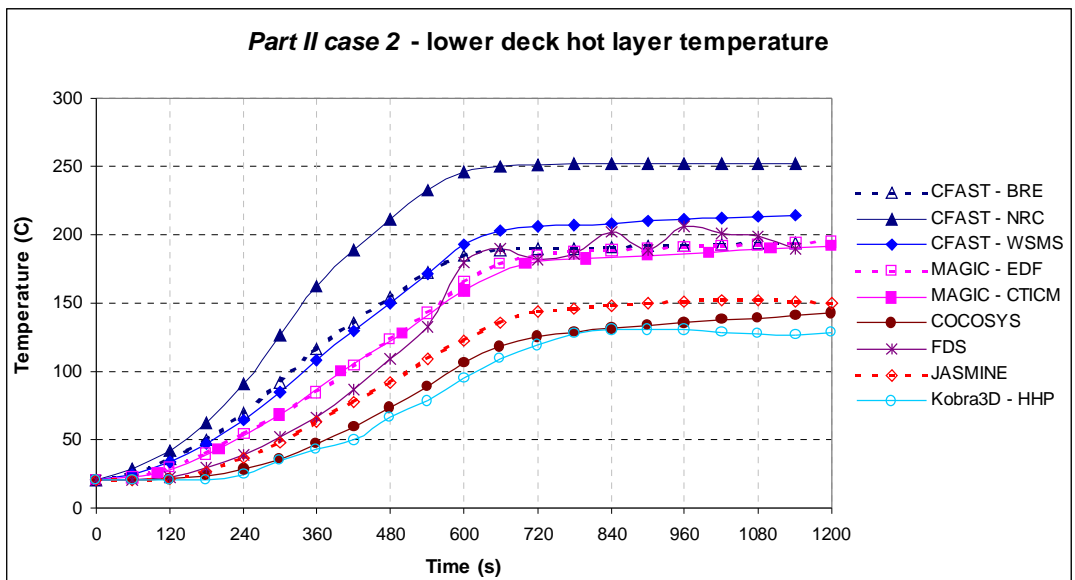
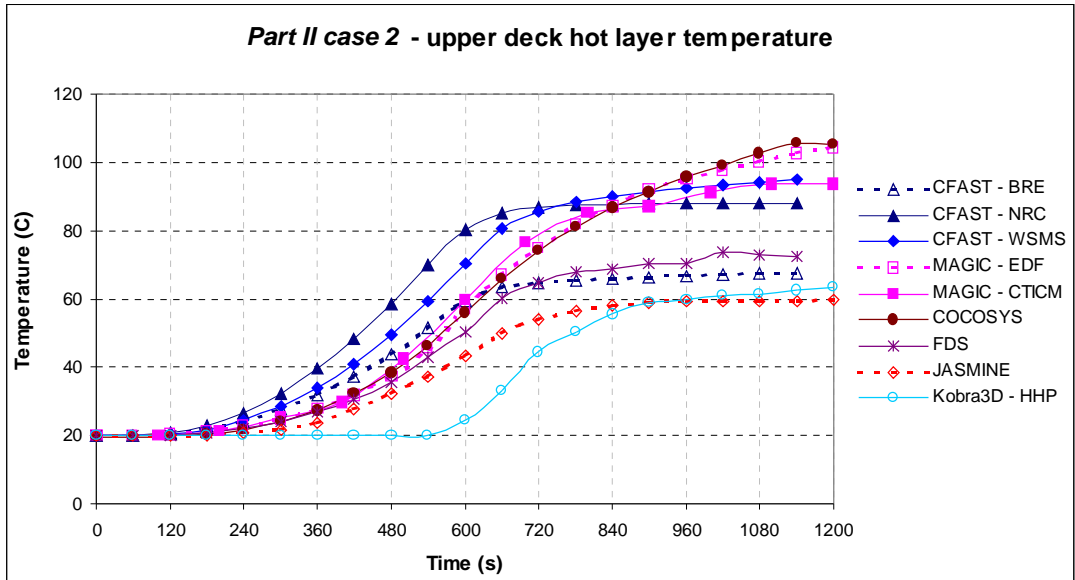


Figure 49 Predicted (Kobra3D) temperatures for *Part II case 1* (taken from Appendix I - J. Will)



Zone models (CFAST and MAGIC) - upper layer temperature plotted
 Lumped parameter and CFD models (COCOSYS, FDS, JASMINE, CFX4 and Kobra3D)
 - average of 'ceiling level' thermocouple tree locations at T1 and T2 plotted.

Figure 50 Inter-code comparison of 'hot layer' temperatures for *Part II case 1*



Zone models (CFAST and MAGIC) - upper layer temperature plotted
 Lumped parameter and CFD models (COCOSYS, FDS, JASMINE and Kobra3D) - average of 'ceiling level' thermocouple tree locations at T1 and T2 plotted.

Figure 51 Inter-code comparison of 'hot layer' temperatures for *Part II case 2*

**Appendix A - K. McGrattan (NIST): Benchmark Exercise #2 - Fire in
a large hall - NIST Fire Dynamics Simulator**

Appendix B - *D. Roubineau (IRSN): Benchmark Exercise 2 - Study of the consequences of a fire in a turbine hall*

**Appendix C - W. Klein-Heßling (GRS): Technical Note TN-KLH
1/2003 - Fire Benchmark #2 - COCOSYS Results**

Appendix D - *L. Gay and B Gautier (EDF): MAGIC Calculation for Benchmark #2 - Fire in a large hall*

**Appendix E - M. Heitsch (GRS): Benchmark Exercise #2
Simulations with CFX**

Appendix F - *M. Dey (USNRC): Analysis of Pool Fires in Large Multi-Level Halls with the CFAST and FDS Fire Codes*

**Appendix G – D. Joyeux and O. Lecoq-Jammes (CTICM):
Simulations with MAGIC (V 3.4.8)**

**Appendix H - S. Miles (BRE): Benchmark Exercise #2 Simulations
with JASMINE and CFAST**

**Appendix I - J. Will (HHP Braunschweig): Benchmark Exercise #2 -
Fire in a Large Hall - Results of Kobra-3D Calculations**